MINISTRY OF NATIONAL EDUCATION

THE ANNALS OF "DUNAREA DE JOS" UNIVERSITY OF GALATI

Fascicle IX
METALLURGY AND MATERIALS SCIENCE

YEAR XXXI (XXXVI),
December 2013, no. 4

ISSN 1453-083X

2013
GALATI UNIVERSITY PRESS

THE ANNALS OF "DUNAREA DE JOS" UNIVERSITY OF GALATI.
FASCICLE IX. METALLURGY AND MATERIALS SCIENCE
N^0. 4 – 2013, ISSN 1453 – 083X

Table of Content

THE ANNALS OF "DUNAREA DE JOS" UNIVERSITY OF GALATI.
FASCICLE IX. METALLURGY AND MATERIALS SCIENCE
N^0. 4 – 2013, ISSN 1453 – 083X

EFFECT OF CURRENT DENSITY ON MORPHOLOGY AND CORROSION RESISTANCE OF EPOXY RESIN /Zn LAYERS

Alina CIUBOTARIU*, Tamara RADU, Alina CANTARAGIU
"Dunărea de Jos" University of Galați, 111, Domnească Street, 800201, Galați, Romania
*Corresponding author
email: Alina.Ciubotariu@ugal.ro

ABSTRACT

In this research we intended to obtain and characteriz composite layers by using epoxy resin (disperse phase) electrodeposited with zinc (metal matrix). The epoxy resin/Zn layers were electrodeposited at two values of current densities: 3A/dm^2 and 5A/dm^2 from a suspension of epoxy resin particles with two mean diameter size particles (0.1 – 5.0µm and 6 – 10µm) in aqueous zinc sulphate electrolyte. Suspension was prepared by adding 10g/L epoxy resin particles into electrolyte solution. The morphology of the layers was investigated by scanning electron microscopy method. The regular crystal structure characteristic of electroplated zinc layers was disturbed by epoxy resin particles that perturb the zinc growth during electrodeposition. The corrosion behavior of the layers in the corrosive solution was investigated by potentiodynamic polarization method. As corrosion test solution 0.5 M sodium chloride was used. The rate of corrosion for layers obtained at 3A/dm^2 was 6.21µm/year for layers with means diameter size particles of 0.1 – 5.0µm, respectively 16.18µm/year for layers with means diameter particles size of 6 – 10µm. It was observed that by increasing the current density to 5A/dm^2 the rate of corrosion for layers was 16.11µm/year for layers with means diameter size particles of 0.1 – 5.0µm, respectively 24.37µm/year for layers with means diameter size particles of 6 – 10µm.

KEYWORDS: epoxy resin particles, electrodeposition, epoxy resin/Zn composite coatings, layers morphology, corrosion rate

1. Introduction

Zinc is an important element in industrial world; it is used in a wide range from metal products to rubber, paint and agricultural industries. Zinc deposits are essentially used to protect steel against corrosion. The protection is principally a result of the zinc's anodic behavior in any electrochemical reaction. Under the same conditions (3.5% sodium chloride solution), the potential of zinc deposits is more negative (-1050mV/SCE) than that of steel (-650mV/SCE). Thus, zinc deposits behave as sacrificial anodes and offer cathodic protection [1, 2]. Surface layers are used to increase the lifetime of components exposed to corrosion and wear condition. It is well known that surface morphology and texture which are both influenced by bath composition and processing parameters have significant effects on the corrosion resistance of zinc electrodeposits [3-5].

Epoxy resins are considered as one of the most important classes of thermosetting polymers and find extensive use in various fields of coating, high performance adhesives and other engineering applications.

Epoxy resins are network-forming polymers displaying several interesting characteristics, e.g. good chemical resistance, adhesion to the most varied substrates, good electrical resistance and mechanical properties. Because of these attributes they have found many applications in different industries (e.g. electronics, aeronautics or astronautics) as protective layers, fiber reinforced plastics, adhesives etc. [6-7].

Considerable efforts have been made not only to improve corrosion resistance property of zinc layers but also to impart other beneficiary properties. One of the possible solutions for this is the incorporation of inert particles (nano or micro sized) into a growing zinc metal matrix during electrodeposition.

The resulted coating generally referred to as metal matrix composite has attracted interest due to its unique functional properties such as higher corrosion and wear resistance, hardness, super conduction and magnetic properties, semiconductor properties, photo catalytic properties compared to pure metal or alloy coatings [8]. However these properties depend on process parameters such as current density, concentration of salts, additives, surfactants and their nature and type of applied current (pulsed current, direct current) [9].

In the present research, efforts have been made to develop a bath solution without additive because they could give reactions with epoxy resin particles and the results could not be interpreted properly. So that, it was proposed to obtain composite layers using epoxy resin type Dinox 110L electrodeposited with zinc.

2. Experimental part

For electrodeposition of coating layers we used an electrochemical cell. The zinc metal plate of 99.99% purity (anode) and DC04 steel plates of 6×3×0.1cm (cathode) were employed. Before electrodeposition mild steel plates were mechanically polished with different grades of emery paper, degreased with alkaline solution and washed with distilled water. Anode was activated by dipping in 10% dilute hydrochloric acid solution for few seconds, washed with water and then placed in bath solution with the composition reported before [10].

Zinc sulphate electrolyte has cathodic polarization bigger than zinc chloride electrolyte so that it was used sulphate electrolyte for electrodeposition. Sodium sulphate increase the conductibility and ability for dispersing and aluminium sulphate was used as buffering agent which stabilized the acidity of electrolyte. Concomitantly we obtain more shining layers.

The pH of the solution was 3.8. Deposition was carried out at current density of 3A/dm^2 and 5A/dm^2, deposition time of 60 minutes and stirring rate of 1000rpm. Electrodeposition experiments were performed at room temperature. In bath solution it was added epoxy resin to give a solution concentration of 10g/L epoxy resin particles with means diameter size particles of 0.1 – 5.0μm and 6–10μm. Epoxy or polyepoxide is a thermosetting epoxide polymer that cures (polymerizes and crosslinks) when mixed with a catalyzing agent or "hardener". Most common epoxy resins are produced from a reaction between epichlorohydrin and bisphenol-A (Fig. 1). The value of n varies from 0 to 25. The resin is liquid when n < 1 and solid when n > 2 [11].

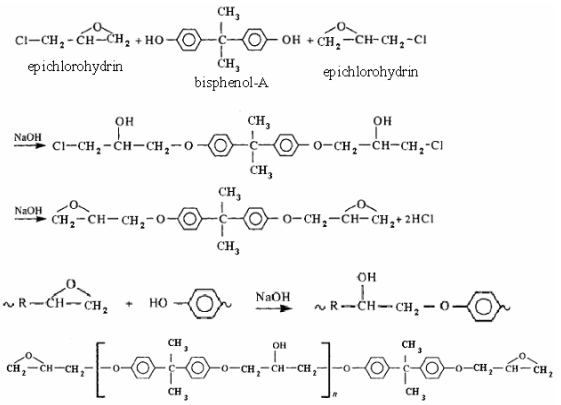

Fig. 1. *Schematic illustrating the formation of the epoxy resin type structures*

Properties of epoxy resin type Dinox 110L used as disperse phase for electrodeposition are presented in Table 1.

The thickness of layers was calculated using gravimetric method.

The morphology of deposits was examined by scanning electron microscopy (SEM) using a microscope type Phylips FEI; QUANTA 200.

Table 1. *Properties of epoxy resin type Dinox 110L*

Molecular weight	500 g/mol
Density	1.18 – 1.25 g/cm^3
Epoxide number	1.85 – 2.20 Eq/kg
Melting point	64 – 76 ºC
Volatile compounds	Max. 1%

For potentiodynamic polarization measurements it was used a three-electrode open cell with epoxy resin/Zn layers as working electrode (WE), a platinum gauze as counter electrode (CE) and a saturated calomel electrode (SCE) as reference electrode (SCE = +241mV/NHE). Initial potential (I.P.) was –1.6 V (Hg/Hg_2Cl_2), final potential (F.P.) was –0.9 V (Hg/Hg_2Cl_2) and a scan rate of 0.5 mV/s. The polarization potentiodynamic curves were recorded after 30 min of immersion. The Tafel parameters for the particular specimens were determined by extrapolating the anode and cathode Tafel curves. As test solution 0.5 M sodium chloride was used.

3. Results and discussions

3.1. SEM analysis

The thickness of epoxy resin/Zn composite layers obtained at 3A/dm^2 was 42.32μm for layer obtained with particles by means diameter size of

0.1 – 5μm and 51.45μm for the layer obtained with particles by means diameter size of 6 – 10μm.

If we increased the current density to 5 A/dm^2 it was found a thickness layer of 70.14μm for the layer obtained with particles by means diameter size 0.1–5μm and 78.34μm for the layer obtained with particles by means diameter size 6 – 10μm (Fig. 2).

It could be observed that by increasing the current density the layers thickness increases. Also it has been observed that by increasing the mean diameter size of epoxy resin particles the layers thickness increased.

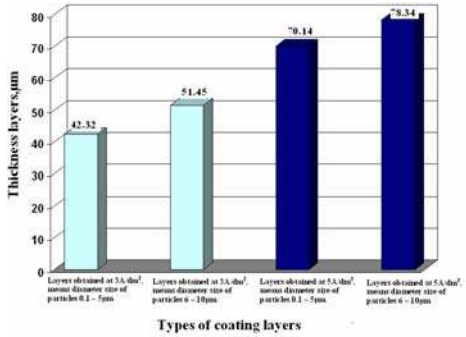

Fig. 2. *Comparative thickness of epoxy resin/Zn layers*

Figs. 3 - 8 compare morphological aspects of pure zinc coatings and epoxy resin composite layers obtained of different current density and different mean diameter particles size under scanning electron microscopy method.

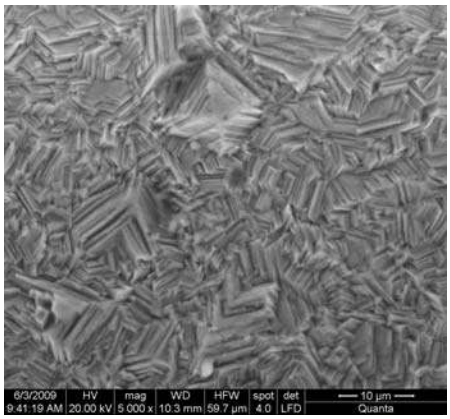

Fig. 3. *SEM surface morphology of pure zinc layers obtained at 3A/dm^2 (x 5000)*

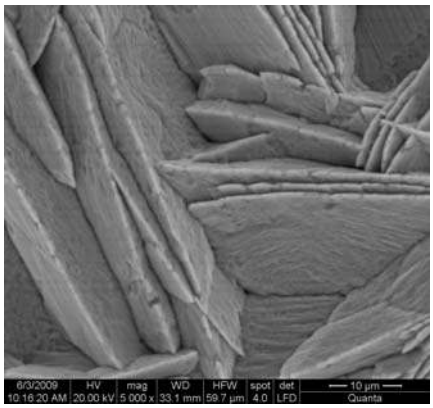

Fig. 4. *SEM surface morphology of pure zinc layers obtained at 5A/dm^2 (x 5000)*

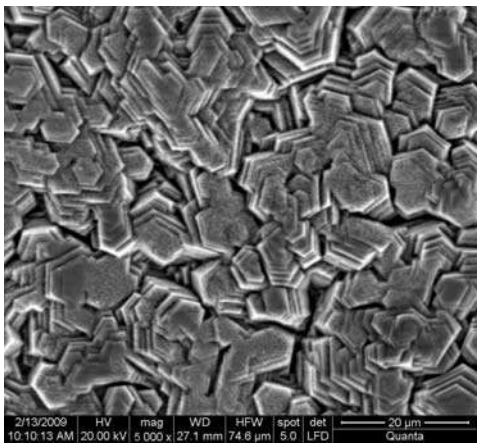

Fig. 5. *SEM surface morphology of epoxy resin/Zn composite layers obtained at 3A/dm^2 with means diameter particles size in electrolyte solution 0.1 – 5 μm (x 5000)*

Fig. 6. *SEM surface morphology of epoxy resin/Zn composite layers obtained at 3A/dm^2 with mean diameter particles size in electrolyte solution 6 – 10 μm (x 5000)*

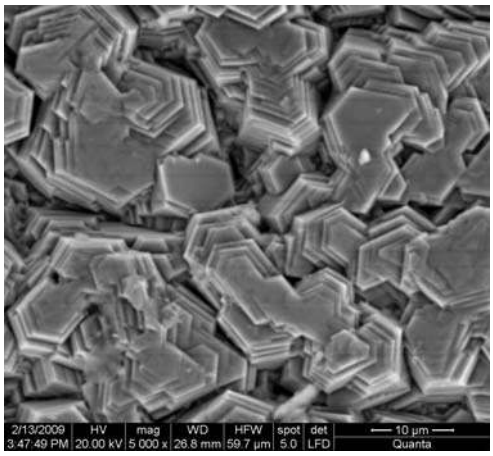

Fig. 7. *SEM surface morphology of epoxy resin/Zn composite layers obtained at 5 A/dm^2 with means diameter particles size in electrolyte solution 0.1 - 5µm (x 5000)*

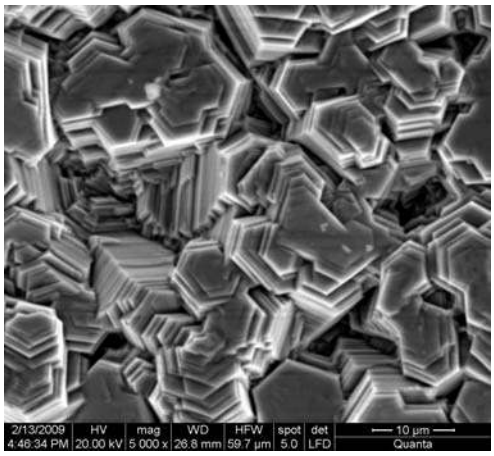

Fig. 8. *SEM surface morphology of epoxy resin/Zn composite layers obtained at 5A/dm^2 with means diameter particles size in electrolyte solution 6 - 10µm (x 5000)*

As it can be seen in Fig. 3 - 8, the addition of epoxy resin particles in electrolyte bath significantly changes the morphology of the zinc deposits as compared to those obtained from solutions without disperse phase. The morphology of coatings layers is different compared to pure coated zinc. The pure zinc coating has a rather regular surface, is bright but not smooth and consists of hexagonal platelets of moderate size having the degree of orientation perpendicular to the substrate surface (Fig. 3 - 4). The morphology of zinc layers obtained at 5A/dm^2 presents a significant increase in the size of the zinc platelets.

For composite layers obtained at 3A/dm^2 it could be observed that the morphology of the surfaces is different function means diameter particles size. It is noted that with increasing means diameter size from 0.1 – 5µm to 6 – 10µm the morphology of the layers is different needle more orderly and smooth (Figs. 5 – 6).

If we increased the current density up to 5 A/dm^2 it was observed that the morphology of the surfaces is changed more to finer crystallites (Figs. 7 – 8). The crystals of coatings were parallelly orientated to the substrate and the hexagonal planes are clearly observed.

The epoxy resin particles act as reducing the crystals size and orientation of electrodeposited zinc during co-deposition.

3.2. Potentiodynamic polarization measurements

The electrochemical investigation of each sample began with the monitoring of the open circuit potential change immediately after the immersion into the testing solutions till reaching a relatively stable stationary value.

The performed potentiodynamic diagrams for epoxy resin/Zn composite coatings in 0.5 M sodium chloride after 30 minutes of immersion are presented in Figure 9.

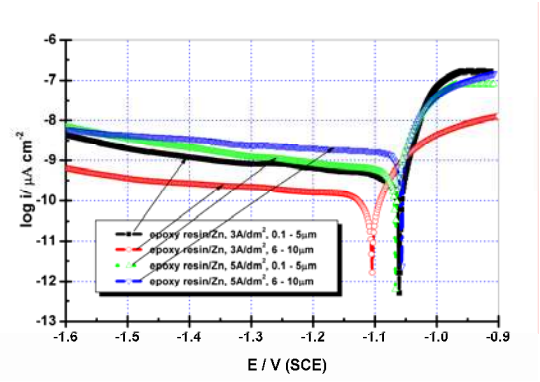

Fig. 9. *Potentiodynamic polarization curves for epoxy resin/Zn layers in 0.5 M sodium chloride solution obtained after 30 minutes of immersion time (log scale)*

In corrosion, quantitative information on corrosion currents and corrosion potentials can be extracted from the slope of the curves, using the Stern-Geary equation [12]:

$$i_{corr} = \frac{1}{2.303 R_p}\left(\frac{\beta_a \cdot \beta_c}{\beta_a + \beta_c}\right) \quad (1)$$

i_{corr} = corrosion current density;
R_p = polarization resistance;
β_a = anodic slope;
β_c = cathodic slope.

Different parameters such as corrosion current density (i_{corr}) and corrosion potential (E_{corr}), cathodic (β_c) and anodic (β_a) Tafel slopes derived from Fig. 9 using Tafel extrapolation are summarized in Table 2.

Corrosion rates (CR) were calculated by the following equation:

$$CR(\mu m / year) = \frac{0.051 \cdot i_{corr} \cdot (E_q.wt.)}{d} \qquad (2)$$

i_{corr} – corrosion current density calculated from Stern – Geary equation;

E_q.wt. is the equivalent weight;

d is the density of the zinc metal in g/cm^3.

The corrosion potential for all types of composite layers is not greatly different; it was observed a very small difference by 30mV.

From potentiodynamic polarization curves the polarization resistance of epoxy resin/Zn layers were been found between 484.82Ωcm^2 (composite layers obtained at 3 A/dm^2 with mean diameter size of resin particles 0.1 – 5μm) and 179.68Ωcm^2 (composite layers obtained at 5A/dm^2 with mean diameter size of resin particles 6 – 10μm).

If we compare corrosion rate of epoxy resin/Zn composite layers with corrosion rate of pure zinc layers [13, 14] we can conclud that by adding epoxy resin particles in zinc electrolyte were obtained epoxy resin/Zn composite layers most resistant to the corrosive attack of the 0.5 M sodium chloride solution than pure zinc obtained from electrodeposition at the same parameters (Fig. 10).

Table 2. *Tafel parameters for epoxy resin/Zn layers calculated from potentiodynamic polarization curves obtained after 30 min from immersion in 0.5 M sodium chloride solution*

Type of coatings	**E_{corr}, V; Hg/HgCl$_2$**	**β_a,**	**β_c,**	**i_{corr},**	**R_p ,**	**V_{corr},**
		[mV/decade]		[μA/cm^2]	[Ω cm^2]	[μm/year]
Epoxy resin/Zn 3A/dm^2, particles size 0.1 - 5μm	- 1.06	18.1	- 78.0	13.16	484.82	6.21
Epoxy resin/Zn 3A/dm^2 particles size 6 - 10μm	- 1.09	35.6	- 55.1	34.32	273.60	16.18
Epoxy resin/Zn 5A/dm^2, particles size 0.1 - 5μm	- 1.07	25.0	- 202.7	34.17	282.76	16.11
Epoxy resin/Zn 5A/dm^2 particles size 6 - 10μm	- 1.08	27.8	- 92.7	51.68	179.68	24.37

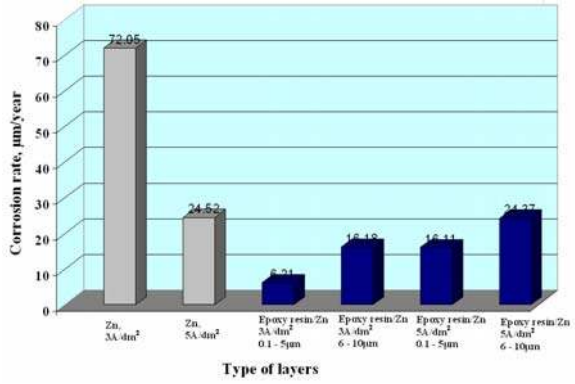

Fig. 10. *Corrosion rate for pure zinc and epoxy resin/Zn composite layers obtained at different values of current densities*

From the results presented in Fig. 10, it can be concluded that, by including epoxy resin particles in zinc sulphate electrolyte bath, the layers obtained are more resistant to the corrosive attack of the 0.5 M sodium chloride. Corrosion rate for pure zinc was 72.05μm/year (layers obtained at 3A/dm^2) and 24.52μm/year (layers obtained at 5A/dm^2). Corrosion rate for epoxy resin/Zn composite layers was between 24.37μm/year (layers obtained at 5A/dm^2 with means diameter size particles of 6 – 10μm) and 6.21μm/year (layers obtained at 3A/dm^2 with means diameter size particles of 0.1 – 5μm) that demonstrate a significant increase of corrosion rate.

4. Conclusions

Our research proved that epoxy resin particles type Dinox 110L could be codeposited with zinc to obtain composite layers without using any surfactants.

It could be observed that by increasing the current density and the mean diameter size of epoxy resin particles the thickness layers increase.

Addition of epoxy resin particles in electrolyte bath significantly changes the morphology of the zinc deposits as compared with those obtained from solutions without disperse phase.

The pure zinc coating has a rather regular surface and consists of hexagonal platelets of moderate size having degrees of orientation perpendicular to the substrate surface. The morphology of the epoxy resin/Zn surfaces is changed more to finer crystallites and crystals of

coatings were parallelly orientated to the substrate and the hexagonal planes are clearly observed.

The epoxy resin particles acts as reducing the crystals size and orientation of electrodeposited zinc during co-deposition. From potentiodynamic polarization curves the polarization resistance of epoxy resin/Zn layers has been found between 484.82Ωcm^2 (composite layers obtained at 3A/dm^2 with mean diameter size of resin particles 0.1 – 5μm) and 179.68Ωcm^2 (composite layers obtained at 5A/dm^2 with mean diameter size of resin particles 6 – 10μm). Corrosion rate for epoxy resin/Zn composite layers was between 24.37μm/year (layers obtained at 5A/dm^2 with mean diameter size particles of 6 – 10μm) and 6.21μm/year (layers obtained at 3A/dm^2 with means diameter size particles of 0.1 – 5μm) that demonstrate a significant increase of corrosion rate versus corrosion rate of pure zinc coatings obtained at the same parameters for electrodeposition. It was demonstrated that the new composite sobtained, epoxy resin/Zn composite layers, have a better corrosion properties than pure zinc layers.

References

[1]. M. Mouanga, L. Ricq, J. Douglade, P. Berçot - *Corrosion behaviour of zinc deposits obtained under pulse current, electrodeposition: Effects of coumarin as additive*, Corrosion Science, 51, (2009), p. 690–698.

[2]. L. Lacourcelle - *Traité de galvanotechnique*, Galva-conseils edition, Paris, (1997).

[3]. S. Khorsand, K. Raeissi, M. A. Golozar - *An investigation on the role of texture and surface morphology in the corrosion resistance of zinc electrodeposits*, Corrosion Science, 53, (2011), p. 2676–2678.

[4]. K. K. Chawla - *Composite Materials: Science and Engineering*, Springer-Verlag, New York, (1998).

[5]. D. Vasilakopoulos, M. Bouroushian, N. Spyrellis, *Electrocrystallisation of zinc from acidic sulphate baths; A nucleation and crystal growth process*, Electrochimica Acta, 54, (2009), p. 2509–2514.

[6]. M. Kubisztal, G. Haneczok, A. Chrobak, A. Kubik, J. Rasek - *Study of epoxy resin curing process by applying internal friction technique,* Materials Science and Engineering A, 521–522, (2009), p. 283–286.

[7]. F. Lionetto, R. Rizzo, V. A. M. Luprano, A. Maffezzoli - *Phase transformations during the cure of unsaturated polyester resins*, Materials Science and Engineering, A, 370, (2004), p. 284–287.

[8]. C. M. Praveen kumar, T. V. Venkatesha, K. G. Chandrappa - *Effect of surfactants on co-deposition of B4C nanoparticles in Zn matrix by electrodeposition and its corrosion behavior*, Surface and Coatings Technology, 206, (2012), p. 2249–2257.

[9]. L. Chen, L. P. Wang, Z. X. Zeng, J. Y. Zhang - *Effect of surfactant on the electrodeposition and wear resistance of Ni–Al_2O_3 composite coatings,* Materials Science and Engineering, A, 434, (2006), p. 319-325.

[10]. Alina Ciubotariu, Lidia Benea, Wolfgang Sand - *Sulphate reducing bacteria in biofilms on thermosetting polymers/zn composite layers*, The Annals of "Dunarea de Jos" University of Galati, Fascicle IX, Metallurgy And Materials Science, N^o. 1, (2011), p. 51-57.

[11]. M. S. Bhatnagar - *Epoxy resins (overview),* The Polymeric Materials Encyclopedia, (1996), CRC Press, Inc.

[12]. M. Stern, A. Geary - *Electrochemical Polarization I. A Theoretical Analysis of the Shape of Polarization Curves*, Journal Electrochemical Society, 104, (1957), 56–63.

[13]. Alina Ciubotariu, Lidia Benea, Olga Mitoşeriu, Pierre Ponthiaux, François Wenger, *Morphological aspects and corrosion behaviour of phenol formaldehyde/Zn composite coatings,* The Annals of "Dunarea de Jos" University of Galati, Fascicle IX, Metallurgy And Materials Science, N^o. 2, (2009), p. 31 – 36.

[14]. Olga Mitoşeriu, Alina Ciubotariu, Lidia Benea, Pierre Ponthiaux, Francois Wenger - *Electrodeposition obtaining and corrosion behaviour of phenol formaldehyde resin / zinc composite coatings*, The Annals of "Dunarea de Jos" University of Galati, Fascicle IX, Metallurgy And Materials Science, N^o. 2, (2008), p. 97 – 102.

THE ANNALS OF "DUNAREA DE JOS" UNIVERSITY OF GALATI.
FASCICLE IX. METALLURGY AND MATERIALS SCIENCE
N^0. 4 – 2013, ISSN 1453 – 083X

ELECTROCHEMICAL MODIFICATIONS OF TITANIUM AND TITANIUM ALLOYS SURFACE FOR BIOMEDICAL APPLICATIONS – A REVIEW

Eliza MARDARE, Lidia BENEA*, Iulian BOUNEGRU
Dunarea de Jos University of Galati, Faculty of Materials Science and Environment,
Competences Center: Interfaces-Tribocorrosion-Electrochemical Systems (CC-ITES),
47, Domneasca Street, RO-800008 Galati, Romania.
*Corresponding author:
email: Lidia.Benea@ugal.ro

ABSTRACT

The field of biomaterials requires the input of knowledge from very different areas such as biology, medicine and engineering so that the implanted material in a living body to not induce any adverse impacts. The paper focuses its attention mainly on titanium and titanium alloys, even though there are biomaterials manufactured from other metals, ceramics, polymers and composite materials. Both electrodeposition and anodic oxidation surface modification methods are discussed with several examples and a brief description of underlying theory, in order to improve the mechanical, chemical and biological properties of these materials.

KEYWORDS: titanium, titanium alloys, electrodeposition, anodic oxidation

1. Introduction

A biomaterial can be defined as any substance or combination of substances synthetic or biological in origin, used in the treatment of disease or lesion, to resolve pathology that cannot be straightened either by the natural healing process or conventional surgical intervention, using a multidisciplinary approach that requires involvement of science such as biology, medicine, and engineering. Biological biomaterials can be classified into soft (skin, tendon) and hard (bone, dentine) tissue types. In the case of synthetic biomaterials, it is further classified into: metallic, polymeric, ceramic and composite [1-2]. The fundamental requirement of a biomaterial is that the material and the tissue environment of the body should coexist without having any undesirable or inappropriate effect on each other. The implanted material should not induce any adverse impacts like allergy, inflammation and toxicity either immediately after surgery or under post operative circumstances [3].

The necessity for biomaterials stems from an inability to treat many diseases, injuries and conditions with other therapies or procedures and biomaterials serve to replacement of body part that has lost function, correct abnormalities improve function and assist in healing. The most important medical applications for biomaterials include orthopedic applications, dental implants, cardiovascular applications, skin repair devices, contact lenses, cochlear replacements, bone plates, bone cement, heart valves, artificial ligaments and tendons.

Metallic biomaterials represent the most highly used class of biomaterials and generally have attributes over other biomaterials in terms of strength, stiffness, toughness, impact resistance, and good processability [4]. The demand for metallic biomaterials is greatly increasing because of aging populations worldwide at a rapid rate and growing demand for a higher quality of life [5].

2. The most essential properties of a metallic biomaterial

In order to be used successfully, metallic biomaterials must have special properties that can be afforded to fulfill the requirements for their intended function, such as mechanical properties, biocompatibility, corrosion resistance, high fatigue and wear resistance. However, depending on the application, differing requirements may appear. Sometimes these requirements can be completely reverse.

2.1. Mechanical properties

Mechanical properties of a biomaterial must be adjusted to its intended applications otherwise the

implant is likely to fail. The mechanical properties such as hardness, tensile strength, modulus, elongation (strain), fracture resistance and fatigue strength or life play an important role in material selection for application in the human body [6].

The most common metals and metals alloys used for implants are fabricated from stainless steel, cobalt alloy and titanium and until nowadays have been used successfully [4-5]. These materials have the requisite strength characteristics but typically have not been resilient or flexible enough to form an optimum implant material. Also many alloys contain elements such as aluminum, vanadium, cobalt, nickel, molybdenum, and chromium which recent studies have suggested might have some long term adverse affects on human patients. Strength of materials from which the implants are made has an influence on them, so that inadequate strength can cause fractures the implant. When the bone implant interface starts to fail, develops at the interface a soft fibrous tissue by releasing tiny particles of the implant and causes pain to the patient [5, 7]. For major applications such as total joint replacement a low Young's modulus equivalent to that of human bone is basically essential in order to prevent bone absorption [8]. These metals typically used for traditional implants have elastic modules much higher than that of bone, for example, cortical bone has a modulus between 15 and 30 GPa depending on the type of the bone and measurement direction – while 316 stainless steel has an elastic modulus of about 190 GPa and that of cast heat-treated Co-Cr-Mo alloy is about 210 GPa. Of these the alloy with the lowest elastic modulus is Ti-6Al-4V with an elastic modulus of about 110 GPa [9-10].

Fatigue strength is defined as the highest periodic stress that does not initiate a failure of the material after a given number of cycles. Metal alloys are used for load bearing applications and must have sufficient fatigue strength to endure the rigors of daily activity (walking, chewing etc). The comparison of mechanical properties of metallic biomaterials with bone is given in table 1 [11].

Table 1. *Comparison of mechanical properties of metallic biomaterials with bone*[*]

Material/ Parameter	Stainless steel	Co-Cr alloy	Pure Ti	Ti-6Al-4V	Cortical bone
Elastic modulus (GPa)	190	210-253	110	116	15-30
Yield Strength (GPa)	221-1213	448-1606	485	896-1034	30-70
Tensile Strength (MPa)	586-1351	655-1896	760	965-1103	70-150
Fatigue Limit (MPa)	241-820	207-950	300	620	-
Density (g/cm^3)	7.9	8.4-9.2	4.5	4.5	-
Elongation (%)	12-40	5-30	15-24	10	1-2

**Adapted from J.B. Brunski. Metals, pp. 37–50 in B.D. Ratner, A.S. Hoffman, F.J. Shoen, and J.E. Lemons (eds.), Biomaterials Science: An Introduction to Materials in Medicine, Academic Press, San Diego (1996).*

2.2. Biocompatibility

There are several characteristics which influence implant biocompatibility. The first is that they should not be toxic to cells. Toxicology deals with the substances that migrate out of biomaterials. It is convenient to say that a biomaterial should not give off anything from its mass unless specifically designed to do so. If a medical implant is fixed and it kills the surrounding cells, this would clearly cause difficulties for the patient. After a certain period the pain becomes insupportable and the implant must be substituted, a method that is called as a revision [7].

Another important factor is the compatibility of synthetic materials with blood and tissue. Interactions at the tissue-material interface may determine whether a material is tissue compatible and can coexist with the physiological environment. A common problem with medical implants is rejection, because every biomaterial has the potential to induce biological dysfunctions such as inflammation and infection in the surrounding tissues after implantation [12]. The immune system identifies the substances from the implant as foreign and attempts to fight them and to remove them and so consequently the foreign materials to be extruded or walled off, in case they can not be removed from the body. The degree of the tissue responses varies according to both physical and chemical nature of the implants. Pure metals tend to evoke a severe tissue reaction, due to the high-energy state or large free energy of them, which tends to lower the metal's free energy by oxidation or corrosion.

2.3. Corrosion

Corrosion, the graded degradation of materials by electrochemical attack, is of concern particularly when metallic biomaterials are placed in the hostile electrolytic environment provided by the human body. The body environment is very aggressive and contains water, complex organic compounds, dissolved

oxygen, proteins, and ions such as hydroxide, sodium and chloride, small amounts of potassium, calcium, magnesium, phosphate, sulphate and amino acids [13-14]. These ions react electrochemically with the surface of metallic biomaterials to cause corrosion. The metallic components of the alloy are oxidized to their ionic forms and the dissolved oxygen is reduced to hydroxyl ions. During corrosion process, the total rates of oxidation and reduction reactions that are termed as electron production and electron consumption respectively, must be equal [13]. The corrosion of biomaterials depends on geometric, metallurgical, mechanical and solution chemistry parameters [15]. The nature of the passive oxide films formed, and the mechanical properties of the materials form some of the essential criteria for selection of alternative or development of new materials.

Resistance to corrosion is extremely important for a metallic material because corrosion can lead to rough surface, lower recovery, and release of elements from the metal or alloy. Release of elements can produce discoloration of adjacent soft tissues and allergic reactions in patients [16]. Corrosion products may be involved in causing local pain, tissue reactions and tumefactions in the region of the implant, in the lack of infection [17].

2.4. Wear properties

Wear properties of an implant material are important, especially for various joint replacements because wear of artificial joints releases particles into the body. Wear cannot be discussed without some understanding of friction between two materials. When metallic implant is subjected to wear, the passive layer can be removed allowing active corrosion to occur while the alloy is repassivates [18]. A fatigue wear process involving fretting causes the generation of wear debris which can produce acute host–tissue reactions and tend to aggravate the fatigue problems of the biomaterial by producing enzymes and chemicals (including fast multiplication of local fibroblast-like cells and activated macrophages) that are highly corrosive and finally implant loosening, a major cause of joint implant failure [19].

2.5. Tribocorrosion synergism

Tribocorrosion is a material degradation process which results from simultaneous mechanical (wear) and chemical or electrochemical (corrosion) effects [20]. It is well known in tribology that a corrosive environment can accelerate the wear rate [20-21]. The results obtained are not just a simply summation of the electrochemical and mechanical effects but represents a complex synergy between wear and corrosion [22]. Tribocorrosion behavior cannot be predicted from wear and corrosion taken separately [23]. If for the titanium and its alloys have been conducted and reported several results on their tribocorrosion behavior, the literature reveals the need for more robust testing techniques, in particular the need for analyze the tribocorrosion behavior of the coatings on their surfaces [24-27].

2.6. Osseointegration

Osseointegration is a recently introduced term that indicates a direct biochemical bond between a non-natural substance and a bony tissue [28]. Osseointegration has made possible the development of a number of clinical applications in the field of hand surgery and orthopedics: finger joint prostheses, thumb amputations, amputation of lower limb etc.

The initial observations of osseointegration were made in the 1952 by Professor Per-Ingva Brånemark of Sweden, in an experiment where embedded titanium device into rabbits' leg bones to study bone healing. At the conclusion of the experiment, after a few months he tried to remove these titanium devices and when he discovered that the bone had integrated so completely with the implant that could not be removed [29-30]. Since Branemark made first observations, osseointegration has been intensively studied and the research is ongoing. Osseointegration is a promising technique for providing function and quality of life.

3. Metallic implant materials

Metallic biomaterials are the most suitable for replacing failed hard tissue up to now. Metals and alloys have been widely used in various forms as implants materials in the medical and dental fields such as devices for bone fixation, partial and total joint replacement, external splints, and traction apparatus as well as dental amalgams, crowns, bridges, and dentures, which provide biocompatibility, the required mechanical strength, high corrosion and wear resistance. The commonly used metallic biomaterials are stainless steels, Co-based alloys, and titanium and its alloys.

3.1. The austenitic stainless steels

The austenitic stainless steels – especially types 304, 316 and 316L – are used for implants fabrication because of a favorable combination of mechanical properties, good corrosion resistance, low cost, availability and easy processing when compared to other metallic implant materials [4-5]. The austenitic class of stainless steels is nonmagnetic and offers the most resistance to corrosion in the stainless group, owing to its substantial nickel 8% content and higher levels of chromium 18%.

Types 316 and 316L stainless steels exhibit better corrosion resistance than type 304 or good elevated temperature strength. The "L" grades are

used to provide extra corrosion resistance after welding. The only difference in composition between 316 and 316L stainless steel is the amount of carbon that is in the material, 316 has 0.08% maximum carbon content while 316L has a 0.03% maximum carbon content. The carbon is kept to 0.03% or under to avoid carbide precipitation. Carbon in steel when heated to temperatures in what is called the critical range (800 degrees F to 1600 degrees F) precipitates out, combines with the chromium and gathers on the grain boundaries. This deprives the steel of the chromium in solution and promotes corrosion adjacent to the grain boundaries. By controlling the amount of carbon, this is minimized.

Chromium is alloying element that is the essential stainless steel material for conferring corrosion resistance. Chromium has a great affinity for oxygen which allows the formation of a strongly adherent, self-healing and corrosion resistant film of chromium oxide on the surface of the steel Cr_2O_3, film that is too thin to be visible, and the metal remains lustrous [4,7,31]. A film that naturally forms on the surface of stainless steel self-repairs in the presence of oxygen if the steel is damaged mechanically or chemically, and thus prevents corrosion from occurring. Molybdenum in the presence of chromium enhances the corrosion resistance of stainless steel. The inclusion of molybdenum enhances resistance to pitting corrosion in salt water. Nickel is another alloying element used as a raw material for certain classes of stainless steel. Nickel provides high degrees of ductility (ability to change shape without fracture) as well as resistance to corrosion. The presence of nickel improves considerably the corrosion resistance when compared to the martensitic and ferritic grades. Surgical implant application for stainless steel include: wire for surgical sutures, fractures plates, pins, screws hip nails and neurosurgical and microvascular clips [12]. Thus, stainless steels are suitable to use only in temporary implant devices because its fatigue strength that is less than other alloys. The wear resistance of austenitic stainless steel is relatively poor and therefore their use in orthopaedic joint prosthesis as metal-on-metal is limited because of high friction and large number of wear debris particles that occurring, resulting rapid loss of the implant [31].

In order to improve corrosion resistance, wear resistance and fatigue strength of these group of stainless steel, can be used surface modification methods such as anodization, passivation, hard coatings, bioceramics, ion-implantation, biomimetic coatings and glow-discharge.

3.2. Co-base alloys

Co-base alloys are generally used in applications which require wear resistance, corrosion resistance and/or thermal resistance. There are basically two types: one is the castable Co-Cr-Mo alloy, which usually has been used for many decades in dentistry and recently, in making joints, and the other is the wrought Co-Ni-Cr-Mo alloy which is a reletive newcomer now used for making the stems of prostheses for heavily loaded joints such as the knee and hip [4, 7].

Co-Cr alloys have an excellent corrosion resistance (better than that of stainless steel), which is provided by a thin adherent layer and passive of chromium-based oxides with additions of Mo on the surface even in chloride environments [7, 31-33]. Ly et al. [34] in their study they report the identification of different Cr and Co species in the passive films formed under different potentiostatic conditions, which play important roles in alloy passivation. Furthermore, they found that Mo is only present in the oxide layer if the film is air formed, but that it readily dissolves upon exposure to the solution [35]. The dissolution rate of Mo was too low to be measured, indicating that the passive film protected further oxidation of underlying Mo in the alloy [34, 36].

The modulus of elasticity for the Co-Cr alloys does not change with the changes in their ultimate tensile strength. These materials have a high elastic modulus (200–220GPa) higher to that of stainless steel (approx. 200GPa), and an order of magnitude higher than that of cortical bone (20–30GPa) [4, 7, 32]. This may have some implications of different load transfer modes to the bone in artificial joint replacements, on contact with bone, the metallic devices will take most of the load due to their high modulus, producing stress shielding in the adjacent bone. The lack of mechanical stimuli on the bone may induce its resorption that will lead to the eventual failure and loosening of the implant [31, 37].

Carbon additions between 0.1 and 0.3 wt% have been shown to favor the formation of carbides which increase wear resistance.

The Co-Ni-Cr-Mo alloy has a high degree of corrosion resistance to seawater under stress than Co-based alloys. The superior fatigue and ultimate tensile strength of the Co-Ni-Cr-Mo alloy make it very suitable for applications that require a long service life without fracture or stress fatigue.

3.3. Titanium and its alloys

Titanium and its alloys are used extensively for implant materials in the medical and dental fields, and offer many advantages such as superior biocompatibility, corrosion resistance, specific strength, relatively low modulus and strong osseointegration tendency compared with other metallic implant materials [38-39]. Among various titanium alloys, pure titanium and Ti-6Al-4V alloy have been and are still most widely used for biomedical applications.

These groups of alloys, as those mentioned above are mainly used for substituting materials for hard tissues.

The greater *corrosion resistance* for titanium and its alloys derives from the spontaneous formation of a titanium oxide film on their surface as long as oxygen is present, its thickness has been evaluated to be approximately 5 nm and which possesses a low level of electronic conductivity [40-44]. This natural oxide layer for commercially pure titanium is composed of titanium oxide in different oxidation states (mainly consists of TiO_2, Ti_2O_3 and TiO), while for the alloys, aluminum, niobium, molybdenum or vanadium are additionally present in oxidized form (Al_2O_3, Nb_2O_5, MoO_2, MoO_3 or V-oxides) oxides which are thermodynamically stable at physiological pH values. The stable oxides are very insoluble in biological fluids and this lead to the excellent localized biocompatibility observed for these classes of alloys [42, 45]. This film acts as an electrochemically passive film and inhibits negative ions from invading the matrix of the titanium or its alloys and in this way prevents the ion release or dissolution of titanium and alloyed elements into the body fluids. This high corrosion resistance of titanium alloys can be strongly decreased by damage of the passive film when the bending stress is loaded on the sample, even if the sample itself is not fractured [5, 38, 40].

The *modulus of elasticity* of these materials is about 100-110GPa, which is half the value of Co-based alloy and is known that a lowest Young's modulus is favorable for homogeneous stress transfer between implant and bone and it was proved that an implanted Ti reduced biomechanical tissue problems, and the fatigue fracture rate following continuous physiological load-bearing is also far lower than it is with other known metals [12]. Niinomi [8] in his study reported that the level of Young's modulus is effective in inhibiting bone absorption after implantation and on the other hand a lowest Young's modulus, even similar to that of bone present some disadvantages because causes large amounts of shear motion between stem and bone, leading to the formation of fibrous tissue and finally failure.

Strong osseointegration tendency. After implantation, the oxygen atoms in the body fluid naturally react with Ti atoms and form the oxidized layer of titanium oxide (TiO_2), and the newly formed and fully mineralized bone is deposited directly upon the metal surface without any interposition [12].

4. Structure, properties and applications of titanium and Ti-6Al-4V titanium alloy

Depending on their microstructure after processing, titanium alloys may be classified into one of five classes: α, near-α, α+β, metastable β or stable β [46].

Alloying elements in Ti are classified into α, β and neutrals stabilizers on the basis of their effects on the α/β transformation temperature or on their differing solubility's in the α or β phases. Pure titanium exists in form of α-phase at temperatures above 882.5^{o}C and in form of β-phase at temperature below 882.5^{o}C [47]. The temperature of allotropic transformation of α-titanium to β-titanium is called Beta Transus Temperature. The α-stabilizing elements extend the α phase field to higher temperatures, while β-stabilizing elements shift the β phase field to lower temperatures. Neutral elements have only minor influence on the β-transus temperature. In crystallographic form of α-titanium atoms are arranged in hexagonal close packed structure (hcp), and in β-titanium atoms are arranged in body centered cubic structure (bcc) [9, 46].

The substitutional element Al and the interstitial elements O, N, and C are all strong α stabilizers and increase the transus temperature with increasing solute content. Among the α stabilizers, aluminum is far the most important alloying element of titanium, because it is the only common metal raising the transition temperature and having large solubilities in both α and β phases. Other α stabilizers include B, Ga, Ge, and the rare earth elements but their solid solubilities are much lower as compared to Al or O and none of these elements is used commonly as an alloying element. The β stabilizing elements are divided into β isomorphous elements (V, Mo, Nb, Ta, Re) and β eutectoid forming elements (Cr, Fe, Si, Ni, Cu, Mn, W, Pd, Bi) depending on the details of the resulting binary phase diagrams. Sufficient concentrations of V, Mo, and Nb elements make it possible to stabilize the β phase at room temperature. The elements Zr and Sn that are found in some Ti alloys are considered to be 'neutral' alloying elements [46].

The α and near-α titanium alloys exhibit superior corrosion resistance but have limited low temperature strength. The β alloys also offer the unique characteristic of low elastic modulus and superior corrosion resistance. The alloys belonging to the α+β system contain one or more α stabilizing element with one or more β stabilizing element. These alloys retain more β phase after solution treatment than do near-α alloys, the specific amont depending on the quantity of β stabilizers present and on heat treatment.

The alpha-beta alloys, when properly treated have an excellent combination of higher strength, ductility and good hot formability. They are stronger than the alpha or the beta alloys due to the presence of both the α and β phases.

Ti-6Al-4V is one of the most widely used

titanium alloys for biomedical application and in generally is used in the (α+β)-annealed condition. Its total production is about half of all Ti alloys. It is an alpha-beta type containing 6 wt% Al and 4 wt% V. Aluminum is added to the alloys as α-phase stabilizer and hardener due its solution strengthening effect. Vanadium stabilizes ductile β-phase, providing hot workability of the alloy [47].

Applications of Ti-6Al-4V. Titanium is one material which receives equal attentions and interest from both the engineering and medical/dental fields. Because of their lightweight, high specific strength, low modulus of elasticity, and excellent corrosion resistance, titanium materials (both unalloyed and alloyed) have become important materials for the aerospace industry, automotive, surgery and medicine, chemical plant, power generation, oil and gas extraction, sports, and other major industries.

In aerospace industry since the early 1950s, was initially used for compressor blades in gas turbine engines. Today, wrought Ti-6Al-4V is used extensively for turbine engine and air frame applications. Engine components include blades, discs, and wheels. Ti-6Al-4V is used in a variety of airframe applications, including cargo – handling equipment, flow diverters, torque tubes for brakes, and helicopter rotor hubs. In missile and space applications, they are used for wings, missile bodies, optical sensor housings, and ordnance. Also, Ti-6Al-4V castings are used to attach the main external fuel tanks to the Space Shuttle and the boosters to the external tanks.

In the automotive industry, wrought Ti-6Al-4V is used in special applications in high – performance and racing cars where is critical, usually in reciprocating and rotating parts, such as valves, valve springs, connecting rods, and rocker arms. It also has been used for drive shafts and suspension springs. Marine applications of wrought Ti-6Al-4V include armaments, sonar equipment, deep – submergence applications, hydrofoils, and capsules for telephone – cable repeater stations. Casting applications include water – jet inducers for hydrofoil propulsion and seawater ball valves for nuclear submarines.

Major medical applications of this alloy are: dental applications, orthopedic applications, cardiovascular applications, cochlear implant, implantable cardiovascular devices, extracorporeal artificial organs, biomedical sensor and biosensors, bioelectodes – electrical stimulation and diagnostic devices.

The popularity of titanium and its alloys in surgical implants fields can be recognized by counting the manuscripts published in literature reports. Thousands of experimental reports have addressed the excellent biocompatibility of titanium and titanium alloy.

5. Surface modification of Ti-6Al-4V for biomedical applications by electrochemical methods

Surface engineering can play a significant role in extending the performance of medical devices made of titanium and its alloys. Surface properties such composition, roughness and topography are the most important factors that depend on cellular interactions on surface engineering [48]. Surface modification is a process that changes a material's surface composition, structure, and morphology, leaving the mechanical properties intact [49].

Titanium and titanium alloys can not meet all of the clinical requirements because of its poor tribological properties such as poor wear resistance and a high co-efficient of friction which can cause problems [50]. In addition, it is dangerous for Ti-6Al-4V to stay in the human body for a long time because undergoes electrochemical exchange releasing metallic ions in the physiological environment and is known that aluminum element has strong neurotoxicity and vanadium is a strong cytotoxin, and over time, the alloy produced adverse reactions in the body tissues. The release of these elements, even in small amounts, may cause local irritation of the tissues surrounding the implant and sometimes can cause the implant failure [51-53]. Therefore, implants of titanium and titanium alloys are not used without some type of surface modification designed to provide a greater wear resistance and to add biofunction, because biofunction cannot be added during manufacturing processes [49]. Various surface modifications have been used for improving the wear, corrosion behaviour and bioactivity of Ti alloys.

The surface modification recently becomes active in the field of implants. In the biomedical domain, coatings have been used to modify the surface of implants, and sometimes to create an entirely new surface which gives the implant properties which are quite different from the uncoated device.

There are a number of methods reported in the literature to modify titanium and titanium alloys for biomedical implants such thermal oxidation [54-56], plasma spraying [57-59], sol–gel method [60-62], biomimetic deposition [63-65], anodic oxidation [66-68], electrophoresis deposition [69-70] and electrochemical deposition [71-74].

5.1. Electrodeposition

Among these techniques which have been developed to deposit bioactive film on titanium and its alloys used for surface modification electrodeposition offers a number of combined advantages such as availability and inexpensive equipment, simple

process, rigid control of coatings thickness, complex shapes and low process temperature [71-72, 74]. Electrodeposition parameters include bath composition, pH, temperature, overpotential, additives type, etc., while important microstructural features of the substrate are grain size, crystallographic texture, dislocation, density, and internal stress [75].

In order to prevent adverse tissue reactions resulting from hard tissue replacements, a bioinert material, which is stable in the human body and is immune at the interaction with body fluids and tissues, is preferred. Some bioactive materials, such as hydroxyapatite, bioactive glasses and glass ceramics are increasingly used as hard tissue replacements due to their ability to induce bone regeneration and bone in growth at the tissue–implant interface without the intermediate fibrous tissue layer by creating a bone-like apatite layer on their surface after implantation. Apatite formation is currently believed to be the main demand for the bone-bonding ability of materials [46, 76].

Hydroxyapatite $Ca_{10}(PO_4)_6(OH)_2$ (HA) is one of the first materials considered for coating metallic implants due to its close similarity of chemical composition and high biocompatibility with natural bone tissue [71-72]. Calcium phosphates are present in bone, teeth and tendons to give these organs stability, hardness, and function [77]. Hydroxyapatite has been widely used for many years as a coating material on titanium and titanium alloys as implant devices in dental and orthopedic fields, and the most important reason for that was selected is its ability to accelerate bone in growth onto the surface of implant during the early stages after implantation.

Table 2. *Various compositions of electrolytes used for electrodeposition of calcium phosphates*

Composition	**pH**	**Ref**
- 1.46 M $CaCl_2$ - 0.87 M NaH_2PO_4	3.89	[71]
- 0.1 M $Ca(NO_3)_2$ - 0.06 M $NH_4H_2PO_4$ - H_2O_2 10 mL/L	4.3	[79]
- 0.042 mol/L $Ca(NO_3)_2$ - 0.025 mol/L $(NH_4)_2HPO_4$	4.4 adjusted by dilute HNO_3 and NH_4OH	[80]
- 0.042 M $Ca_2(NO_3)_2$ x $4H_2O$ - 0.125 M $NH_4(H_2PO_4)$	4.4	[81]
- 0.04 mol/L $Ca(NO_3)_2$ - 0.027 mol/L $(NH_4)_2HPO_4$ - 0.1 mol/L $NaNO_3$	4.5	[82]
- 0.021 M $CaCl_2$ - 0.0225 M $NH_4H_2PO_4$	4.5	[83]
- 0.61 mM $Ca(NO_3)_2$ - 0.36 mM $NH_4H_2PO_4$	6	[84]
- 137.8 mmol/L NaCl - 1.7 mmol/L K_2HPO_4 x $3H_2O$ - 2.5 mmol/L $CaCl_2$	7.2 Adjusted with tris-hydroxymethylaminomethane $[(CH_2OH)_3CNH_2]$ and hydrochloric acid	[85]
- 1.67 mM phosphate containing salt, in the form of either $NH_4H_2PO_4$ or K_2HPO_4 - 2.5 mM calcium containing salt in the form of either $CaCl_2$ or $Ca(NO_3)_2$	7.2 by addition of tris(hydroxyl aminomethane), (hereafter referred as Tris) and hydrochloric acid	[72]

There are a number of additional benefits with this coating: faster adaptation of implant and surrounding tissue with reduced healing time, firmer implant bone attachment and the reduction of metallic ion release.

Several compositions of solutions indicated in Table 2, have been used as electrolytes in order to coat calcium phosphates using the electrodeposition method: acidic solution (pH≤4); basic solution (pH>9) and nearly neutral modified simulated body fluid (SBF) (pH=7.2–7.6) [78].Today electrodeposition is much more than just a coatings technology. Recent literature on the electrodeposition of metallic and nonmetallic coatings containing nanosized particles is intensely investigated. The incorporation of nanosized particles can give an increased microhardness and corrosion resistance, modified growth to form a nanocrystalline deposit and a shift in the reduction potential of a metal ion [75].

Due to the rapid development of nanotechnology, the potential of nano-calcium phosphates has received considerable attention. Recent developments in biomineralization and biomaterials have demonstrated that nano-calcium phosphate particles play an important role in the formation of hard tissues [77]. Literature reports indicate that cumulative adsorption of proteins from body fluids is significantly higher on smaller nanometer grain size materials compared with conventional scale size [77].

In the past decades extensive research on hydroxyapatite coated implants have focused on the tissue–implant interface and also on the problems associated with the coating process and optimization of coating parameters to enhance tissue response [76]. Hydroxyapatite coating of Ti substrate by electrodeposition has been investigated by many research groups [69, 72, 86-87]. Electrochemical deposition of hydroxyapatite coating on titanium surface is an attractive process because irregular surfaces (porous, complex shape of substrate) can be coated relatively quickly at low temperatures and therefore unwanted phase changes could be avoided [72, 82]. Additionally, the thickness, chemical composition and microstructure of the deposit can be well controlled through adequate parameters of the electrodeposition process. Several recent studies have focused on the introduction of intermediate layers, as examples of controlled anodic TiO_2 film, between bioactive HA coating and metal substrate.

5.2. Anodic oxidation

Electrochemical anodizing is one of the simplest among the different techniques employed to form rough, porous and uniform films (generally oxide/hydroxide combination) across which oxygen ions can diffuse and oxidize the substrate, increasing the thickness of the film and in this way decreases ion release, modify and enhances the in vitro corrosion resistance and biocompatibility of Ti and its alloys [88]. Recently, anodic oxidation has become an attractive method for preparing oxide films on titanium, because the porous oxide films insure apatite formation in physiological environment in order to improve implant bioactivity for biomedical applications [66, 88-90]. It is generally accepted that rough and porous surfaces have a more pronounced and beneficial influence on cellular activity than smooth ones [68]. Porous implants layer have lower density than respective bulk and good mechanical strength is provided by bulk substrate [91].

Electrochemical anodic oxidation is an electrochemical process, which after application of direct-current voltages to electrodes immersed in electrolyte leads to oxidation of metal anode that forms a solid oxide layer on the surface [92]. The type, concentration and pH of electrolyte solution as well as the electrochemical parameters such as the applied current density, the voltage, the time of oxidation can affect the surface morphology, the chemical composition and the crystalline structure of the oxide films formed by anodic oxidation [93-95].

The electrolytes most commonly used to anodize Ti and its alloys are sulphuric and phosphoric acids at different degrees of dilution and Ca-P based solutions [93,96]. An important condition which the electrolyte solution must meet is that should not chemically attack the growth of oxide, to prevent its dissolution during the anodization process, or at least it should be guarantee that the oxide growth percentage is higher than the dissolution one [93]. The rate of anodic film formation is much higher than its dissolution rate in acidic electrolytes like sulfuric acid, acetic acid, and phosphoric acid compared to alkaline electrolytes [97-98].

The electrical potential difference imposed between cathode and anode and the current density imposed to reach that value of potential difference can vary within a wide range of values. In fact, low potentials (1–130V) causes the formation of a smooth, amorphous oxide, about 3–300 nm thick, whose color changes as a function of thickness and, consequently, of applied voltage (interference color) [93, 99]. On the contrary high potentials (100–500V), combined with high current densities, are the parameters used in anodic spark deposition (ASD) processes, which lead to a crystalline or semi-crystalline oxide that can range from few tens to hundreds micrometers thick [93,99]. The crystal structures of the titanium oxide have revealed different oxide structures at different thickness: TiO_2 with anatase structure was observed at 90 V [91,100], mixture of anatase and rutile structure was formed at 155 V and a single rutile phase was produced at 180 V, respectively [91, 100].

The properties of anodic oxide films strongly depend on their composition, structure, and thickness. As the voltage increases, the thickness of the layer also increases and particular colors will arise at specific voltage rates. The transition from one color to another is not evident defined, but rather by nuances gradually through a limited spectrum. The apparent color transmitted to the metal is induced by interference between specific wavelengths of light reflecting off the metal and oxide coated surface [101]. Light which crosses through the oxide layer, then reflecting off of the metal, must pass farther than light reflecting directly off the surface of the oxide. If one wave type is not synchronized with the other, they will annul each other out, making that color "darker" or invisible. If through the thickness of the oxide layer is obtained a wave pattern whose path is similar to the path of a certain wavelength of light and it closely follows its path, then the wave amplitude will be increased, and this color would appear brighter. When the wave patterns cancel each other, the process it is called destructive interference, and when they match, it is constructive interference. Sometimes it is possible that the thickness of the oxide layer to create a combination of effects at the same time.

The main reactions leading to oxidation at the anode are as follows [46]:

At the Ti/Ti oxide interfaces:

$Ti \leftrightarrow Ti^{2+} + 2e^-$

At the Ti oxide/electrolyte interface:

$2H_2O \leftrightarrow 2O^{2-} + 4H^+$ (oxygen ions react with Ti to form oxide),

$2H_2O \leftrightarrow O_2$ (gas) $+ 4H^+ + 4e^-$ (O_2 gas evolves or stick at electrode surface).

At both interfaces:

$Ti^{2+} + 2O^{2-} \leftrightarrow TiO_2 + 2e^-$

The titanium and oxygen ions resulted from these redox reactions are actuated through the oxide by the externally applied electric field thus achieving the oxide film. Is know that titanium oxides obtained by anodic processes have a high resistivity relative to the electrolyte solution and the metallic components of the electrical circuit and therefore the applied voltage drop will mainly occurs across the oxide film of the anode. As long as the electric field is high enough to lead the ions through the oxide, a current will flow and the oxide will continue to grow [46].

6. Conclusions

In this review, an overview of metallic implant application especially Ti and its alloy and the need of electrochemical surface modification methods used to improve the mechanical, chemical and biological properties of these have been given. The properties of titanium and its alloys can be upgraded to some extent after their surfaces are modified by electrochemical anodic oxidation and electrodeposition of HA.

Electrodeposition of HA to the titanium substrate is of utmost importance for the implant to function properly in physiological conditions. The application and prospective use of nano-calcium phosphate in the biological repair of bone and enamel are promising work. It is suggested that nano-HA may be the ideal biomaterial due to its good biocompatibility and bone/enamel integration.

One possible solution to improve the adhesion is to form an intermediate bonding layer between the titanium substrate and the HA coating, by anodic oxidation method. As a result of this anodic treatment, the surface of the Ti substrate is much rougher and porous. In summary, researches performed until now suggested that the anodic oxidation method followed by electrodeposition of HA is an effective way to prepare bioactive titanium surfaces.

With the development of the surface engineering, more new surface modification technologies will be introduced to improve the properties of titanium and its alloys for meeting the clinical needs.

Acknowledgements

The authors gratefully acknowledge both Bilateral Research Agreement between Competences Center: Interfaces-Tribocorrosion-Electrochemical Systems (CC-ITES) from Dunarea de Jos University of Galati and Department of Metallurgy and Materials Engineering (MTM) from Katholieke Universiteit Leuven and research project CEA-IFA C2-02 / 01-03-2012.

References

[1]. G. Binyamin, B.M. Shafi, C.M. Mery - Seminars in Pediatric Surgery **15**, 276 (2006).
[2]. B.D. Ratner, S.J. Bryant - Annu. Rev. Biomed. Eng. **6**, 41 (2004).
[3]. G. Manivasagam, D. Dhinasekaran, A. Rajamanickam - Recent Patents on Corrosion Science **2**, 40 (2010).
[4]. M.B. Nasab, M.R. Hassan - Trends Biomater. Artif. Organs, **24**, 69 (2010).
[5]. K.H. Frosch, K.M. Stürmer - Eur J Trauma **32**, 149 (2006).
[6]. D.H. Kohn - Curr. Opin. Solid. State Mater. Sci. **3**, 309 (1998).
[7]. J. Alvarado, R. Maldonado, J. Marxuach, R. Otero - Mech. Mater.–**I**, INGE 4011, 1 (2003).
[8]. M. Niinomi - Journal of the Mechanical Behavior of Biomedical Materials **I**, 30 (2008).
[9]. M. Long, H.J. Rack - Biomaterials **19**, 1621 (1998).
[10]. K. Wang - Mater. Sci. Eng. A **213**, 134 (1996).
[11]. J.B. Brunski - Metals, pp. 37–50 in B.D. Ratner, A.S. Hoffman, F.J. Shoen, and J.E. Lemons (eds.) - Biomaterials Science: An Introduction to Materials in Medicine, Academic Press, San Diego (1996).
[12]. H. Suh - Yonsei Med. J. **39**, 87 (1998).
[13]. U.K. Mudali, T.M. Sridhar, B. Raj - Sadhana **28**, 601 (2003).
[14]. D.C. Hansen - The Electrochemical Society Interface 31 (2008).

[15]. J.J. Jacobs, J.L. Gilbert, R.M. Urban - J Bone Joint Surg Am. **80**, 268 (1998).
[16]. N. Adya, M. Alam, T. Ravindranath, A. Mubeen, B. Saluja - J. Indian Prosthodont. Soc. **5**, 126 (2005).
[17]. D. Sharan - Orthopaedic Update (India) **9**, 1 (1999).
[18]. M.A. Khan, R.L. Williams, D.F. Williams - Biomaterials **20**, 765 (1999).
[19]. S.H. Teoh - Int. J. Fatigue **22**, 825 (2000).
[20]. Y. Yan, A. Neville, D. Dowson, S. Williams - Tribol. Int. **39**, 1509 (2006).
[21]. J.R. Goldberga, J.L. Gilbert - Biomaterials **25**, 851 (2004).
[22]. M. Azzi, J.A. Szpunar - Biomol. Eng. **24**, 443 (2007).
[23]. D Landolt - J. Phys. D: Appl. Phys. **39**, 3121 (2006).
[24]. S. Barril, S. Mischler, D. Landolt - Wear **256**, 963 (2004).
[25]. J. Komotori, N. Hisamori, Y. Ohmori - Wear **263**, 412 (2007).
[26]. H. Ding, Z. Dai, F. Zhou, G. Zhou - Wear **263**, 117 (2007).
[27]. S. Kumar, B. Sivakumar, T.S.N.S. Narayanan, S.G.S. Raman, S.K. Seshadri - Wear **268**, 1537 (2010).
[28]. T. Albrektsson, C. Johansson - Eur. Spine. J. **10**, 96 (2001).
[29]. R. Brånemark, P.I. Brånemark, B. Rydevik, R.R. Myers - J. Rehabil. Res. Dev. **38**, 175 (2001).
[30]. R. Dimitriou, G.C. Babis - J Musculoskelet Neuronal Interact **7**, 253 (2007).
[31]. M. Navarro, A. Michiardi, O. Castaño, J.A Planell - J. R. Soc. Interface **5**, 1137 (2008).
[32]. J.J. Ramsden, D.M. Allen, D.J. Stephenson, J.R. Alcock, G.N. Peggs, G. Fuller, G. Goch - Annals of the CIRP **56**, 687 (2007).
[33]. R. Zupančič, A. Legat, N. Funduk - Mater. Tehnol. **41**, 295 (2007).
[34]. Y.S. Li, K. Wang, P. He, B.X. Huang, P. Kovacs - J. Raman. Spectrosc. **30**, 97 (1999).
[35]. A.W.E. Hodgson, S. Kurz, S. Virtanen, V. Fervel, C.-O.A. Olsson, S. Mischler - Electrochim. Acta **49**, 2167 (2004).
[36]. I. Milošev, H.-H. Strehblow - Electrochim. Acta **48**, 2767 (2003).
[37]. R. Huiskes, H. Weinans, B. Van Rietbergen - Clin. Orthop. Relat. Res. **274**, 124 (1992).
[38]. M.Niinomi - Mat. Sci. Eng. A **243**, 231 (1998).
[39]. M. Niinomi - Metall. Mater. Trans. A **33**, 477 (2002).
[40]. M. Masmoudi, M. Assoul, M. Wery, R. Abdelhedi, F. El Halouani, G. Monteil - Appl. Surf. Sci. **253**, 2237 (2006).
[41]. R. Chiesa, E. Sandrini, M. Santin, G. Rondelli, A. Cigada - J. Appl. Biomater. Biomech. **1**, 91 (2003).
[42]. C. Sittig, M. Textor, N.D. Spencer, M. Wieland, P.-H. Vallotton - J. Mater. Sci. – Mater. M. **10**, 35 (1999).
[43]. C. Fonseca, M.A. Barbosa - Corros. Sci. **43**, 547 (2001).
[44]. Y. Yang, N. Oh, Y. Liu, W. Chen, S. Oh, M. Appleford, S. Kim, K. Kim, S. Park, J. Bumgardner, W. Haggard, J. Ong - Journal of the Minerals, Metals and Materials Society **58**, 71 (2006).
[45]. J.A. Disegi - Injury, Int. J. Care Injured **31**, 14 (2000).
[46]. X. Liu, P.K. Chu, C. Ding - Mater. Sci. Eng. R **47**, 49 (2004).
[47]. C.E.B. Marino, S.R. Biaggio, R.C. Rocha-Filho, N. Bocchi - Electrochim. Acta. **51**, 6580 (2006).
[48]. M. Geetha, A.K. Singh, R. Asokamani, A.K. Gogia - Prog. Mater. Sci. **54**, 397 (2009).
[49]. T. Hanawa - Japanese Dental Science Review, **46**, 93 (2010).
[50]. K. Niespodziana, K. Jurczyk, M. Jurczyk - Rev. Adv. Mater. Sci. **18**, 236 (2008).
[51]. Boon Sing Ng, I. Annergren, A.M. Soutar, K.A. Khor, A.E.W. Jarfors - Biomaterials **26**, 1087 (2005).
[52]. Y. Okazakia, E. Gotoh - Biomaterials **26,** 11 (2005).
[53]. Y. Li, C. Wong, J. Xiong, P. Hodgson, C. Wen - J. Dent. Res. **89**, 493 (2010).
[54]. P.A. Dearnley, K.L. Dahm, H. Çimenoğlu - Wear **256**, 469 (2004).
[55]. S. Kumar, T.S.N.S. Narayanan, S.G.S. Raman, S.K. Seshadri - Mater. Chem. Phys. **119**, 337 (2010).
[56]. S. Kumar, T.S.N.S. Narayanan, S.G.S. Raman, S.K. Seshadri - Mater. Sci. Eng. C **30**, 921 (2010).
[57]. S. Yang, H.C. Man, W. Xing, X. Zheng - Surf. Coat. Tech. **203**, 3116 (2009).
[58]. H. Wang, N. Eliaz, Z. Xiang, H.-P. Hsuc, M. Spector, L.W. Hobbs - Biomaterials **27**, 4192 (2006).
[59]. C.H. Hager Jr., J.H. Sanders, S. Sharma - Wear **265**, 439 (2008).
[60]. L. Gan, J. Wang, R.M. Pilliar - Biomaterials **26**, 189 (2005).
[61]. D. Wang, C. Chen, T. He, T. Lei - J. Mater. Sci.-Mater. M. **19**, 2281 (2008).
[62]. Y.-M. Lim, K-S. Hwang, Y-J. Park - J. Sol-Gel Sci. Techn. **21**, 123 (2001).
[63]. Q. Zhang, Y. Leng, R. Xin - Biomaterials **26**, 2857 (2005).
[64]. J. Wang, P. Layrolle, M. Stigter, K. de Groot - Biomaterials **25**, 583 (2004).
[65]. F. Barrère, P. Layrolle, C.A. van Blitterswijk, K. de Groot - J. Mater. Sci.-Mater. M. **12**, 529 (2001).
[66]. X. Cui, H.-M. Kim, M. Kawashita, L. Wang, T. Xiong, T. Kokubo, T. Nakamura - Dent. Mater. **25**, 80 (2009).
[67]. R. Narayanan, P. Mukherjee, S.K. Seshadri - J. Mater. Sci.-Mater. M. **18**, 779 (2007).
[68]. F. Variola, J.-H. Yi, L. Richert, J.D. Wuest, F. Rosei, A. Nanci - Biomaterials **29**, 1285 (2008).
[69]. I. Zhitomirsky, L. Gal-Or - J. Mater. Sci.-Mater. M. **8**, 213 (1997).
[70]. M. Wei, A.J. Ruys, B.K. Milthorpe, C.C. Sorrell, J.H. Evans - J. Sol-Gel Sci. Techn. **21**, 39 (2001).
[71]. A. Raknga rm, Y. Mutoh - Mater. Sci. Eng. C **29**, 275 (2009).
[72]. A. Kar, K.S. Raja, M. Misra - Surf. Coat. Tech. **201**, 3723 (2006).
[73]. S. Miao, W. Weng, Z. Li, K. Cheng, P. Du, G. Shen, G. Han - J. Mater. Sci.-Mater. M. **20**, 131 (2009).
[74]. P. Kern, P. Schwaller, J. Michler - Thin Solid Films **494**, 279 (2006).
[75]. C.T.J. Low, R.G.A. Wills, F.C. Walsh - Surf. Coat. Tech. **201**, 371 (2006).
[76]. S.R. Paital, N.B. Dahotre - Mater. Sci. Eng. R **66**, 1 (2009).
[77]. Y. Cai, R. Tang - J. Mater. Chem. **18**, 3775 (2008).
[78]. Q. Yuan, T.D. Golden - Thin Solid Films **518**, 55 (2009).
[79]. Y.W. Song, D.Y. Shan, E.H. Han - Mater. Lett. **62**, 3276 (2008).
[80]. Y.-Y. Zhang, J. Tao, Y.-C. Pang, W. Wang, T. Wang - Trans. Nonferrous Met. Soc. China **16**, 633 (2006).
[81]. N. Dumelie, H. Benhayoune, D. Richard, D. Laurent-Maquin, G. Balossier - Mater. Charact. **59,** 129 (2008).
[82]. Y.-Q. Wang, J. Tao, L. Wang, P.-T. He, T. Wang - Trans. Nonferrous Met. Soc. China **18**, 631 (2008).
[83]. D.J. Blackwood, K.H.W. Seah - Mater. Sci. Eng. C **29**, 1233 (2009).
[84]. N. Eliaz, T. M. Sridhar - Crystal Growth & Design **8,** 3965 (2008).
[85]. X. Zhao, L. Yang, Y. Zuo, J. Xiong - Chinese J. Chem. Eng. **17**, 667 (2009).
[86]. N. Eliaz, M. Eliyahu - J. Biomed. Mater. **80A**, 621 (2007).
[87]. X. Cheng, M. Filiaggi, S.G. Roscoe - Biomaterials **25**, 5395 (2004).
[88]. R. Narayanan, S.K. Seshadri - J. Appl. Electrochem. **36**, 475 (2006).
[89]. D. Velten, V. Biehl, F. Aubertin, B. Valeske, W. Possart, J. Breme - J. Biomed. Mater. Res. **59**, 18 (2002).
[90]. E. Krasicka-Cydzik, K. Kowalski, I. Glazowska - Journal of Achievements in Materials and Manufacturing Engineering, **18**, 147 (2006).
[91]. J. Jakubowicz - Electrochem. Commun. **10,** 735 (2008).
[92]. H. Lukáčová, B. Plešingerová, M. Vojtko, G. Bán - Acta Metallurgica Slovaca, **16**, 186 (2010).
[93]. M.V. Diamanti, M.P. Pedeferri - Corros. Sci. **49**, 939 (2007).
[94]. H.H. Park, I.S. Park, K.S. Kim, W.Y. Jeon, B.K. Park, H.S. Kim, T.S. Bae, M.H. Lee - Electrochim. Acta. **55**, 6109 (2010).

[95]. J. Kunze, L. Müller, J.M. Macak, P. Greil, P. Schmuki, F.A. Müller - Electrochim. Acta. **53,** 6995 (2008).
[96]. H.Z. Abdullah, C.C. Sorrell - J. Aust. Ceram. Soc. **43**, 125 (2007).
[97]. A. Karambakhsh, A. Afshar, P. Malekinejad - J. Mater. Eng. Perform. **19**, 1 (2010).
[98]. Y.-T. Sul, C.B. Johansson, Y. Jeong, T. Albrektsson - Med. Eng. Phys. **23**, 329 (2001).
[99]. M.V. Diamanti, M. Ormellese, M.P. Pedeferri - Corros. Sci. **52**, 1824 (2010).
[100]. B. Yang, M. Uchida, H.-M. Kim, X. Zhang, T. Kokubo - Biomaterials **25**, 1003 (2004).
[101]. S. Van Gilsa, P. Mast, E. Stijns, H. Terryn - Surf. Coat. Tech. **185**, 303 (2004).

THE ANNALS OF "DUNAREA DE JOS" UNIVERSITY OF GALATI.
FASCICLE IX. METALLURGY AND MATERIALS SCIENCE
N^0. 4 – 2013, ISSN 1453 – 083X

COMPOSITE BASED ON AlMg ALLOYS OBTAINED BY GAS INSUFFLATION

Oana BĂLŢĂTESCU, Raluca Maria FLOREA, Costel ROMAN, Ioan CARCEA
"Gheorghe Asachi" Technical University of Iaşi, Faculty of Materials
email: oana84rou@yahoo.com

ABSTRACT

Composite materials are the most advanced class of materials invented and produced by humans in modern times as well as a challenge for the future in the field of scientific and technological performance. They are made up of at least two phases of different nature which are so combined to form a new material with a superior combination of properties. They are generally materials with unusual performances on the relationship between properties and specific gravity. Composites are multiphase materials with distinct and well-defined interface between the constituent phases ensuring a transfer of property but can lead to obtaining a product with exceptional performance from the starting material. Stabilized Aluminum Foams (SAF) are new class of materials with low densities and novel physical, mechanical, thermal, electrical and acoustic properties. They offer potential for lightweight structures, for energy absorption, and for thermal management; and some of them, at least, are cheap. Metal foams offer significant performance gains in light, stiff structures, for the efficient absorption of energy, for thermal management and perhaps for acoustic control and other, more specialized, applications. They are recyclable and nontoxic. They hold particular promise for market penetration in applications in which several of these features are exploited simultaneously. Metal foams are metal matrix composites (MMC) characterized by: higher specific properties, high capacity vibration damping and sound, mechanical energy absorption etc. The wide range of possible properties can lead to innovative applications, which is a strong driving force for the improvement of metal foam production technologies. Investigated and studied materials are composite of aluminum alloy matrix where the stabilisation of the gas bubbles has been done by ceramic particle added. To obtain SAF we have focused research on Al-Mg alloys with different concentrations of magnesium and silicon carbide (SiC). To obtain these materials has been chosen a different gas blowing method (N_2, SO_2 şi C_4H_{10}). It was observed that the best results in terms of pore volume gave the blowing with C_4H_{10}. The samples obtained were analyzed by electron microscopy.

KEYWORDS: AlMg alloys, gas insufflations, metal foams, stabilized aluminum foams (SAF), porous metals, cellular materials

1. Introduction

Metal foam or metallic foam has become a very popular term which is nowadays used for almost any kind of metallic material which contains voids. It might be useful to distinguish various expressions:

- cellular metal: space is divided into distinct cells. The boundaries of these cells are made of solid metal, the interior are voids. Ideally, the individual cells are all separated from each other by metal but often this restriction is relaxed.

- porous metal: the metal contains a multitude of pores, curved gas voids with a smooth surface.

- metal(lic) foam: foams are special cases of porous metals. A solid foam originates from a liquid foam in which gas bubbles are finely dispersed in a liquid.

- metal sponge: space is filled by pieces of metal that form a continuous network and co-exist with a

network of empty space which is also interconnected [1].

Aluminum foams are a new class of materials with low densities, large specific surface and novel physical and mechanical properties. Their applications are extremely varied: for light weight structural components, for filters and electrodes and for shock or sound absorbing products. Recently, interesting foaming technology developments have proposed metallic foams as a valid commercial chance; foam manufacturing techniques include solid, liquid or vapor state methods. The foams presented in this study are produced by Melt Gas Injection (MGI) process starting from melt aluminum [2, 3].

There are a lot of applications of metallic foams, but most of them are in the automotive, aircraft and building industries, in which the SAF manufacturers have the objective to achieve a market penetration that will bring stabilized aluminum foam to where magnesium is today (e.g. light weight structures, sandwich cores, strain isolation (compression), mechanical damping, biomedical industry, acoustic absorption, acoustic control, kinetic energy absorbers (compressive), blast resistance, storage and transfer of liquids, fluid flow control, heat exchangers/refrigerators, thermal isolation, electrical shielding, electrodes and catalyst carriers, electrode material, spargers, sporting equipment, decoration and arts [4].

2. Experimental procedure

The injected air causes bubbles to rise to the surface of the melt, forming liquid foam which is stabilized by the presence of solid ceramic particles on the gas liquid interfaces of the cell walls. The stabilized liquid foam is then mechanically conveyed off the surface of the melt and allowed to cool to form a solid slab of aluminum foam. The aluminum foam structure (cell size and cell wall thickness) is controlled by the process variables such as the volume fraction of the solid particles; foaming temperature, airflow rate, and impeller design the foam making process. Unfortunately, no publication has been found in the work on the influence of the process in variables on the cell structure of aluminum foam. In the future we will study and investigate the effect of the concentration of SiC particles on the cell structure and mechanical properties.

The experimental equipment consists of an electric resistance furnace (maximum heating temperature 800 ºC), which was adapted for insufflations gas (C_4H_{10}) It is also equipped with a wide agitator and a trough acquisition of foam formed (Figure 1). Has been obtained metal foam by mixing the alloy melt AlMg10 with 20% SiC powder 120µm size, at a temperature of 710 ºC and with C_4H_{10} injection at 1.2 atm pressure. The obtained foam was analyzed by electron microscopy.

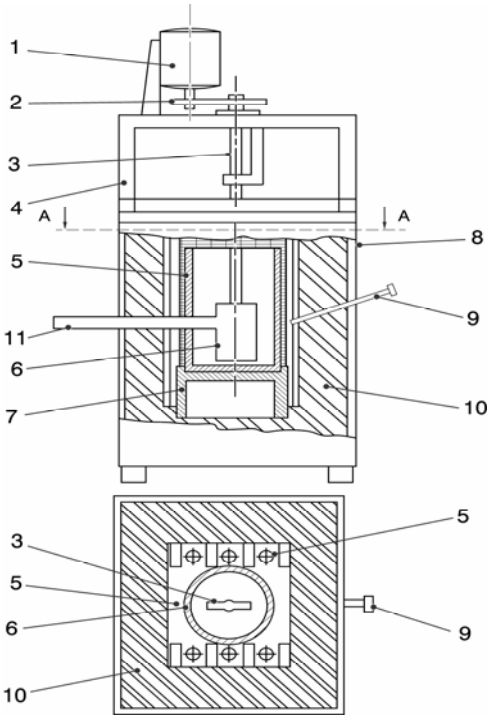

Fig. 1. *Electric resistance furnace. 1 – engine, 2 – reductor, 3 – port rod paddle, 4 – metal frame, 5 – crucible, 6 – paddle, 7 - crucible support, 8 – silica bars, 9 – thermocouple, 10 – refractory shield, 11 – collecting gutter foam [5]*

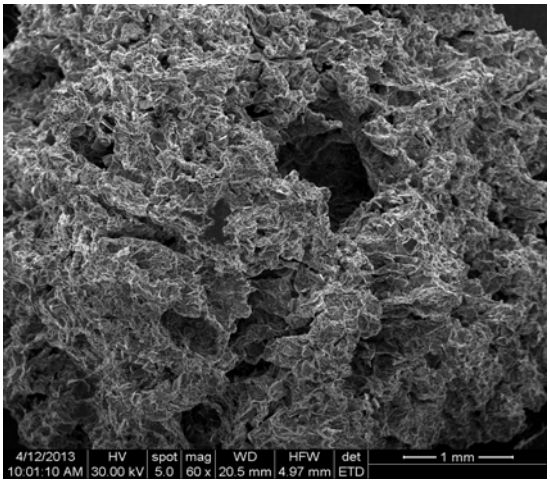

Fig. 2. *Analysis by scanning electron microscopy SEM to highlight the overall appearance of the overall composition and the morphology of the constituents and distribution of the pores in the matrix of the composite. It is noted that the pores are imbued each other and also appear ligament bridges porous*

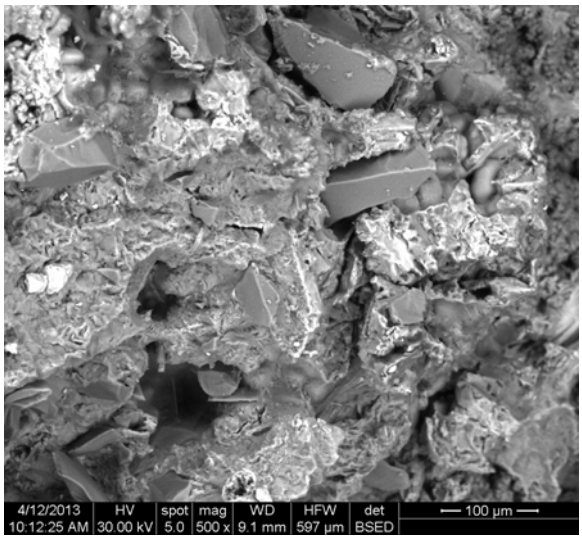

Fig. 3. *SEM image highlighting the distribution and morphology of carbides and the porosity that was formed in the composite structure. Are shown a variety of hydrocarbons as well as pores which have dimensions of the order of 50 µm which are distributed throughout the mass of the composite. X 500*

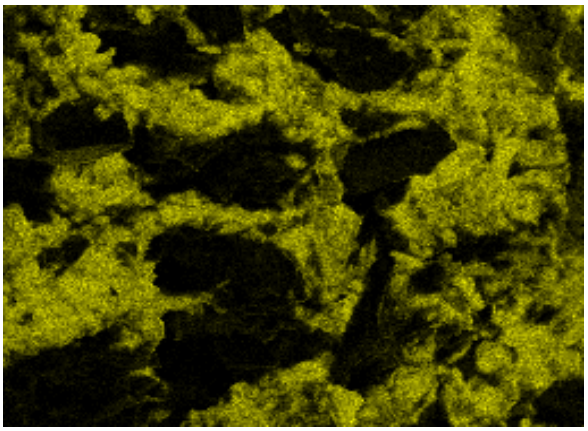

Fig. 5. *EDX qualitative analysis to highlight the detail of the map matrix aluminum alloy. We are identified spherulites on the basis of aluminum oxide, and the network of pores was also developed around the carbides of silicon*

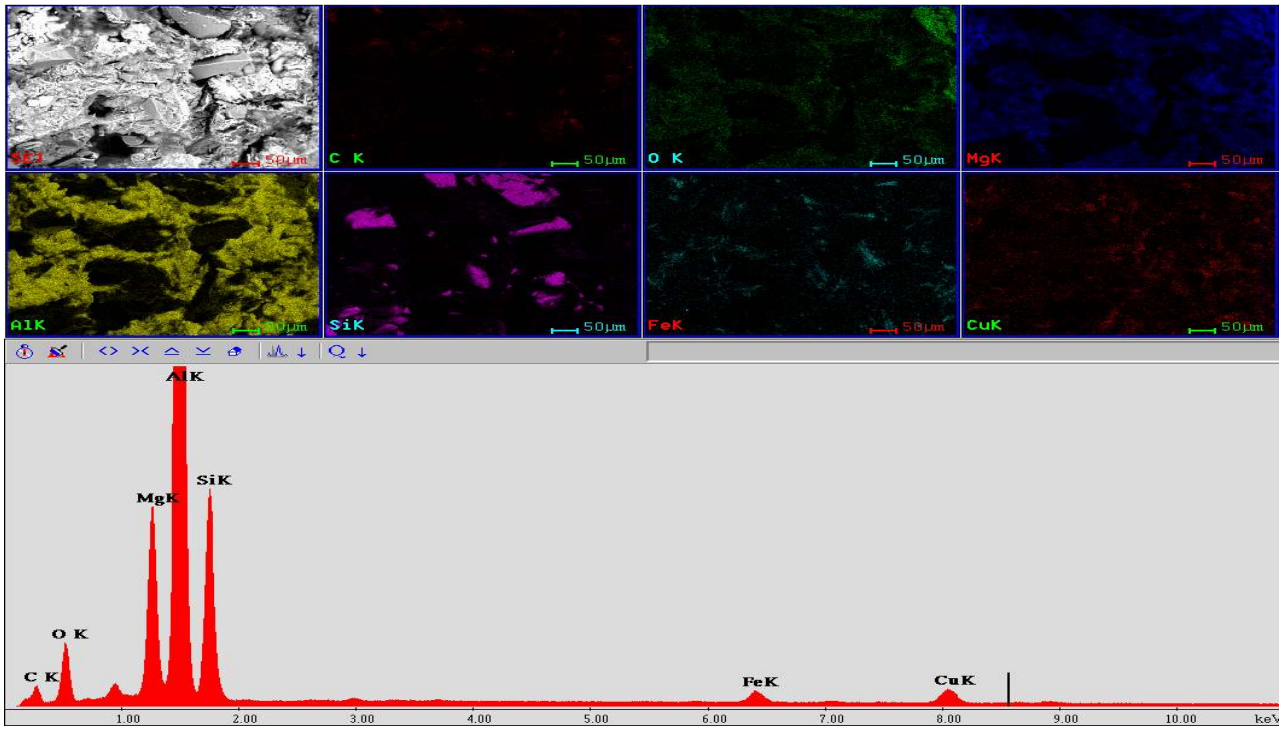

Fig. 4. *Analysis by electron diffraction EDX with SEI images distribution maps that highlight the main constituents of the composite. The colors are chosen in order to differentiate the distribution of the constituents on the basis of: Al, Si, Fe, Cu, Mg, O and C*

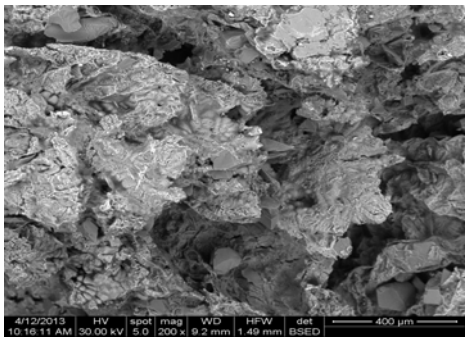

Fig. 6. *SEM image shown the porous internal structure of walls ligaments and inclusions (catches) of silicon carbide in these areas. X 200*

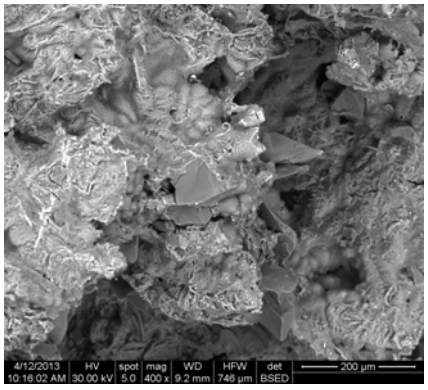

Fig. 7. *It is observed at the same time the intercommunicated area between pores. Detail of the previous image that highlights how silicon carbonates are embedded on the walls of ligaments. X 400*

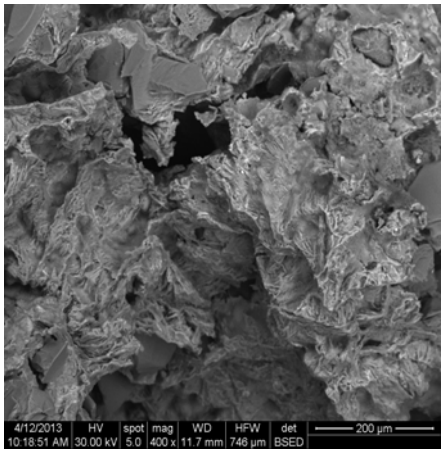

Fig. 8. *Detail of the surface morphology of cavities that can be found in the matrix composite. It is noted the "sponge" structure of the matrix and a plurality of multifilament growth (formation resulting from the segregation of the AlMgSi compounds which appeared to solidify the matrix) in preference to the surface of the mold cavity solidification*

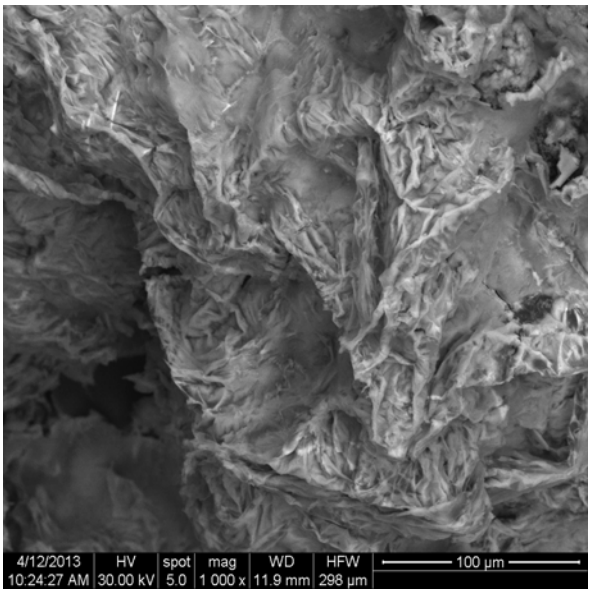

Fig. 9. *Analysis of the structure and morphology of a part of the cells formed shows that they have spongiosal consistency, and partially with micro-lamellar appearance or foil. This result we believe that emerged as a result of penetration modeling gas (butane) that we put in the whole mass of the composite before solidification. X 1000*

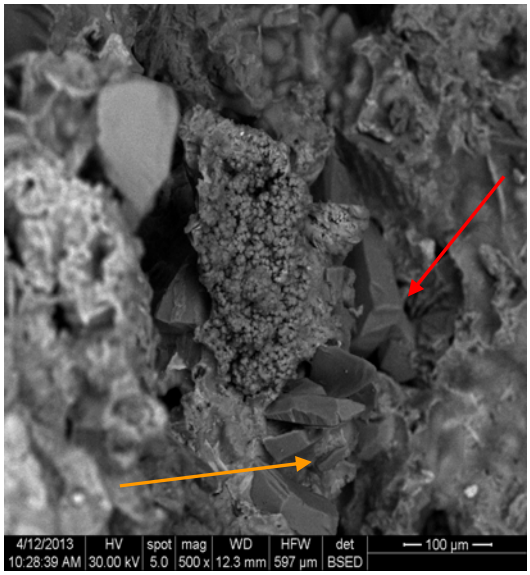

Fig. 10. *The butane gas concentration area and near the concentrations of silicon carbide (as marking) following the non-homogeneous gas bubbling can be formed in the matrix of the composite tinted conglomerate and some conglomerates of cluster-like structure (cluster structure). This cluster morphology can be observed in the SEM image shown in the center. X 500*

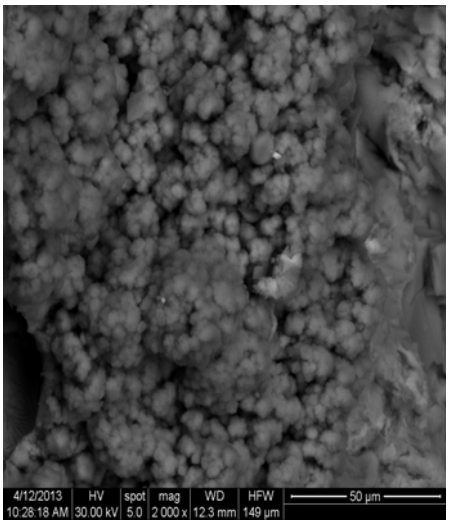

Fig. 11. *Detail of morphology development and solidification zones in the cluster. It point out that high degree of porosity exists in the solidification morphologies that are found in areas with clusters of carbides. X 2000*

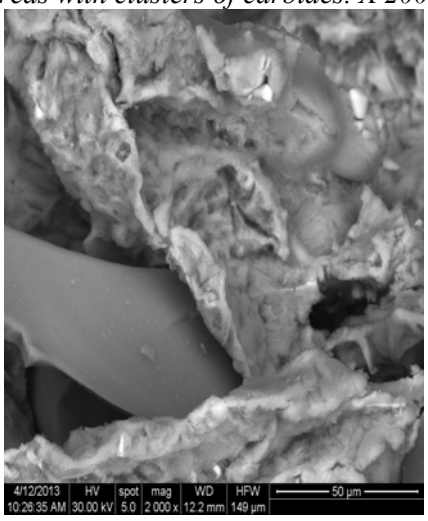

Fig. 12. *SEM image which shows the way solidification of the matrix alloy in the vicinity of the silicon carbide particles. At the interface it is found that there is a strong segregation of the alloy matrix, there is no adhesion between the matrix and the contact carbide. It is possible that butane bubbling it have leaked carbide particle surface, thus increasing trend of detachment from the matrix and carbides significantly increased the porosity of the composite. X 2000*

3. Conclusions

The laboratory equipment allowed us to obtain a metal foam by mixing the alloy melt AlMg10 with 20% SiC powder 120µm size. We used an injection of butane at 1.2atm pressure and 710ºC melt temperature.

In the metal foam microstructure obtained is observed that a network of pores penetrated it with ligaments porous bridges between them, developed around silicon carbide. Pore size is over 50µm.

Multifilament increases resulting in segregation of the AlMgSi compounds that have occurred in the solidification of the matrix, mainly on the surface of the mold cavity solidification.

We have observed the silicon carbide based on spherulites of aluminum oxide.

The formed cells, besides the spongiosal consistency, have a partial aspect or micro-laminated foil, gas ingress occurred as a result of modeling.

The gas it was observed at the interface in the absence of adhesion between matrix and silicon carbide, apparently due to "flow" surface carbides butane.

Acknowledgement

This paper was realised with the support of POSDRU CUANTUMDOC "DOCTORAL STUDIES FOR EUROPEAN PERFORMANCES IN RESEARCH AND INOVATION" ID79407 project funded by the European Social Found and Romanian Government.

References

[1]. J. Banhart - *Metallic foams: challenges and opportunities*, Eurofoam2000, Editors: P. Zitha, J. Banhart, G. Verbist (MIT-Verlag Bremen), (2000), 13-20.

[2]. J. T. Wood - *Production and applications of continuously cast, foamed aluminum*, Proceedings of Fraunhofer USA Metal Foam Symposium, Verlag MIT Publishing, (1997), 31-35.

[3]. P. Asholt - *Aluminum foam produced by the melt foaming route process, properties and applications*, Proceedings of Int. Conf. on Metal Foam and Porous Metal Structures, MIT Publishing, (1999), 133-140.

[4]. M. F. Ashby, A. G. Evans, J. W. Hutchinson, N. A. Fleck - *Metal Foams: a Design Guide*, ISBN 0-7506-7219-6, (2000).

[5]. O. Bălţătescu, R. M. Florea, C. Roman, I. Rusu, I. Carcea - *Stabilized aluminum foams, unique material for industrial applications*, Journal of Optoelectronics and Advanced Materials Vol. 15, No. 7- 8, (2013), 823-832.

THE ANNALS OF "DUNAREA DE JOS" UNIVERSITY OF GALATI.
FASCICLE IX. METALLURGY AND MATERIALS SCIENCE
N^0. 4 – 2013, ISSN 1453 – 083X

DUST EMISSIONS FROM AN INTEGRATED STEEL MILL IN CORRELATION WITH HUMAN EXPOSURE AND THEIR ADVERSE HEALTH EFFECTS

Anișoara CIOCAN, Tamara RADU
Faculty of Materials Science and Environment, "Dunărea de Jos" University of Galaţi,
111, Domnească Street, 800201, Galaţi, Romania
email: aciocan@ugal.ro

ABSTRACT

Many of the metallurgical operations contribute to generation of the dust emissions if these are not properly controlled and managed. The relevant sectors as important sources for airborne dust are: coke oven plant, sintering equipments, blast furnaces, basic oxygen steelmaking, steel mills and also handling, preparation and transport of raw materials, products, by-products and residues. The annual average values of dust for metallurgical plant and period analysed not exceeds allowable level. The measurements showed that the daily average determined for settled dust varies very high. Sometimes, certain of these exceed the limits of the rules in force for air quality indicators. As result at exposure to generated dust (especially to particulate matter) appear adverse health problems at workers and population that lives in the neighbourhood of steelwork plant. Impact of dust emissions as air pollutant on the population of the vicinity areas is correlated with levels of incidence and prevalence of some specifically diseases. The indicators calculated for evaluation the health status (severity index, relative risk, professional etiological fraction) did not demonstrate the adverse health effects determined by exposure to dust particles in suspension on population that lives in vicinity of the plant. This influence is more likely to workers directly involved in metallurgical activity.

KEYWORKS: dust emissions, particulate matter, integrated steel mill, health status

1. Introduction

In terms of environmental protection, metallurgical processes involve operations that are dangerous because generate pollutants [1-3]. Emissions of pollutants represent one of the criteria for assessing the occupational risk associated with the work environment from metallurgical plants. Under European guidelines, for each sector must be identified the sources of pollutants emissions, the quantity of pollutants released to environment, their toxicity and their degree of hazard. The characteristics of pollutants are determined by the nature of the materials processed, the processes that happen (mechanical, thermal, physical, chemical) and by properties of products or by-products resulted (physical and chemical) [4]. One of the primary pollutants with adverse impacts on environmental from workplaces and from surrounding areas is dust. Many of the metallurgical operations contribute to generation of the dust emissions if these are not properly controlled and managed. As result, may appear health problems at exposure to generated dust.

The risks from exposure to dust emissions are dependent characteristics of dust emission, i.e. the quantity, chemical composition and species, particle shape and size as well as their biological aggressiveness. The major exposure of workers and population that lives in the neighbourhood of steelwork plant is achieved on air way by inhalation, ingestion and skin absorption of the dust particles present in the ambient air. Directive 2008/50/EC on ambient air quality and cleaner air for Europe has set mandatory limits for particulate matter. It is the first EU directive that includes limits on air concentrations of $PM_{2.5}$ (fine particulate matter). In these circumstances, the Directive requires Member States by 1 January 2015, the emission limit value for

particulate matter should not exceed 25 micrograms per cubic meter as an annual average, while in 2020 to decrease to 20 micrograms per cubic meter [5].

For integrated steel mills, standards impose for particulate matter the following air emission levels: 20-50 mg/Nm^3 (lower value is for presence of toxic metals, reference conditions for thee limits are different). According to studies conducted in different countries, there is a correlation between respiratory systems and long-term exposure to particulate concentrations of approx. 30 - 35mg/m^3. More, simultaneous presence of dust and other pollutants cause synergetic negative effects for human health. The synergistic relationships between the airborne dust, sulphur dioxide and nitrogen oxides are relevant. To minimize the adverse effects on health and environmental, it is necessary the continuous management of all metallurgical activities and the application of emissions monitoring programs for all sectors of the integrated steel plant. This is based on evaluation of direct or indirect indicators of emissions and the effluents in the environmental factors. It is imposes the sources identifying and the emissions with significant impact on the human health and environment, during normal working operations and for special conditions. Thus may be taken measures for reducing of the pollution level (with dust and other pollutants) in accordance with environmental standards [6-8].

This paper presents an analysis of metallurgical activities in relevant sectors of an integrated steel mill in terms of dust emissions (especially particulate matter), that is necessary to identify sources of emissions released into the air. Dust emission levels generated for a certain period of time are presented, recommending solutions to reduce them in order to comply within the limits of the rules in force for air quality indicators. It also discusses the adverse effects of dust emissions on the health of workers and the population from surrounding areas of the plant, based on indicators that quantify the health of workers and the people from surrounding areas of the plant.

2. Sources of dust emissions and their level for a integrated steels mill

In all steps of steels production flow based on the blast furnace/basic-oxygen route can be identified important sources of dust emissions.

The relevant sectors are: coke oven plant, sinter equipments, blast furnaces, basic oxygen steelmaking and casting, steel mills and also handling, preparation and transport of materials, products, by-products and residues. The major part of dusts generated at modern steel works are controlled by adequate equipments (cyclones, wet scrubbers, electrostatic precipitators, bag filters).

The dust collected is recycled or controlled dumped. However, variable quantities of dusts are issued directly or indirectly to air as suspended particulate matter (PM), depending of efficiency of cleaning facilities. These particles can be classified by more properties: shape, physical behaviour in the air, size, biological activity, chemical species etc. [8-10]. The most common parameter used in occupational hygiene for defining the particulate matter is the aerodynamic diameter (Table 1) [8].

Table 1. *Fractions of particulate matter, defined by aerodynamic diameter*

Particulate matter fraction	**Aerodinamic diameter**, μm
Total suspended particulates (TSP)	≤ 10
PM_{10} or coarse fraction	≥2.5; ≤10
$PM_{2.5}$ fraction	≥1; ≤ 2.5
PM_1 or fine fraction	≥1; ≤0.1
Ultra fine fraction (UFP)	≤0.1

The airborne dust (formed by fine and very fine fractions of particulates with aerodynamic diameter) is susceptible to cause adverse health effects more than coarse particulates [11, 12]. Chemical composition emphasizes their biological aggressiveness. These particles may contain varying concentrations of mineral oxides, metals (e.g. arsenic, cadmium, mercury, lead, nickel, chromium, zinc, manganese), and the metal oxides. Also on their surface can adsorb some persistent organic pollutants (dioxins, furans and so on). The coarse fractions of particles remain airborne for short periods and are therefore deposited very close to the generation sources. Even these fractions of particles can be entrained in airflows and wind and carried on short distances [8].

In ferrous metallurgy, the particulate matter can be generated by physical processes (manipulation, transport of the raw materials, their storage on sol, the handling and processing of the materials), thermal and chemical processes (combustion, oxidation, condensation, reduction, etc.).

The main sectors that generate the largest quantities of dust are ordered according to the amount as shown in Figure 1 [13].

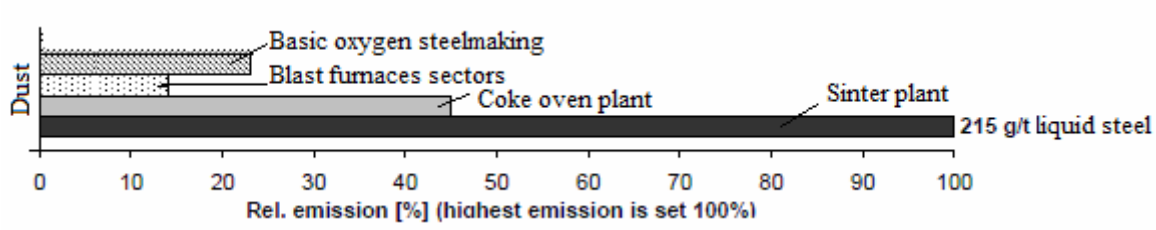

***Fig. 1**. Relative emissions of dust released from main sectors of integrated steel plant*

• Coke oven plants are the first production units of an integrated steelwork. They are placed on second place after sinter plants from point of view of the generation processes of the dust emissions as air pollutants. The conveying operations, handling, crushing, screening and loading of the coal are susceptible to generate important dusts quantities. Principally from coke ovens, the continuous emissions of particulate matter are the result of thermal processes. Intermittent emissions and fugitive can come from a large number of sources including oven doors, valves, charging holes etc. Other emissions may arise from processing of coke (quenching, crushing, sieving) and from the treatment of the off-gas (discontinuous emissions). For coke-oven plants in different EU Member States, 2005 year, the dust emissions to air ranged from 15.7 to 298g/t coke (higher value is for old plants with cracks in the oven walls) [14].

• Sinter plants generate the most significant amount of particulate matter in an integrated steel mill. From sintering operations may result amounts of dust about 20kg/t of steel (80% of particles smaller than 100 microns in diameter) [15]. Emissions from the sinter plant arise primarily from handling/preparation operations of the materials (transport, loading, unloading, crushing, sieving, mixing). The sintering strand and the wind-boxes are the primary sources of particulate emissions (mainly as iron oxides) for sinter machines. At the download area of the agglomerate from belt, emissions are mainly formed by oxides of iron and calcium. The crushing of the hot sinter, quenching and sieving are next hot-point for dust emissions [16, 17].

Generally, the dust emissions from sinter machine are controlled by capture and directed to de-dusting facilities. Only particles entrained by off-gas, which could not be kept entirely reach the air. These emissions can be a significant problem for people and the environment. In accordance with the literature, even performed electrostatic precipitators that equipped modern sinter plants have a low efficiency for fine fractions (rich in heavy metals and other hazardous compounds). From this reason, to minimise the dust, as advanced de-dusting technique considered for best available technique (BAT), is recommended the bag filter installed downstream to the existing electrostatic precipitator. Fabric filters enhanced with additives are highly efficient at reducing particulate matter emissions in the waste gas stream. They reduce emissions of PCDD/F, hydrochloric acid, hydrofluoric acid. Also, some emissions of VOCs and PAHs are more efficient reduced [18, 19]. To minimize pollutant emissions released and to reduce the amount of off-gas requiring end-of-pipe treatment, some modern sinter plants apply the recirculation of waste-gas through sinter strand [20].

• Particulate matter emissions generated by the blast furnace plant include emissions from the cast house and the cleaning of BF gas. The casting operation is higher source of particulate emissions from this sector (400 - 1500 g/t iron, depending on applied technique) [18]. Principally they are formed by iron oxides, magnesium oxide and carbonaceous compounds as particulate. Molten iron and slag emit smoke while travelling from the taphole to ladle and also to installation or pit for slag granulation. They are firstly determined by the contact of molten iron and slag surface with air. Also the drilling and plugging of the taphole can cause dusts emissions. These increase by utilisation of oxygen to open a clogged taphole. Casting emissions are controlled by capture hoods and gas cleaner facilities (usually the fabric filters). Also it can prevent the formation of pollutants with covered runner systems that exclude the ambient air contact with the molten surface. The following operations that generate dust emissions are mechanical processes at handling of materials. The transport of raw materials, loading and unloading of materials in and from bunkers at scaffold are the source of dusts formed from ores, sinter and coke particles. Gas leakage, from aspiration facility for space between cones, contain fine particles. Such particles can be simultaneous emitted with gas released in air at the blast furnace top, by opening of relief valve to the atmosphere for the pressure equalization. In these areas, dust emissions are controlled by gas cleaner facility (electrostatic precipitator).

The emissions are captured and cleaned in multistage de-dusting systems: bag filters to capture coarse fractions; Venturi scrubbers for fine particulates containing heavy metals and other

compounds. The dust unloading from dry cleaning facilities can be emitted as particulates to air. Minor emissions may arise from firing process of combustible gas (blast furnace gas and methane) to hot stoves (cowpers).

• Particulate matter emissions from basic oxygen steelmaking arise from pre-treatment of hot metal(including hot metal transfer, desulphurization and deslagging processes); charging operations; oxygen blowing for reducing of carbon level and oxidation of impurities; tapping operations. The sources of pollutants emissions are grouped as sources of primary emissions (pre-treatment of hot metal, oxygen blowing into furnace, secondary metallurgy) and sources of secondary emissions (deslagging of hot metal, charging into furnaces of hot metal and scraps, tapping of liquid steel and slag from furnaces and ladles, secondary metallurgy, tapping operations, handling of additives, continuous casting) [14]. Most of dust emissions to air from all these processes (named point-sources or hot points) are controlled (by capturing in de-dusting systems). Some of these are dispersed into air and as result, the environment conditions are negative affected (principally the ambient air from workplaces). The gas released from the furnace during oxygen blowing contain an important quantity of particulate matter (mainly consisting of metal oxides, including heavy metals). Particulate matter are usually removed from gases by means of Venturi scrubbers or dry electrostatic precipitators. When suppressed combustion is applied, Venturi scrubbers may achieve a particulate matter concentration of 5-10mg/Nm^3 (but concentrations up to 50mg/Nm^3 are possible also) in the gas. This corresponds to 1g/t liquid steel [14]

3. Analyse of the dust emissions customized for a Romanian integrated iron and steel plant

The integrated steel mill has in operation in period analyzed the following: coke ovens, sinter plants, blast furnaces, basic oxygen steelmaking plants and steels mills. Also, there are supplementary facilities for: unloading of materials from ships and trains; transport and storage of materials on soil; raw materials preparation (crushing, sieving, weighing etc.). There were also additional facilities for: unloading of materials from ships and trains; transport and storage of materials on soil; materials preparation (crushing, sorting, weighing etc.). Practically, majority of the activities developed in these sectors generate dust. In terms of potential effects on human health and environmental quality, the air factor is the main medium to transfer the fugitive emissions from the source to receivers (workers, population from vicinity of the metallurgical plant). Air emissions were sometimes visible from distance and perceived not only in industrial area but also in large neighbouring areas.

Air pollution in coking plants is mainly due to diffuse emission sources rather than those controlled by de-dusting plants. Transport facilities, crushing and screening of coal and coke, which are likely to generate significant quantities of dust are equipped with electrostatic precipitators. Because the concentration of the particulates contained by off-gas released to air from these facilities was in 1997 about 100 mg/Nm^3, was imposed their modernisation. As result of insufficient capture capacity, during the preparing operations of coals, the diffuse emissions were at higher level, 0.6 – 1.5 g/Nm^3. For this reason was necessary the resizing of suction facilities. The emissions generated from combustions chambers were mostly captured and was directly discharged to stack. Coke batteries release important dust quantities, consisting of a complex mixture of organic and inorganic compounds, past including heavy metals. The raw gas resulted from coking process was captured and directed to chemical section for cleaning and recovering of valuable elements. To diminish the diffuse emissions from loading and unloading of coke batteries, these were equipped with hydroinjection installations. Their modernisation led to decreasing of dust emissions from 35 – 40 mg/Nm^3 to 18 – 20 mg/Nm^3. The transport operations, related to coke quenching, produce particulate matter in range of 0.5 – 0.7 mg/Nm^3. The filter bags reduce these emissions to 0.03 – 0.04 mg/Nm^3. Inherent particulate emissions from coke quenching were substantially reduced by adopting a dry technique. The level of particulates released from discharging zone of coke after its quenching was high. For decreasing of emission from quenching facilities was proposed a multistage cleaner solution: multistage cyclone and the wet scrubber followed by fabric filters. These ensures reaching an emission level of 38 - 45 mg/Nm^3. The diffuse emissions dust quantified to coke transport on the conveyer belts, especially at discharge ends (points transhipping) were high, 1.2 – 2.7g/Nm^3 [21, 22].

For these hot-points were recommended and applied the solution: wet cyclone and fabric filter to ensure the level 38 - 42mg/Nm^3. An electrostatic precipitator can be supplementary attached to sieving area of coke for maximal reducing of the dust emissions. On the flow of sinter - blast furnaces, the first major sources of diffuse emissions are from the storage of raw materials piles on uncovered sites. The particulate matter emitted carry with them variable concentrations of heavy metals (Pb, Zn, Mn, Cr, Cu, Ni, Cd etc.). In these areas heavy metals present in dusts (especially those generated from ores) are mainly accumulated in/on soil. Sometimes wind

drives the fine fractions to neighbouring areas, generating a significant hazard to the environment and humans. The materials preparation (crushing, sieving, mixing, transport) and their conveying on belts generates also dust emissions. These were captured and removed with an electrostatic precipitator. Because suction network of cleaner facility that stretched on large areas, the efficiency of capture was low. This makes visible dust sitting on the ground of the preparing materials sector. Resizing of network suction and the installation of equipment in local emission points can improve system efficiency. Homogenization of raw materials in mixing drums and loading on sintering belts do not generate significant dust emissions because the material handling is wet. Agglomeration process itself generates large quantities of dust that contain heavy metals and alkali metal compounds, (due to the high temperatures in the combustion zone and to the high depression). From sinter strand results a high flow of gases (about 5.000 m_3/m_2 sinter belt surface). These carries the important quantities of dust (coarse and fine particles) to electrostatic precipitator. Coarse particles (of approx. 100 microns) come from the loading of materials mixture and from bottom layer of sintering strand.

They have the composition in correlation with the mixture subjected to sintering. Fine particles (0.1-1 microns) are formed in the sintering zone, after complete evaporation of moisture from the mixture. These are rich in heavy metals (Pb, Zn) and the chlorides of Na and K. These chlorides from the fine dust lead to low efficiency of removing at only 60% (functioning of electrostatic precipitator is worsened as result of increasing of dust resistivity), and the emissions were located between 50-100mg/Nm^3. Unloading on sintering belts, hot crushing, sieving and especially sinter cooling are other important emissions sources for the dust. In Table 2 are given the dust emissions levels that were measured at suction hoods of electrostatic precipitator in different areas of this sector.

***Table 2**. Dust level for various sites of sintering installations, 1997 [21]*

Different areas from sintering process		**Level,** mg/m^3
Raw materials preparation	Crushing installations	295 – 300
Weighting	Weighting station	185 – 205
Homogenizing of raw material	Primary mixing drum	167 – 180
	Secondary mixing drum	135 – 148
	Belts for fines return	178 – 195
Sinter sieving	Hot sinter screening	302 – 353
	Cooled sinter sieving	245 – 265
Cooling sinter	Cooling installation (without fan function)	272 – 286
	Cooling installation (with fan function)	180 – 196

After de-dusting by electrostatic precipitator, the dust emission were diminished in the range 40 - 70mg/Nm^3 (higher values are in correlation with some leaks from conveyors mantles and also from incorrectly utilisation of de-dusting equipments).

As a final conclusion it was found that significant environment problem in the sintering sector is represented by diffuse dust emissions which are present practically on all flow line. Because in the period under review (1997), the dust content in air was higher that the values admissible from European standard, were recommended the adoption of following measures for the reduction these diffuse particulate emissions from sintering flow: enclosures for transhipment areas of raw materials; modification of discharging hoppers of materials; wetting of material in summer; placing of the additional de-dusting systems to raw material sector. Also, was required the upgrading of the capture systems and de-dusting installations type electrostatic precipitator to reduce diffuse emissions in the zone of sintering machines. Better for the sector would be to use the dusting equipment, bag filters.

In sector of blast furnaces were identified sources of dust generation, some emissions exceed admissible levels. The solid particles (generated from transport, loading and unloading of materials from bunkers at blast furnace scaffold) released to stack with off-gas were in 1997 in the range of 44 - 69 mg/Nm^3 (between 7 and 40 kg/t iron). About 3 – 5 % of this amount was released to air at pressure equalisation operations between the bells of charging installation. Off-gas released of blast furnace top is treated and used in various combustion processes. The preparing of coal for injection into blast furnace is a minor source for dust (about 2 - 50 g/t iron), the installation for injection being equipped with adapted systems for emissions control. Same situation is considered at firing process of combustible gas (mixture consisting of blast furnace gas and methane) to cowpers, typically emissions were limited to about 10 mg/Nm^3 [21]. At casting of iron and slag are released great and variable quantity of brown fumes,

400 – 1500 g/t pig iron. These are the result of interaction of hot iron and oxygen from air, being largest to skimmer gate and tilting runner areas. Also casting house air are polluted with dust emitted at beginning and ending of tapping due the ramming mass and its utilisation.

Emission sources of air pollutants at basic oxygen furnaces steelmaking are grouped into primary and secondary emission sources. Most emissions generated can be partial controlled (captured and conducted to cleaner systems). A small amount of these is dispersed in air, and lead to worsening of environmental conditions in the workplaces. The emissions from pre-treatment of the iron (desulphurization, slag separation etc.) are diminished by simultaneous suction with gases in local hoods and by further treatment into fabric filters. Thus the dust emitted to air is reduced below admissible level. For the pig iron mixers not equipped with special facilities for gas capture were assessed following quantities of dust: 12 g/t iron for loading of furnace; 18 g/t iron for unloading from furnace. During oxygen blowing, the gas emitted is polluted with 15 – 20 kg particulate matter/t steel. These emissions are retained in wet cleaners Venturi (until 25 - 100 mg/Nm^3). When applying wet scrubber, air pollution problems transferred to other environmental factors: to water-waste water is polluted with solid suspensions containing heavy metals, cyanides, nitrogen compounds etc.; to sol – sludge is formed, from which a little fraction is recycled, most being uncontrolled dumped. The air emissions from the secondary treatment of the steels are minor. AOD installation was equipped with filter bags. The pig iron pouring, loading of furnace, steel and slag tapping from furnaces and ladles, treatment with additives and continuous casting are operations characterized by dust emissions (brown fumes).

Measured or estimated dust emissions shows that many workplaces were affected by exceeding the level of dust emissions allowed. Besides air pollution in work areas, metallurgical activities from this metallurgical plant had negative effect on air quality from adjacent areas. To illustrate the level of population exposure at this pollutant released from Romanian steel plant, can analyse data presented in Tables 3-5. There are the results of statistical processing of the data measured by legal environmental control institutions and laboratory of steel plant itself [22].

Although the annual average values exceeds allowable level, it appears that the daily average determined for settled dust varies very high. For same class of dust, the annual average monitored in certain areas of Galati town was normal.

Similar conclusions arising from the analysis of isoconcentration curves of daily and annual average concentrations presented as cartographic maps made by modelling of temporal and spatial dispersion of particulate matter. Modelling dust emission for the Romanian steel plant and its surrounding residential area was conducted by ICEM Bucharest [21].

Table 3. *Airborne dust: annual and daily average*

Year	Mean annual value,	Maximum daily value	Minimum daily value	Frequency of exceed	Total number of samples
	[mg/m^3]		[mg/m^3]	[%]	
1999	0.0520	0.149	0.002	0	1012
2000	0.0560	0.145	0.016	0	304

Table 4. *Dust settled, annual and daily average*

Year	Mean annual value,	Maximum daily value	Minimum daily value	Frequency of exceed	Total number of samples
	[mg/m^3]		[mg/m^3]	[%]	
1996	24.15	95.01	2.61	56.38	94
1997	28.90	217.4	2.32	60.8	97
1998	29.01	92.42	2.53	50	104
1999	14.45	363.04	1.02	15.6	96
2000	9.42	254.78	0.51	28.18	110

Table 5. *Mean annual values of settled particles, according to monitoring by the Department of Public Health Galati, mg/m^3*

Collection points	Year										
	1991	1992	1993	1994	1995	1996	1997	1998	1999	2000	2001
Domnească Street	20.2	36.8	21.3	18.9	18.5	26.5	19.8	17.8	16.7	15.2	15.3
Traian Street	20.7	23.4	23.6	22.3	19.4	21.0	18.2	21.5	24.2	22.6	35.6
Filesti Station	25.7	30.5	26.2	26.9	18.6	22.2	23.2	19.3	18.8	19.6	16.5
Drumul Viilor Street	20.1	22.2	22.3	30.9	17.8	22.9	21.9	17.3	18.3	19.0	19.5
Moruzzi Place	-	17.7	20.8	16.1	14.4	24.8	24.4	19.0	25.0	19.0	19.1
Pensioners Home	-	19.0	24.4	20.6	22.6	20.9	17.0	16.8	15.8	13.5	19.6

For modelling of the concentrations of dust (and other air pollutants), the Gaussian model, ISC - AERMOD View, was used. Maps obtained (Figure 2 and Figure 3) show that annual average concentrations of particulate matter shall not exceed the limits imposed by European regulations on air quality.

For steel mill and in its vicinity areas were exceeded hourly average concentrations of particulate matter.

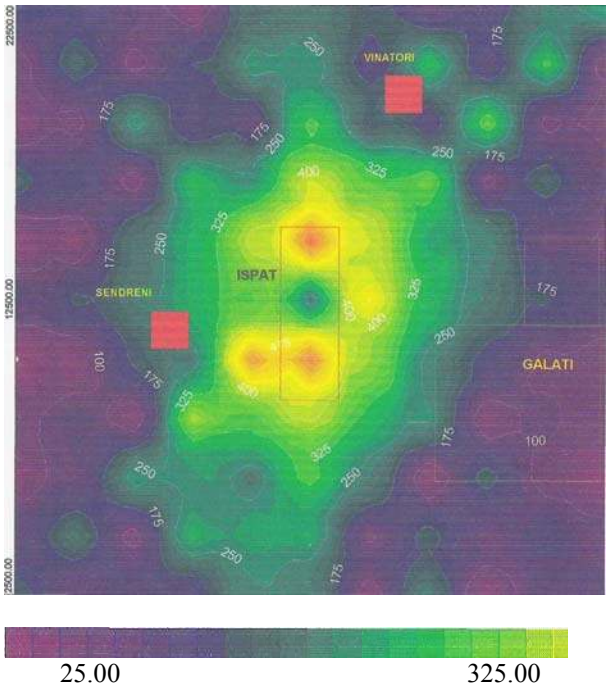

Fig. 2. *Map of particulate matter dispersion (hourly concentration, µg/Nm^3)*

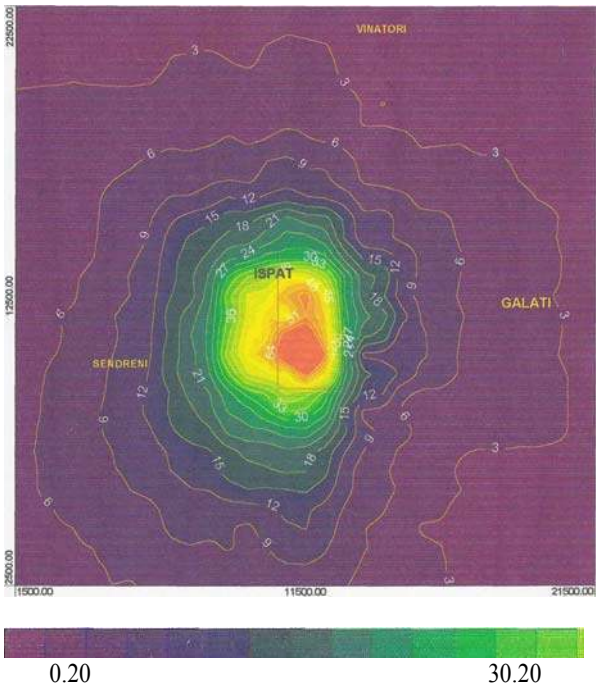

Fig 3. *Map of particulate matter dispersion (annual concentration, µg/Nm^3)*

4. Effects of exposure of workers and population to dust emissions

Air pollution is a real risk to human health and disease incidence is linearly proportional to the nature and concentration of the pollutant that exceeds the reference value and the number of people exposed. For integrated iron and steel plant, is predominant the continuous exposition to low concentrations of dust emissions during normal operation of the plant. Incidentally, people may be exposed to high concentrations of pollutants for a short period of time following the occurrence of undesirable events. Their action on the human body translates into acute and chronic effects that can be quantified by modifying

some specific indicators (mortality, morbidity and so on). Fraction of fine particles ($PM_{2.5}$ and PM_{10} even) is a special health problem because they can penetrate deep respiratory system and can be absorbed into the blood. Effects of exposure depends on the air concentration, aerodynamic diameter of the dust particles in question, and exposure time/duration. The studies have found the causing of chronic respiratory diseases both for workers and for people in adjacent areas [23].

The dust released affect the immediate worker, leading to occupational disease or work-related diseases. The evaluation of demonstration causal relationship between pollution and diseases can be discussed by way of the analysis of mortality and morbidity indicators. To determine these indicators for Romanian integrated steel plant were used clinical data available on the situation of occupational health office.

The dust emissions can be linked mainly to respiratory diseases (asthma, chronic bronchitis) and sometimes to other like skin diseases (contact dermatitis) or medical diseases of the eyes. The situation of occupational disease cases, as severity index (IG - as number of days of temporary disability relative to the average number of employees) reported in the period 1996-2001 and calculated by ICEM Bucharest [21] is presented in the Table 5. We chose only the data for sectors for which the dust emissions are analysed in this paper.

Table 5. *Severity index (IG) for sectors of Romanian steel plants, during 1996-2001, %*

Years	1996	1997	1998	1999	2000	2001
Coking sector	846.9	781.01	866.77	844.29	778.43	596.22
Blast furnaces	709.08	709.82	689.06	681.84	615.97	569.47
BOF sector	761.41	771.9	801.65	599.47	618.83	598.6

The aetiology of respiratory diseases is difficult to be discussed in correlation only with a particular pollutant. Studies relating to diseases caused only by exposure to dust can not be achieved. However it can appreciated that exposure to high fugitive emissions of fine dust particles of coal/coke and brown fumes (together with exposure to irritants and toxic gases emissions) it favourable to emergence and negative evolution of the diseases in some workplaces. The eye diseases manifest themselves in areas where personnel are exposed to harmful dust (metals, coal/coke) and also to irritating gas or overexposure to light in welding operations.

The severity index on group of diseases determined by exposure to dust emissions (together with other pollutants) is given in Table 6. The highest value was recorded for coke, which is higher than that of the entire factory. This can be attributed to the simultaneous action of dust with more pollutants (BaP, HPA, BTX, PAHs) generated by activities developed in this sector.

Also, the values of indicator named professional etiological fraction (PEF) for the sectors of integrated plant are evaluated by ICEM Bucharest [21]. To evaluated this indicator was used the values of relative risk (RR as ratio of incidence in terms of occupational exposure and incidence in the benchmark group). Professional etiological fraction (EFF) based on RR, validates the percentages above 20% the causality of work-related diseases.

Table 6. *IG on group of diseases in relationship with dust exposure, during 2000-2001, %*

Group of diseases	**All sectors of metallurgical plant**	**Sector**		
		Coking	**Blast furnaces**	**Basic oxygen furnaces**
Respiratory diseases (without flu and pneumonia)	6.31	7.45	4.65	6.17
Skin diseases	3.59	3.9	3.25	3.4
Eyes diseases	1.29	1.42	1.20	1.17

Highest relative risk value was recorded for the period 1999-2000 to coke ovens plants: risk of disease was 3-4 times higher. Simultaneously, the highest percentage of PEF were recorded to sectors: coke oven plants, pig iron making (including sinter sectors), basic oxygen steelmaking (Table 7) [21]. Analyzing indicators, is find that between 1998 1999, professional etiological fraction (EFF) was significant at Romanian integrated plant, representing 25 to 33% compared with benchmark group, illustrating a link between work-related diseases and conditions relating to microclimate.

Table 7. *Professional etiological fraction (PEF) in sectors of integrated plant*

Sector	1997	1998	1999	2000	2001
Coking sector	50.82	43.79	68.01	75.49	53.85
Blast furnaces	45.14	8.97	60.43	51.56	32.55
BOF sector	44.35	40.75	53.43	67.97	52.08
All sectors of integrated plant	37.30	28.52	66.76	65.39	49.09

Impact of dust emissions as air pollutant on the population of the vicinity areas can correlate, especially, with incidence levels and prevalence of respiratory diseases. Health Department of Galati district has selected 35 diseases likely to be affected by air pollution, classified into 5 categories: airborne infectious diseases, acute respiratory diseases, conjunctivitis diseases, ENT diseases, chronic diseases. Environmental report conducted by ICEM Bucharest [21], to express morbidity in investigating the relationship between air pollution and health have used „incidence" and „prevalence": for acute diseases - their incidence was calculated (for 1995) by class of diseases (number of diagnosed new cases reported per 100,000 inhabitants); for chronic diseases was calculated the prevalence (for 1995) by classes of disease (number of existing cases reported per 100,000 population).

Levels of incidence and prevalence by classes of diseases were calculated for Galați town separately for areas that have different exposures (as exposed and unexposed areas) for 1995, Table 8. [21].

Table 8. *Levels of morbidity indicators in Galați*

Diseases	**Areas**			
	Exposed		**Unexposed**	
	Adults	**Children (under 14 years)**	**Adults**	**Children (under 14 years)**
infectious diseases	70.54	9312.6	146.09	6466.49
conjunctivitis diseases	30.41	1985.49	55.10	1423.54
ENT diseases	160.55	3910.50	249.89	3175.97
acute respiratory diseases	3521.09	84015.31	2688.65	54392.54
chronic respiratory diseases	108.25	372.91	78.15	3295.42
other chronic diseases	42.57	377.94	4.48	263.43

To estimate the effects of pollution on the health of the population has become analyzing the morbidity levels (expressed as all phenomena of disease) that can be considered an indicator of the body's response to exposure.

Examination of the trend morbidity levels over a long period of time and comparing them to the national average can confirm or disprove if there is any influence of the presence of pollutants in the environment on the levels of these indices. Table 9 shows the comparative evolution of morbidity for Galati and Romania during 1991-2000 in terms of respiratory diseases.

In terms of respiratory diseases percentage in Galati town compared to the situation on at national level, they were below 1%.

It can be appreciated that the industrial activity of integrated steel mill from Romania (including also the exposure to dust emissions) does not a major negative impact on the health of the population.

Table 9*. Respiratory diseases for all Romania and Galati, during 1991-2000**

Year	1991	1992	1993	1994	1995
România	6350	6887	7188	7321	7439
Galați	52070	63235	55381	48822	43211
	0.82	0.91	0.77	0.66	0.58
Year	1996	1997	1998	1999	2000
România	8060	7160	6913	6584	6749
Galați	42635	11109	29144	42547	40540
	0.52	0.15	0.42	0.64	0.60

* Data provided by the Ministry of Health.

5. Conclusions

Particulate matter (PM) may be generated by multiple sources identified in each process step of an integrated iron and steel plant. They may contain varying concentrations of mineral oxides, metals, metal oxides and some adsorbed organic pollutants.

Sources include thermal processing of materials (coal processing; coke quenching; sinter process; tapping and casting of pig iron, steel and slag; melting and refining into blast furnaces, basic oxygen furnaces, pig iron mixers; installations of secondary metallurgy etc.); air heating furnaces (cawpers); mechanical actions (e.g. crushing, sieving, conveying weighing, loading, unloading etc.); and handling of materials (e.g. raw materials, additive, recycled and waste materials, and by-products).

The level of dust emissions in point-sources placed on industrial site and also on surrounding areas requires a continuous monitoring. The results allow to take necessary measures to reduce the level of dust emissions at hot sources. A dust release affect the immediate worker, but it may spread throughout the workplace and affect the population of the vicinity areas. Based on the analysis of air quality monitoring data and morbidity data can not demonstrate with certainty affirm the influence air pollution (including dust particles in suspension) on the population living in vicinity of the plant. This influence is more likely to plant workers directly involved in its activity.

References

[1]. *** - *Best Available Techniques Reference Document on the Production of Iron and Steel*, December 2001, available on www.epa.ie/downloads/advice/brefs/Iron%20&%20Steel.pdf

[2]. **H. Schoenberger** - *Final draft: best available techniques reference document on the production of iron and steel,* Publications of EC: European Commission, Joint Research Centre, IPTS, European IPPC Bureau, 2001

[3]. **R. Remus, M.A. Aguado-Monsonet, S. Roudier, L. Delgado Sanch** - *Best Available Techniques (BAT) Reference Document for Iron and Steel Production,* European Commission Joint Research Centre Institute for prospective technological studies, 2013, available on http://eippcb.jrc.es/reference/BREF/IS_Adopted_03_2012.pdf

[4]. *** - *Environmental, Health, and Safety Guidelines for Integrated Steel Mills*, WORLD BANK GROUP, apr. 2007, www.ifc.org/ifcext/enviro.nsf/Content/EnvironmentalGuidelines

[5]. *** - *Directive 2008/50/EC on ambient air quality and cleaner air for Europe,* available on http://ec.europa.eu/environment/air/legis.htm

[6]. H.U. Wanner - *Effects of atmospheric pollution on human health*, Journal of Aerosol Science**,** Volume 21, Supplement 1, 1990, pp. S389–S396, Proceedings of the 1990 European Aerosol Conference

[7]. *** - *U.S. Environmental Protection Agency, National Emission Standards for Hazardous Air Pollutants: Integrated Iron and Steel Manufacturing; Final Rule*, (United-States: 40 CFR Part 63, Federal Register/ Vol. 68, No. 97, May 20, 2003), www.epa.gov

[8]. **R. Heather** - *Particulate emissions from a steel works: A quantitative ecological assessment, thesis for the degree of Master of Philosophy*, 2008, http://etheses.dur.ac.uk/2063/

[9]. *** - *Monitoring of particulate matter in ambient air around waste facilities*. Rep. No. 1 844 322610. 2004, Environment Agency, Bristol

[10]. **D.A. Grantz, J.H.B. Gamer, D.W. Johnson** - *Ecological effects of particulate matter. Environment International*, **29** (2-3), 2003, pp.213-239

[11]. *** - *Hazard Prevention and Control in the Work Environment: Airborne* Dust WHO/SDE/OEH/99.14, Chapter 1 - Dust: Definitions and Concepts, http://www.who.int/occupational_health/publications/en/oehairbornedust3.pdf

[12]. *** - *Pollution Prevention and Abatement Handbook*, WORLD BANK GROUP, Airborne Particulate Matter, July 1998, www-wds.worldbank.org

[13]. *** - *Integrated pollution prevention and control, Production of Iron and Steel, draft* February 2008, http://eippcb.jrc.es

[14]. *** - *Best Available Techniques (BAT) Reference Document for Iron and Steel Production*, Industrial Emissions Directive 2010/75/EU (Integrated Pollution Prevention and Control), JOINT RESEARCH CENTRE, Institute for Prospective Technological Studies Sustainable Production and Consumption Unit, European IPPC Bureau, http://eippcb.jrc.ec.europa.eu/,

[15]. Nalini Bhat et.al. - *Technical EIA guidance manual for metallurgical industry,* Prepared for Ministry of environment and forests, Government of India, august 2010

[16]. *** - *Iron And Steel Production, Metallurgical* Industry, 10/86 (Reformatted 1/95), http://www.epa.gov

[17]. *** - *General review of Sintering section of BREF,* Eurofer 2007

[18]. *** - *02 First draft of the revision of the BREF on Production of Iron and Steel* (Feb 2008), http://eippcb.jrc.es/

[19]. **W. Lemmon & Associates Ltd**. - *Research on Technical Pollution Prevention Options for Iron Sintering,* Draft of 2003/05/17 (Canada: prepared for the Canadian Council of Ministers of the Environment, 2003

[20]. P. Finlay et.al. - Section V.D.2**.,** *Guidance by source category: A*nnex C, Part II Source Categories, *Sinter plants in the iron industry*, DRAFT 22/04/04

[21]. *** - *Studiu de evaluare a riscului la ISPAT*-SIDEX Galaţi, ICEM S.A. Bucureşti

[22]. *** - *Raport la Bilanţ de mediu nivel II pentru ISPAT-SIDEX Galaţi. ICEM S.A. Bucureşti*

[23]. M. Koponen, T. Gustafsson, K. Kalliomäki, P.L. Kalliomäki, M. Moilanen, L. Pyy - *Dusts in a steel-making plant, International Archives of Occupational and Environmental Health, October* 1980, Volume 47, Issue 1pp 35-45

THE ANNALS OF "DUNAREA DE JOS" UNIVERSITY OF GALATI.
FASCICLE IX. METALLURGY AND MATERIALS SCIENCE
N^0. 4 – 2013, ISSN 1453 – 083X

RESEARCH REGARDING WORK SAFETY IN THE LOADING ZONE FURNACE

Stefan DRAGOMIR, Marian BORDEI, Viorel DRAGAN
"Dunărea de Jos" University of Galaţi, 111, Domnească Street, 800201, Galaţi, Romania
email: sdragomir@ugal.ro

ABSTRACT

The loading zone furnace is the place where we find work belt conveyors, vibrating screens and feeders, 5-ton hoist, cyclone, scale hoppers, troughs for routing and carriage of waste materials.

The work consists in storing the sorts of raw materials and of used coke and in delivering them to the furnace load recipes.

KEYWORDS: furnace, evaluation, risk level, job security

1. Components of the evaluated work system

1.1. Workload

The task of the worker in the loading zone with raw materials of the furnace is described in the technical working instructions provided by UAF-furnaces section, as follows:

- working instruction at scaffold loading bunkers furnace [1];
- working instruction on unlocking and cleaning pellet hoppers and hopper weighing pad [2];
- technical Instructions regarding the operation and maintenance of protection and safety belt conveyors [3];
- technical instructions on performing cleaning in the pit skips [4].

1.2. Work environment

The main characteristics of the work environment are specified in Analysis reports. According to the analysis report there are exceeds of the permitted values of the following pollutants: particulate coke, ammonia and the presence of noise has also been revealed [5].

The work environment is characterized by:

- high temperature in the warm season;
- low temperature in cold season;
- low lighting level at night;
- presence of draft in some areas of work;
- the presence of carbon monoxide (CO).

2. Research on risk factors at the furnace

2.1. Mechanical risk factors

The main mechanical factors that may jeopardize the safety of furnace worker are:

- grip, drive, crushing by moving machine parts;
- mechanical transmissions without defenders (eg mechanical couplings, drive roller rubber mats from conveyor bands etc.);
- hitting by the auto transport and / or CF during move through the inside unit during travel from home to work and vice versa;
- slip parts, materials, stored without stability at the end of conveyor belts;
- rolling cylindrical parts and materials in storage at the end of conveyor belts;
- fall due to cable breakage skip tank traction;
- flip pieces, parts, materials stored without ensuring stability;
- free fall of parts, tools, supplies from higher rates of employment;
- accidental release of raw material from feed hopper of the furnace;
- throwing objects or particles (eg dust, coke particles of ore, limestone, pellets, nuts, screws, rubber sleeves etc.);
- deviation from the normal trajectory of skip movement or conveyor belts (eg the running line derailment of skip, deviation of rubber mat, etc.).
- jet, eruption of methane or oxygen from the distribution outlets or cracking storms connecting the outlets of distribution and oxy-fuel appliances;

- dangerous contact surfaces or contours (pungent, sharp, slippery, abrasive, adhesive) – not deburring surfaces, hazardous contours in work areas;

- electric or pneumatic vibration of pikamer used for cleaning hoppers, vibrations of vibrating sieves and power during operation.

2.2 Heat risk factors

The main heat risk factors are:

- lowered temperature of metal surfaces affected by cold weather;

- flames - short circuit appeared in electrical installations at buildings or work equipment, fire danger.

2.3 Electric risk factors

The main electric risk factors are:

- electrocution by direct contact – unprotected current paths (eg welding machine terminals);

- electrocution by indirect contact or by electricity or voltage step appearance – metal extended structure, damaged protection, water reservoirs near the current paths, etc.

2.4 Physical risk factors

The main physical risk factors are:

- high air temperature in warm weather;

- low air temperature in cold weather;

- airflow - because of work quota, without effective seal (broken or missing windows), and so on;

- low lighting level during the night;

- noise beyond permissible limit (in pit skip) and below the maximum permissible levels at other limits on the scaffold (as of the analysis);

- natural disasters - ex. earthquake, lightning etc.;

- pneumoniconiosis powders present in workplace air (according to the attached ballot determinations).

2.5. Chemical risk factors

The main chemical risk factors are:

- airborne dusts, gases or vapors or explosive dusts coke, ore, gas leaks and oxygen distribution outlets, and so on;

- the presence of carbon monoxide in the atmosphere of the working area (derived from adjacent work areas - furnace itself).

2.6. Physical stress

The main physical risk factors are:

- state effort - working mainly in the "orthostatic" position [3]

- dynamic effort at work;

- high travel route during the inspection (verification) of work equipment, manual handling of heavy weights during the cleaning and so on;

- vicious positions while replacing rollers on conveyors to unclog funnels at work inside the funnels (enclosed space) etc.;

2.7. Mental stress

The main mental stress risk factors are:

- overwork during weekdays;

- psychological stress because of injury risk.

2.8. Mistreatment of employees

The main mistreatment of employees risk factors are:

- implementation of contingency work operations or other kind of technical work provisions [2];

- wrong positioning of the protective grates storage bunkers;

- incorrect core attached to the lifting installation hook hoist;

- walking in dangerous areas - on the access roads, car travel zone of sieves vibratory conveyors climbing during their operation into the hoppers, and so on;

- entry into the buffer zone from the skip during its operation;

-- confined space entry work without authorization, no access allowed without CO detectors without security measures of labor under the specific instructions;

- fall on the same level: the imbalance, sliding through foreclosure - uneven surfaces loaded with dust, blocked traffic routes, and so on;

- falls from heights: by stepping into the void, the imbalance by sliding;

- accident communications - ex. the other furnace operator on the trestle, with workers of repairing teams, with cowper operator at CAMC, with the head of the band and so on;

- use of work equipment with inadequate technical condition.

3. Measurements and recordings of specific risk factors in the furnace area

After studies and research, targeting the risk factors of furnace workers, there has measured a total of 47 cases from the furnace corresponding specific activities, with each level corresponding to the hazard of the job analysis (diagram of Figure 1).

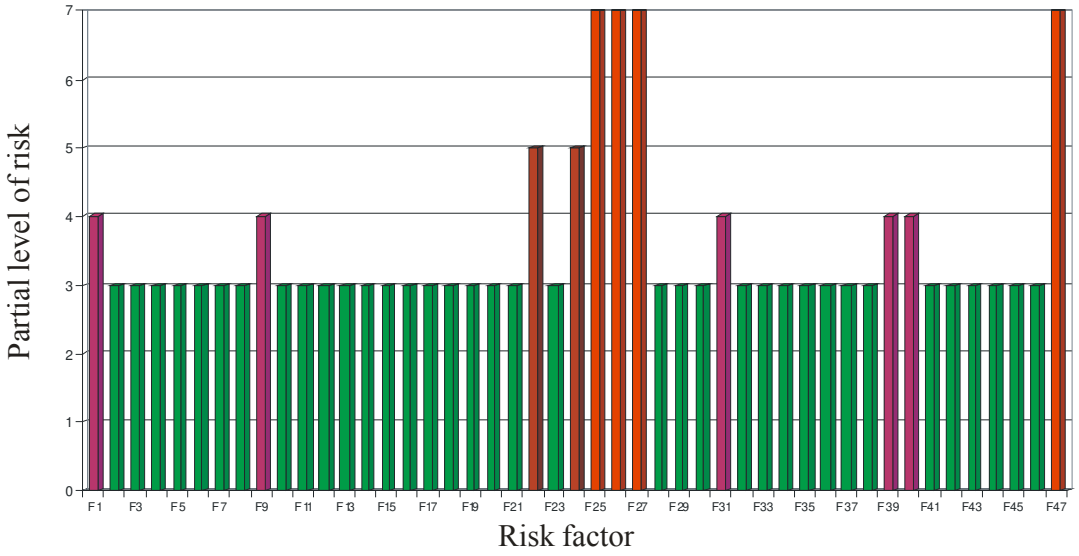

Fig. 1. *Risk factors furnace diagram (partial levels of risk) [2]*

Explaining risk factors F1 to F48, [5] are explained below:

F1-Gripping, driving, crushing by moving machine parts - mechanical transmissions without defenders (eg mechanical couplings, drive roller rubber mats from bands transporter etc.).

F2-Flicking the auto transport and/or CF to move through the inside unit to travel from home to work and vice versa.

F3-Sliding parts, materials, stored without stability at the end of the conveyor belts.

F4-Rolling cylindrical parts and materials in storage at the end of the conveyor belt.

F5-Fall of tank skip traction because of cable breakage.

F6-Flipping pieces, parts, materials stored without ensuring stability.

F7-Free fall of parts, tools, supplies from higher heights.

F8-Accidental discharge of material from the furnace feed hopper.

F9-Design objects or particles (eg dust, coke particles of ore, limestone, pellets, screws, rubber sleeves, elastic couplings, etc.).

F10-Deviation from the normal path of travel of the conveyor belts or skip (eg running line derailment of skip, deviation rubber mat, etc.).

F11-Jet eruption of methane or oxygen distribution outlets or cracking storms connecting the outlets of distribution and oxy-fuel equipment.

F12- Dangerous contact surfaces or contours (stinging, sharp, slippery, abrasive, adhesive) - not deburring surfaces, contours in hazardous work areas.

F13-Electric or pneumatic pikamer vibration used for cleaning hoppers, vibrating sieves vibration and power during operation.

F14-Lowered temperature of metal surfaces touched during winter.

F15- Short flames appeared in electrical installations for buildings or work equipment, fire hazard.

F16-Indirect contact with electricity or voltage step appearance - extensive metal structure, damaged protection, accumulation of water in the vicinity of the current paths etc.

F17-High air temperature in the warm season.

F18-Low air temperature in the cold weather.

F19-Airflow - because of work quota, without effective seal (broken or missing windows) etc.

F20-Low level lighting during nights.

F21-Above the maximum permissible noise -in the pit skip.

F22-Natural disasters - ex. surprise earthquake, lightning etc.

F23-Pneumoniconiosis dust present in workplace air (according to the attached ballot determinations).

F24-Particulate matter in the air, gases or vapors or explosive dusts coke, ore, gas leaks and oxygen distribution outlets etc.

F25-The presence of carbon monoxide in the atmosphere of the working area (derived from adjacent work areas.

F26-Technological process which provides a working environment in accordance with the legislation in force.

F27-Working with one furnace operators in trestle sector in certain areas (isolated).

F28- Blast-furnace work one on trestle in certain areas (isolated) - after taking exchange the inspection or the other Blast-furnace is free, C.O., Bo.
F29-Inadequate training of staff – ex.: work instructions and safety incomplete, etc.
F30-Static effort – work mainly in the „orthostatic".
F31-Dynamic effort at the working activity – high travel route during the inspection (verification) work equipment, manual handling of heavy masses during the cleaning etc.
F32-Vicious positions in the replacing rollers conveyors, hoppers unclog at work inside the funnels (enclosed space), etc.
F33-High rate of activity in some days.
F34-Psychological stress linked to risk of injury.
F35-Execution of contingency operations during work or in a different way than technical norms of work.
F36-Wrong positioning of the protective grates on storage bunkers.
F37- Incorrect attach of the corfs at hook lifting (hoist).
F38- Blast-furnace trouble with each other on the trestle, with workers repair teams with cowper operator at CAMC, the head of the band etc.
F39-Furnace operator other trouble with the trestle, with teams of repair workers with cowper operator at CAMC, the head of the band etc.
F40-Walking in hazardous areas - the car doorways in the range of the vibrating sieves, climbing belt conveyors during their operation into the hopper access door area etc.
F41-The entry in the buffer of the skip during its operation.
F42-Entry into confined spaces without work permit without permit access without CO detectors without security measures of labor under the specific instructions.
F43-Fall on the same level: the imbalance, sliding through foreclosure - uneven surfaces loaded with dust, blocked traffic routes etc.
F44-Falls from height: by stepping into the void, the imbalance by sliding.
F45-Communication accidents - ex. the other furnace operators in trestle sector, with workers repair teams, with cowper operator at CAMC, with the head of the band etc.
F46-Use of work equipment of inadequate technical condition.
F47-Omission of performing operations that ensure safety at work.
F48-Failure to use safety equipment and facilities provided.

Using the risk factors for workers in the furnace can be calculated the overall risk level of the workplace using the formula:

$$\mathbf{N_{rg} = \Sigma R_i r_i \ / \ \Sigma r_i}$$

which:

$\mathbf{\Sigma R_i r_i}$ - is the sum of risk factors considered in the work area;

$\mathbf{\Sigma r_i}$ - is the sum of the partial workplace risk assessment.

To work from the furnace after the introduction of related parameters in Figure 1, level of risk is achieved $N_{rg} = 3.92$.

4. Interpretation of the results of the evaluation of risk factors

Overall risk level calculated for working furnaces equals 3.92, within the "furnace operator" workplace and placed the jobs in the category of jobs with unacceptable level of risk.

This result is supported by the "Assessment sheet furnace operator job boom" which is observed that out of 47 risk factors identified (Fig. 1), 11 above, as part of the risk level, the value of 3, and 4 value fall within the category of risk factors, two being in the category of high risk factors (NVPR = 5), and the other five being in the category of environmental risk factors (NVPR = 4). The 11 risk factors that are unacceptable in the range: F25, F26, F27, F47, F22, F24, F1, F9, F31, F39, F40.

To reduce or eliminate the 11 risk factors (which are ranged as the unacceptable), it is necessary to carry out the general measures listed in "Safety measures proposed" to work "furnace operators in trestle sector."

Regarding the distribution of risk factors generating sources, the situation is as follows (Fig. 2):

- specific risk factors to the means work/equipment work: 36.17%
– specific risk factors to the performer: 27.66%
- specific risk factors to the task: 17.02%
- specific risk factors to the work environment: 19.15%.

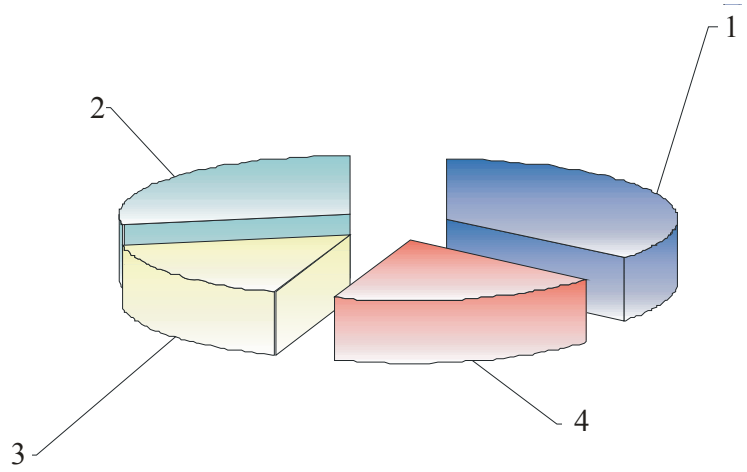

1 – specific risk factors to the means work/equipment work: 36.17%;
2 – specific risk factors to the performer: 27.66%;
3 - specific risk factors to the task: 17.02%;
4 - specific risk factors to the work environment: 19.15%;

Fig. 2. *Distribution of risk factors on sources of job of the furnace insecurity. [2].*

The analysis of the *Evaluation form* shows that 74.47% of the identified risk factors may have irreversible consequences on the performer.

5. Measures and proposals

For job security in the loading zone of the furnace raw materials it is proposed to:

- compliance with legislation on working in areas where toxic substances are present;
- always use the protective equipment supplied;
- monitor the health of furnalists when performing work in areas where toxic substances are present;
- mark of hazardous areas;
- supplies and equipment furnalists sector on trestle with portable detection and signaling the presence of carbon monoxide;
- clearly identify areas where accidents with carbon monoxide frequently occur;
- indicat through safety signs the areas where carbon monoxide may occur;
- develop clear guidelines/procedures in case of carbon monoxide alert;
- monitor the health of the furnace operators in trestle sector;
- review all working procedures and internal guidelines and implications for occupational safety updates, to achieve economic activity at least by the minimum security requirements of the law;
- equip the furnace operator on trestle sector with low voltage lamps (24V) while working in confined spaces;
- compulsory used by the furnace operator on trestle sector with low voltage lamps (24V) while working in confined spaces;
- verify the trestle furnace operator by permanent control of the head band, and/or by sampling the upper superiors on how to perform work in confined spaces;
- mark areas that appear to surpass the maximum allowable noise level;
- supply equipment sector furnace operator trestle with earplugs;
- mandatory use earplugs by furnace operator trestle sector when working in areas where they found exceeded the maximum allowable noise level is excluded;
- conduct periodic medical examination in due time;
- train trestle sector furnace operators to HG No. 493/2006 regarding the exposure of workers to risks arising from noise;
- verify the trestle furnace operators by permanent control of the head band, and / or by sampling from more senior leaders on how to use earplugs;
- repair and install all protective devices in moving organs;
- prohibit removal of protective devices in moving bodies;
- check the physical condition of protective devices for machine parts before work starts;
- mark according to regulations, all hazardous areas that may manifest risk of clamping, training, crushing, impact, etc. by moving machine parts or the mobile parts;
- prohibit the initiation or continuation of work when missing damaged or incorrect placement of protective devices in moving bodies is noticed;
- correct physical demarcation and visible signs of circulation areas;
- train furnace operators in trestle sector about obeying the working instructions and the importance of compliance and job security.

6. Conclusions

To ensure job security at the furnace, the following main conclusions are very important:

- delineation and marking access routes and circulation;
- prohibit climbing or crossing conveyor during operation;
- training of the furnace operators in trestle sector on how to travel in dangerous areas;
- physical demarcation correct and visible signaling to skip buffer zone;
- prohibition of entries in the buffer SCHIP during its operation;
- training furnace operators trestle sector on how to perform the cleaning pads skip;
- verification of the trestle furnace operators by permanent control of the head band, and / or by sampling the upper superiors on how to perform cleaning in holes in the pads of skip.

The work on the furnace does not provide a working environment in accordance with the legislation in force - ex.: area with low lighting, dust presence, use of lighting that is not explosion-proof, the use of lighting lamps that are not under construction explosions and low voltage to perform work in confined spaces (ore and pellet hopper and hopper scales buffer) – the right inspection of the staff and the use of complete and corresponding working instructions.

References

[1].* - Instrucţiunea de lucru la încărcarea buncărelor de la estacada furnalului nr. 5
"I.L. – U.A.F. – F – 001/2006, rev. 0";
[2]. *** - Instrucţiunea de lucru privind deblocarea şi curăţatarea pâlniilor cântar minereu şi pelete şi pâlnilor tampon "I.L. – UAF-F -101/2007, rev.0";
[3]. *** - Instrucţiunea tehnică de lucru privind exploatarea şi întreţinerea sistemelor de protecţie şi siguranţă ale transportoarelor cu bandă „I.L. – U.A.F.-F – 015/2007, rev. 1";
[5]. *** - Instrucţiunea tehnică de lucru privind efectuarea activităţii de curăţenie în groapa schipurilor „I.L. – U.A.F.-F – 086/2007, rev. 2".
[6]. *** - Cartea lucratorului la furnal- Ed. Interna .U.A.F.sect. Furnale. Rev. 2012.

THE ANNALS OF "DUNAREA DE JOS" UNIVERSITY OF GALATI.
FASCICLE IX. METALLURGY AND MATERIALS SCIENCE
N^0. 4 – 2013, ISSN 1453 – 083X

PARTICULAR ASPECTS CONCERNING INSTABILITY AT INTERFACE LCAK STEEL - SLAG (CaO-Al_2O_3) DUE TO TRANSFER OF SULPHUR, EVALUATED USING THE MODEL REICHENBACH-LINDE ADAPTED

Petre Stelian NITA
"Dunărea de Jos" University of Galaţi, 111, Domnească Street, 800201, Galaţi, Romania
email: pnita@ugal.ro

ABSTRACT

Based on the model of Reichembach and Linde, adapted to the interface in the system LCAK steel-(CaO-Al_2O_3) slag at temperature 1873.15K, it is shown that transfer of sulphur from steel to slag could promote interfacial Marangoni instability, proven by positive and relative small values of Marangoni dimensionless number, related to slag. Positive values of critical Marangoni number have been found in the rage of dimensionless wavenumber a $a_0<a<a_\infty$, $a_0 = 2.881255 \pm 5 \cdot 10^{-6}$ and $a_\infty = 3.0058 - 3.006$ (asymptote) for a characteristic length d=100μm. In the range of values of the dimensionless wavenumber a=2.9−3.0, corresponding to wavelength λ= 216.66−209.44μm, a relation $Ma_{c,slag} = (0.0957a + 0.618 + \frac{1}{L_S \cdot D^*}) \cdot e^{168.69a^2 - 947.51a + 1331.7}$, *containing also the sulphur partition ratio between slag and steel L_S and ratio of diffusion coefficients of sulphur in slag and steel D^*, was established giving values of critical Marangoni dimensionless number. Values $Ma_{c,\ slag}=20-5200$ are obtained for $L_S=10-1000$, supporting the idea that slag is active in the dynamics of interface steel-slag with consequences on the steel quality and kinetics of important processes of refining, contrary to certain evaluations seeming to be insufficiently substantiated. Stationary instability in the form of short wavelength waves could develop in the mentioned conditions or, considering the asymptote found at $a_\infty = 3.0058-3.006$ oscillatory waves could develop.*

KEYWORDS: interface, steel, slag, sulphur transfer

1. Introduction

Capillarity during steelmaking and refining is recognized as an important phenomenon in hydrodynamics of interface in liquid systems in general, including those formed by ferrous alloys, slags and atmospheres[1]-[7], but the analysis of its manifestations, according to the well known achievements in related systems, also following a philosophy close to them, is not yet approached practically. In most of cases, facts derived from technological practice and results of experiments are linked only qualitatively or empirically with certain parameters of capillarity. A more consistent analysis is imposed by needs of high quality steels characterized, among other requirements, by low and extremely low contents of harmful elements as oxygen, sulphur and phosphorus and a high cleanliness state, concerning different non-metallic inclusions.

Some qualitative considerations have been reported [2]-[5], also some quantitative but restricted to particular cases [6][7] and in both situations without treating in particular manner specific capillarity aspects related to each of fluids forming the interface.

Based on the simplified "one layer" model applied to slag, it was shown[8][9] that sudden local variations of the sulphur content, taken as inhomogeneities, of order $10^{-3} \div 10^{-2}$ mass% in CaO-Al_2O_3 slags, typical for desulphurization process, could excite a Marangoni instability and could lead to enough high values of solutal Marangoni number (Ma), overcoming also enough its critical threshold value $(Ma_c \cong 80)$ established according to Pearson

[10]. These suggest that Marangoni flow and convection could take place at a scale of several hundreds of micrometers at interface steel-slag by advection and further by convection, considering the continuity law. The respective analysis was performed in certain established conditions, ensuring the most favorable conditions, i.e. minimal conditions required for solutal Marangoni instability, based mainly on an argued scaling of the characteristic lengths and characteristic time durations of different competing physico-chemical actions at interface on slag side.

Sternling and Scriven [11], based on their linear analyze of stability and in absence of any scaling of characteristic time and length, have established seven cases when interfacial turbulence is usually promoted, in a system of two superposed immiscible fluids of semifinite heights. From them, the main situations are: 1-solute transfer out of the phase of higher viscosity; 2- solute transfer out of the phase in which its diffusivity is lower; 3- large differences in kinematic viscosity and solute diffusivity between the two phases; 4- steep concentration gradients near the interface; 5- interfacial tension highly sensitive to solute concentration. Taking into account data from the Table 1, according to statements of Sternling and Scriven statements [11], there is no interfacial convection due to sulphur transfer from steel into slag, because it is against of points 1 and 2 from above. In the same time, according to point 3 and possible to point 4, interfacial turbulence could be promoted at interface steel-slag.

Several factors and parameters oppose to instability in a system of two immiscible fluids with interface. Firstly, the presence of the heavier fluid (steel) bellow the lighter one (slag) acts to stabilize the interface. Secondly, the presence of the interfacial tension between two immiscible fluids is a stabilizing factor of interface and in a certain configuration of the system it introduces a particular minimal wavelength necessary to promote instability.

Regarding the system steel-slag, evaluations using related criteria based on a generally accepted procedure, are totally missing. In the case of desulphurization process of LCAK steels treated under $CaO-Al_2O_3$ slags, the missing could be due perhaps to the transfer of sulphur from steel into slag, despite this solute is a surface tension active both in slag as in steel, according to the first two criteria [11] cannot promote interfacial turbulence, contrary to the physical evidence of an observed strong turbulence accompanied by emulsification [1]. Another reason could be that in steel refining frequently intended external actions during technological process could be totally prevalent at macro-scale, shadowing the surface driven phenomena at micro-scale, further making them to seem as negligible.

When the two layer model is considered in the system liquid steel-slag, important problems appear because it is necessary to establish how the interface could be considered, sharp or diffuse. Because steel and slag are immiscible liquids of extremely different nature and properties, the interface is considered in this paper as a sharp one. This seems to be quite acceptable for stationary cases corresponding to resting state or to zero relative velocity of the liquids forming the interface, on certain substantial depths of the layers in both liquids. This option is in connection with the present analysis which is dedicated to establish the minimal conditions of the marginal hydrodynamic stability (Marangoni) when the interfacial tension is perturbed by variations of solutal origin, enough strong, continual and persistent, i.e. local fluctuation of concentration of a surface tension active solute, able to promote Marangoni flow.

The approached problems in this paper are:

i) to evaluate the numerical evolution of Ma_c upon characteristics of wave function when sulphur is transferred from steel to slag through the interface;

ii) to establish the domain of positive values of Ma_c related to slag properties, proving that possible Marangoni instability takes place at an interface steel-slag when sulphur is transferred from steel to slag.

This is done in the case when the interface between steel and slag results from boundary layers of thickness resulting from theory of momentum dissipation and the whole system is reduced by truncation at layers having such established thicknesses.

2. Adaptation of the model Reichenbach-Linde to the particular case of LCAK steel – CaO - Al_2O_3 slag interface

The main chemical reaction describing the desulphurization process of LCAK steel under $CaO-Al_2O_3$ slags is the following:

$$[S]+(CaO)+2/3[Al]\Leftrightarrow(CaS)+1/3(Al_2O_3)\ \Delta G_T^0<0 \quad (I)$$

In the analysis performed in this paper the thermochemical effects at interface in both liquids will be neglected because corresponding thermal diffusion coefficients in steel and slag are higher with one to two order of magnitude than the corresponding mass diffusion coefficients, also because of the considered smallness of the concentration inhomogeneity of sulphur [7]. The analysis is focused on the capillary consequences of the main process consisting in the transfer of sulphur from steel into slag, mainly to promote the Marangoni flow and convection in slag, which at the first sight is in contradiction to behavior predicted by Sternling and Scriven model[11]

Microconvection is a flow which originates from random disturbances in the temperature or concentration field. For these random disturbances to amplify, the system needs to be unstable.

The Marangoni number for the solutocapillarity case is frequently expressed as it is shown in the rel. (1), according to [10]:

$$Ma = \frac{\left(-\frac{\partial\sigma}{\partial c}\right)\cdot c_0 \cdot L}{\mu \cdot D} \quad (1)$$

The form given in rel.(2) was used in the model Reichembach-Linde [12]:

$$Ma = \frac{\left(-\frac{\partial\sigma}{\partial c}\right)\cdot \frac{\partial c}{\partial z}\cdot d^2}{\mu \cdot D} \quad (2)$$

Significance of factors in the rel. (1) and (2) is the following:

$(\partial\sigma/\partial c)-$ is the dependence of surface/interface tension on concentration; it is called frequently surface/interface concentration coefficient; it is taken as a constant value in order to be in agreement with the Boussinesq approximation extended to surface/interface tension dependence on concentration of surface active solute, procedure being necessary to perform a linear analyses;

c_0- is a characteristic concentration or a characteristic difference of concentration Δc (rel.1);

$\frac{\partial c}{\partial z}-$ is the concentration gradient (rel.2);

L – is a characteristic length (rel.1) [10];

$d-$ unit length (rel.2) [12];

D – is the diffusivity of the surface active solute in the phase of interest;

$\mu-$ is the dynamic viscosity of the considered phase.

Marangoni number expresses a ratio of a characteristic diffusion or diffusion-viscosity time and a characteristic time for Marangoni driven flow. Different relations of Marangoni number appear in the literature, which makes any comparison to be difficult in certain conditions. Marangoni numbers express the ratio of surface tension forces and viscous drag. In this respect, the critical value of The Marangoni dimensionless number is Ma_c and shows how many times the perturbation of the surface tension has to be greater than the visco-diffusion forces, in order to promote flow.

A characteristic concentration gradient is incorporated in the Marangoni number given in rel. (2) and it could be evaluated quantitatively in the form of ratio of finite differences $\frac{\Delta c}{\Delta z}$.

The establishing of the depth Δz represents the main challenge and requires a more substantial comment in order to be solved correctly. The same is valid also for the finite difference of concentration c which could take naturally a wide range of values related to slag, from those of magnitude of statistical concentration fluctuations (3-5% from the mean value obtained by chemical analysis inclusive the maximal solubility value of sulphur), up to major inhomogeneities, as it was signaled in steel [6] and which could be several hundreds times higher than the bulk concentration of sulphur in steel.

Depending on the system, many other expressions available in literature may be used, but this must be done carefully because wrong selections of representative parameters and of edificatory considered experimental data have been signaled, in analyzing the Marangoni effect based on them.

The model Reichenbach-Linde [12] investigates the stability of plane interface using the linear hydrodynamical stability theory and it is was used in evaluation of neutral and oscillatory marginal stability. Values of critical Marangoni dimensionless number from rel. (2), related to upper phase (1), have been computed for marginal states of stationary and oscillatory instabilities. A flat interface between two immiscible fluid layers of finite height was used and a term, expressing the gravity effect (Weber dimensionless number), was introduced as required in the balance of forces on the normal direction in order to obtain critical Marangoni numbers.

Finite depths of the layers in each fluid are taken those where the temperature perturbation vanishes, and it is shown that all considerations and relations from thermocapillarity case and could be used in the solutocapillarity case, respecting the equivalence principles in replacing the involved quantities from thermocapillary case to solutocapillary case. Flatness of interface was introduced in the form of capillary dimensionless number as Crispation number, for which condition $Cr=0$ is required.

The resulting set of basic relations and definition of parameters is in the form of the relation presented bellow. Further, the authors used in their numeric simulations relative arbitrarily selected value of ratios of important parameters of the liquid phases forming the interface in question and they did not established characteristic lengths using the method of scaling, but only a generic unit length d. The intrinsic interfacial viscosity is neglected in the model Reichembach-Linde [13] similarly to in the model Sternling-Scriven [11]. The main relations, quantities and parameters of the model Reichembach-Linde [12], adapted to the mass transfer of sulphur from steel (phase 2) to slag (phase 1) are the following:

$$Ma_{slag} = \frac{\left(\varepsilon + \frac{1}{L_s \cdot D^*}\right) \cdot \left(H_1 + H_2 \frac{G_1}{\mu^* \cdot G_2}\right)}{-\frac{1-E_2}{(1-E_1)(1+E_2)} L_1 + \frac{D^*}{1+E_2}\frac{G_1}{G_2} L_2} \quad (3)$$

Ma_{slag} – critical Marangoni dimensionless number related to slag phase;

$$D^* = \frac{D_{(S)}}{D_{[S]}}; \quad (4)$$

where: $D_{(S)}$, $D_{[S]}$ – is the mass diffusion coefficient of sulphur in the slag and respective in the steel.

$$\mu^* = \frac{\mu_{slag}}{\mu_{steel}} \quad (5)$$

where: μ_{slag}, μ_{steel} – is the dynamic viscosity of the slag and respective of the steel.

$L_{[S]} = \frac{(\%S)}{[\%S]}$-is the instant partition ratio of sulphur, between slag(%mass) and steel[%mass]; (6)

$$\varepsilon = \frac{(1-E_2)(1+E_1)}{(1+E_2)(1-E_1)} \quad (7)$$

$a = k \cdot d$ - is the dimensionless wave number; (8)

d - is a characteristic length, in [m]; (9)

k - is the wave number, in [m^{-1}]; the wavelength is $\lambda = 2\pi/k$, in [m]; (10)

$$l_i = \frac{h_i}{d} \quad (11)$$

h_i -is the thickness of layer i (1,2), in [m]; (12)

$$E_i = e^{-2al_i} \quad (13)$$

$$H_i = 8a^2\left(1 - E_i^2 - 4al_iE_i\right) \quad (14)$$

$$G_i = -(1-E_i)^2 + 4a^2 l_i E_i \quad (15)$$

$$L_i = (1-E_i)^3 - 4a^3 l_i^3 E_i (1+E_i) \quad (16)$$

Relations (7), (14)-(16) are computational parameters obtained by grouping, with no physical meaning, but useful for easiness of computations.

The model [12] contains mathematical expressions based on exponential functions in base e (Euler number e ≈2.71828) and due to this, the Marangoni dimensionless number according to the relation(3) never could reach the value zero and the graphic of Ma=f(k) never could intersect the axis of abscise containing the wave number in any form (explicit or implicit variable). Therefore the graphic, either is over abscise, or below it. This means the Marangoni number reaches only a strictly positive value or a strictly negative one.

Also, it is shown in many basic papers that if an asymptote to the graphic would appear, than the development of a possible instability will change from short waves stationary instability to an oscillatory instability even in the form of dilatational waves. The results found in the present paper based on the model [12] show that such zone was found.

For the first time the model [12] was adapted in the present paper to the particular interface LCAK steel-(CaO-Al_2O_3) slag at temperature 1873.15K. From the whole configuration of the technological system steel-slag, which is extended at infinity, in rectangular coordinates, a small portion will be considered, this having the height of layers according to the preliminary scaling of the characteristic heights and length. This is a first difference in comparison with the approach used in the basic model [12], where arbitrary dimensions and their ratios have been considered. In the present paper all ratios containing quantities h_i, d and their ratios, involved in the model, have fixed values, because of the real case considered. In what it follows the adapted model from the present paper is used to evaluate conditions of stability/instability of the mentioned interface in flatness conditions under other particular conditions which are imposed either by the specific values of parameters of phases, or due to the specific scaling which is used. Careful scaling of specific and characteristic lengths and dimensions involved in the present analysis is an important key for a correct approach of the problem, even from its starting point, especially as this has not been done before from various reasons, in many other previous analyzes. Many papers report theoretical analyzes, considerations presented as pertinent, experimental and modeling results, in various liquid systems, which present a certain degree of similarity with the system steel-slag, considered in the present paper. There are different characteristic lengths, specific to each dominant action, therefore the analysis of stability/instability at interface steel-slag and of the neighboring regions in each phase must be performed in known conditions, acceptable physically for all physical and physicochemical competing actions. Scaling had in view conditions ensuring that the Marangoni effect will be the dominant action, among the other physical and physicochemical competing actions, in such high degree prevalence that it will be possible to be directly evaluated as state.

3. Evaluation of marginal stability at interface in established conditions

3.1. Establishing relevant values of parameters involved in the adapted model

Preliminary testing of the model to predict conditions of occurrence stability/instability of the flat interface LCAK steel-(CaO-Al_2O_3) slag is

performed for the following conditions exposed in the Table 1.

The layer thicknesses (h_1,h_2) selected for computations, in the present paper, are slightly higher than the values given in the Table 1. This represent an acceptable truncation of the boundary layer, used frequently in large open systems in nature and the manner to treat similar problems could be validated also in systems at low dimensional scales, like the system in question in the present problem.

Fully respecting the established notations and their meanings, the selected values are respectively h_1=400x10^{-6} m on the slag side, h_2=50x10^{-6}m on the steel side and d=100x10^{-6}m along the interface slag-steel, related to the slag side, with double function. Thus, in the acceptance of the present paper d represents the characteristic length, according to the definition given initially [12], but also represents a distance, along the interface, on which the perturbation of surface tension, due to perturbation of interfacial concentration of sulphur related to the slag side is enough strong, continual and persistent, to produce Marangoni flow and convection. Computations of edifying dimensionless numbers for values of interfacial tension in the range of sulphur content in slag (0-2.92mass%S and σ_i =1.235-1.285 N·m^{-2}) and gravitational acceleration g=9.81m·s^{-2} give the following results:

-Bond number at interface on the slag side:

$$Bo=\frac{\rho_{slag}\cdot g\cdot d^2}{\sigma_i}=(2.05-2.13)\cdot 10^{-4} \qquad (17)$$

Bo number is used instead of Weber dimensionless number.

-Crispation number representing the inverse of capillary number:

$$Cr=\frac{\mu\cdot D}{\sigma_i\cdot d}=(2.29-2.38)\cdot 10^{-7} \qquad (18)$$

The values express that interfacial tension prevails very strong over gravity ($Bo<1$ for simply prevailing) and the necessary required condition for flatness of interface ($Cr<10^{-5}$) is accomplished. More, in the case of a small perturbation of interfacial tension slag – steel $\Delta\sigma_i$ due to an inhomogenity of sulphur content in slag Δ(S), the condition ($Bo<1$) still is satisfied if Δ(S)> 0.01%mass, using a modified Bo dimensionless number, containing at denominator $\Delta\sigma_i$ instead of σ_i in the rel. (17).

The parameters considered in the present paper, referring to the considered slag-steel system and the adapted model, fully satisfy the set of conditions of the initial model Reichembach-Linde[12].

Following values of computational parameters in the adapted model have been established using data from Table 1.

$$\frac{h_1}{d}=8\ ;\ \frac{h_2}{d}=0.5 \qquad (19)$$

Table 1. *Physico–chemical quantities and parameters of (60%)CaO-(40%)Al_2O_3 slags and LCAK steels, at the temperature 1873K*

Quantity, symbol, units	phases, values, references	
	(1)Slag	(2)Steel
Density, ρ, kg·m^{-3}	2685 [13]	7000[14]
-Dynamic viscosity, μ, Pa·s;	0.1184 [13]	0.007 [14]
	$4.41\cdot10^{-5}$	$1\cdot10^{-6}$
-Kinematic viscosity, ν , m^2/s	$\eta^*=\eta_1/\eta_2=16.914$	
Diffusion coefficient of sulphur D_S, m^2·s^{-1}	$2.48\cdot10^{-10}$ [16]	$4{,}4\cdot10^{-9}$ [14]
	$D^*=D_1/D_2=56.36\cdot10^{-3}$	
Solubility of sulphur, %mass	2.092 [17]	high
Concentration coefficient of interfacial tension , $\frac{\partial\sigma_i}{\partial(\%S)}$, 10^{-3}N·m^{-1}· (%)$^{-1}$	-23.9 - average of values related to sulphur content in slag and using relation: $\sigma_i=0.7353(\%S)^2-25.504(\%S)+1284.8$ [9]	
Boundary layer thickness, based on concept of energy dissipation in the boundary layer, h_i, x10^{-6} m	358.933 (*)	43.035 (*)
	355.76 (**)	49.021 (**)
	$h^*=h_1/h_2=\{8.34;7.257\}$	

(*) obtained using rel.given in [18];
(**) obtained using rel. given in [19]

3.2. Computational results

The results of computation using the adapted model, the values of ratios of involved quantities (Table 1) and the parameters given in the rel. (19) are presented in the fig. 1 and fig.2 where the specific dispersion relation of the critical values of Marangoni factor Ma' are given in the form $Ma_c=f(a)$ (a-dimensionless wave number, rel. 8), because of the smaller values on the abscise.

The critical Marangoni factor Ma' is derived from rel. (3) and represents the part of the critical Marangoni dimensionless number (rel.3), depending purely of geometrical configuration of the interface and the elements derived from expanding the perturbation in Fourier components (normal modes).

$$Ma'=Ma_c/F \qquad (20)$$

The factor F contains the influence of mass transfer and partition ratio of sulphur:

$$F=\left(\varepsilon+\frac{1}{L_S\cdot D^*}\right) \qquad 21)$$

The magnitude of the factor F also depends on the dimensionless number a because of ε (rel.7) and according to the figure 3 it has slight dependence on values of a, but represents the main part of factor F in real technical situation because $L_S>1$. Therefore the fraction in rel.(21) has negligible value compared to value of ε.

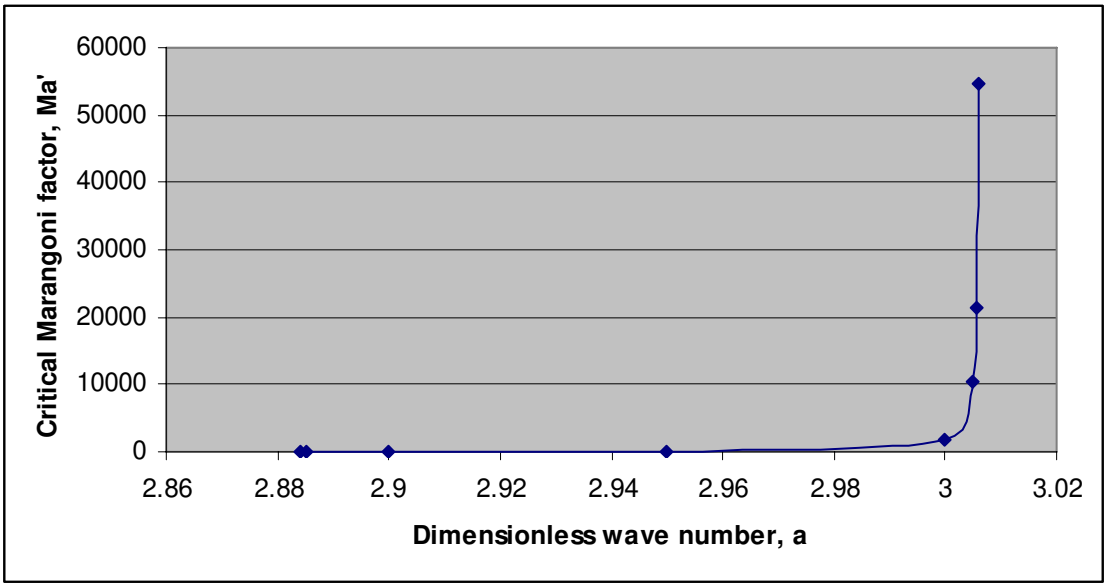

***Fig. 1**. Marangoni Factor Ma' function of dimensionless wave number a*

The graphic of function is below the abscise up to a point of a value a_0 =2.881255±5·10^{-6}, not belonging to the domain of values of the dimensionless wave number, that means negative critical Marangoni numbers. Further, this means that in this range no instability occurs when sulphur is transferred from steel to slag through interface, fully in agreement with case presented by Sternling and Scriven [11] but valid in case of interface of infinite depths layers. Further, the numerical evolution of dispersion relation $Ma_c=f(a)$ is extremely interesting and it is shown in this paper for the firs time.

The most important part and in the same time a contribution revealed in the present paper, to these specific problems, consists in the fact that further, overcoming the value a_0, values of Ma_c become positive and evolve by positive values to an asymptote which was established numerically in this case at the value a_∞=3.0058−3.006. A better resolution in positioning the asymptote was not possible based on the computations technique used, though other three decimals have been computed. However, the results are very good because the values of a_∞ give by conversion, using rel. (8)-(10), an extremely narrow interval of the wavelength value , λ=209.021−209.035)·10^{-6} m. An exact finite value could not be obtained because of the exponential functions based on rel.(8).

The values of Ma_c evolve in the interval $0<Ma_c<\infty$ upon values of dimensionless wave number a, $a_0< a < a_\infty$ and represents limits of marginal state of stationary and/or oscillatory instabilities.

From the fig.2 an interval of values a=2.883 −3.0 results, where Ma'= 1.667− 1662 that lead to moderate values of Ma_c as it is shown in the Fig. 3. These values suggest that interfacial instability of interface steel-slag could occur in the form of short waves, due to the transfer of sulphur from steel to slag.

In the range of dimensionless wave number a=2.9 − 3.0, Marangoni factor Ma' presents a strong linear dependence given by the relation:

$$Ma' = e^{168.69a^2-947.51a+1331.7} \qquad (22)$$

Presenting the coefficient of determination R^2 = 1.0.

Further it results that the values of the critical dimensionless number Marangoni are given by the simple relation:

$$Ma_{c,slag} = F\cdot Ma' = (0.0957a + 0.618 + \frac{1}{L_S \cdot D^*})\cdot \cdot e^{168.69a^2-947.51a+1331.7} \qquad (23)$$

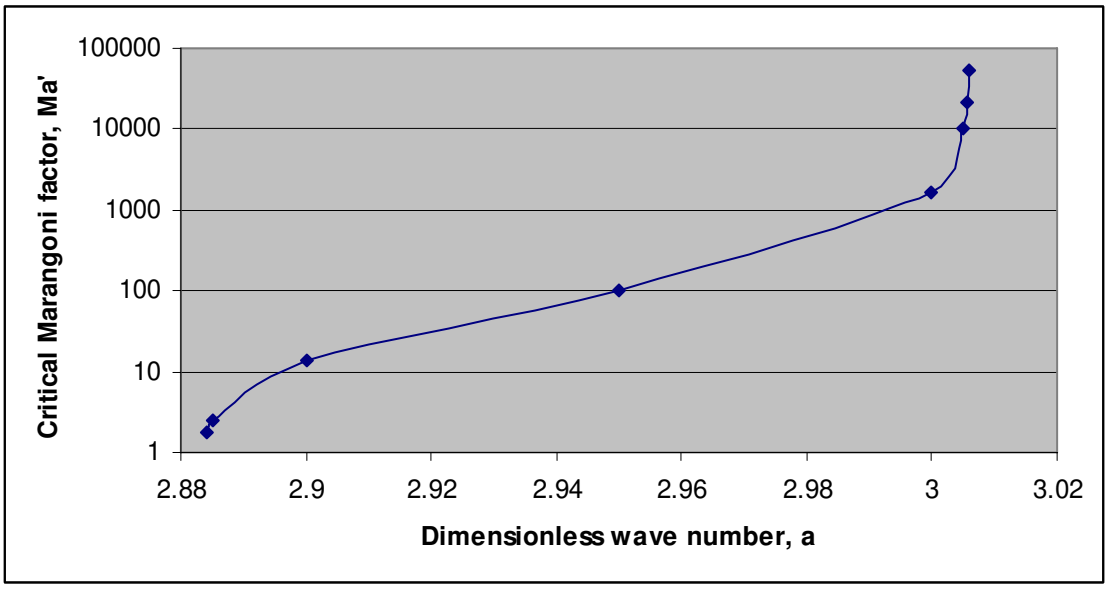

Fig. 2. *Marangoni Factor Ma' (in logarithmic scale) as function of dimensionless wave number a*

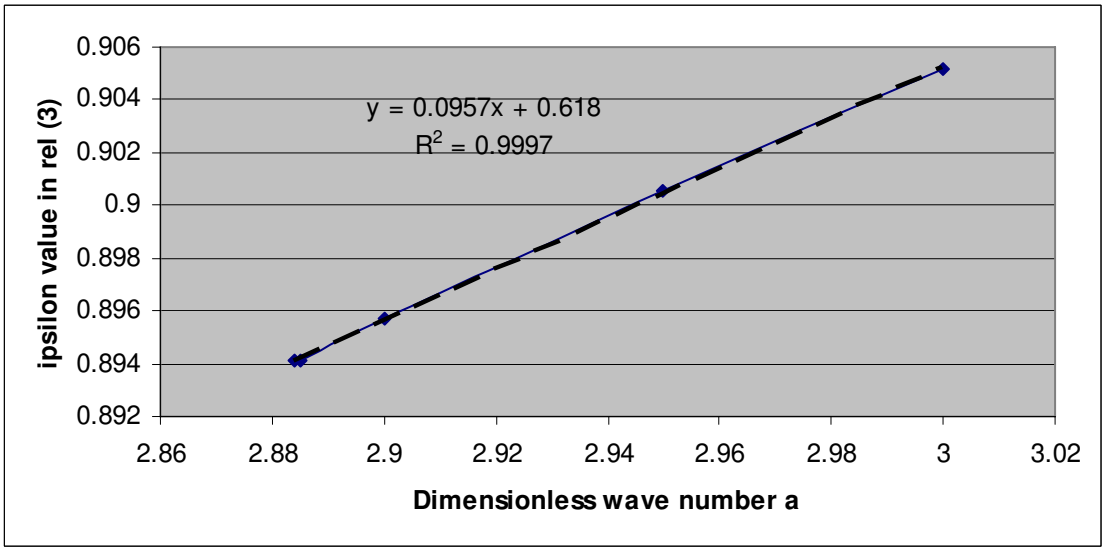

Fig.3*. Values of ε factor, in rel.(3), upon the dimensionless wave number a*

Rel. (23) is valid in the interval of dimensionless wave number values $a = 2.9 - 3.0$ and values of critical Marangoni number Ma_c are presented in the Table 2 for the system considered here and values of the sulphur partition ratio $L_S \in \{1; 10; 100; 1000\}$ which are frequent in practice of desulphurization under slag.

Table 2. *Values of $Ma_{c,slag}$ in the domain of values a=2.9−3.0, at representative values of L_S.*

L_S / a	1	10	100	1000
2.9	259.053	43.214	21.630	19.471
2.92	514.364	86.053	43.221	38.938
2.94	1168.859	196.117	98.843	89.115
2.96	3039.036	511.543	258.704	233.42
2.98	9048.512	1527.086	774.943	699.73
3.0	30824.812	5217.453	2656.717	2400.643

4. Commentaries and conclusions

It was shown that the system LCAK steel−(60%Ca0+40%Al_2O_3) slag at temperature 1873.15 K , during transfer of sulphur from steel to slag could be evaluated from the point of view of stability/instability induced by this transfer. This was done using Reichembach-Linde model [12] which was adapted on the base of physico-chemical parameters of steel and slag. The necessary condition consisting in limited heights of the layers of steel and slag has been realized by truncation method based on the theory of momentum dissipation, using relations that give data in good agreements [18][19].

The results are finally presented in the form of data in table 2 as values of $Ma_{c,slag} = f(a)$ using preliminary results in form of factors f and Ma'. These results show that the condition $Ma_{c,alag} > 0$ is accomplished in a small region of values of the dimensionless wave number a, $a_0 < a < a_\infty$, $a_0 = 2.881255 \pm 5 \cdot 10^{-6}$ and $a_\infty = 3.0058 - 3.006$. From this region, an even smaller extended region of a values ($a = 2.9 - 3.0$) equivalent to wave lengths $216.6 - 209.44 \mu m$ corresponds to low and moderate values of $Ma_{c,slag} = 20 - 5217$ at $L_s = 10\text{-}1000$, which seems to be enough easy to be touched and overcome in the technical conditions of desulphurization in current refining processes.

A shorter explanation of this behavior of the system LCAK steel−(60%Ca0+40%Al_2O_3) slag at temperature *1873.15K*, could be that sulphur, once being transferred at interface on the slag side, at certain values of its partition ratios L_s because of the resistance to mass transfer by diffusion inside of slag, acts as an interfacial inhomogeneity and produces a perturbation of the surface tension which is relaxed by flow(mass transport) along the interface, if this perturbation is enough high, persistent and continual. In these conditions, current values of $Ma_{slag} > Ma_{c,slag}$ and ratios $Ma_{slag} / Ma_{c,slag}$ have high values leading to occurrence of Marangoni convection. Stationary instability in the form of short wavelength waves could develop in the mentioned conditions or, considering the asymptote found at $a_\infty = 3.0058 - 3.006$ oscillatory waves could develop.

The narrow interval of a/λ values, found in this research, where the values of $Ma_{c,slag}$ are positive and relative small, allowing occurrence of instability enough easy, could represents what is called a selection mode of wavelength in Marangoni convection, concept which is not enough clarified and argued, but frequently signaled and presented, often with some restraint and caution.

References

[1]. Deng J., Oeters F. - Steel Res., **61**(1990), 438
[2]. Olette M. - ISIJ International, **33** (1993) 1113-1124
[3]. Belton G.R., Evans T.J., Strezov, L. Phil - Trans. R. Soc. London A, **356**(1998), 941-953
[4]. Chung. Y., Cramb A.W. - Metall. Mater.Trans.B, **26**(2000) 957-971
[5]. Yin H, Emi T. - Metall Mater Trans B, **34B**(2003), 483-492
[6]. Rhamdhani M.A., Brooks G.A. and Coley K.S. - Metall. Mater.Trans.B, **36B**(2005), 219-227
[7]. Rhamdhani M.A., Brooks G.A. and Coley K.S. - Metall. Mater.Trans.B, **36B**(2005),591-604
[8]. Nita P.S. - Mat.Sci. EngA Struct, **495**(2008) 320–325
[9]. Nita P.S. - The Annals of "Dunarea de Jos" University of Galati Fascicle IX Metallurgy and Materials Science 3(2010), ISSN 1453-083X, 5-14.
[10]. J.Pearson - J.Fluid Mech., **4**(1958), 489-500
[11]. Sternling C.V., Scriven, L.E. - AIChE Journal, **5** (1959) 514 – 523
[12]. Reichenbach J., Linde H. – J Colloid Interf Sci **84**(2) (1981) 433-443
[13]. *** - Slag Atlas, 2nd Editions, Verlag Stahleisen, D-Dusseldorf, (1995)
[14]. Kawai Y. and Shiraishi Y. - Handbook of Physico-Chemical Properties at High Temperatures, ISIJ, Tokyo (1988).
[16]. Jonsson L., Du Sichen, Jonsson P. - ISIJ int. **38**(1998) 260
[17]. Özturk B., Turkdogan E.T. - Met. Sci. 15(1984) 260
[18]. Bulicka J., Prochàzka - J. Chem. Eng. Sci., **31**, 1976, pp. 137–146.
[19]. L.D. Landau, E. M. Lifshitz - Fluid Mechanics, Pergamon Press, Oxford, (1984)

THE ANNALS OF "DUNAREA DE JOS" UNIVERSITY OF GALATI.
FASCICLE IX. METALLURGY AND MATERIALS SCIENCE
N^0. 4 – 2013, ISSN 1453 – 083X

STATIC ANALYSIS OF THE STRUCTURE TYPE TANK THERMALLY

Ionel PETREA
"Dunărea de Jos" University of Galaţi, 111, Domnească Street, 800201, Galaţi, Romania
email: ipetrea@ugal.ro

ABSTRACT

This paper consider finite element analysis for structural analysis of a tank under thermal loadings. Geometric modeling is done in CATIA and for finite element analysis the author used FEA module in Catia. The aim is to determine von Mises stress field, deformed mesh and thermal loadings.

KEYWORDS: thermal fields,Von Mises stress, displacement field, restrictions, loads

1. Introduction

Finite element method (FEM - Finite Element Method) is one of the best methods of performing calculations and simulations in engineering.

CATIA software contains Structural Analysis modules, which is a suitable for advanced finite element analysis.

The steps in finite element analysis are as follows:

- three-dimensional modeling of components assembled using CATIA Part Design and CATIA sketcher modules;
- insert all component parts using CATIA Assembly Design module;
- application of a material to the assembly components;
- accessing CATIA Structural Analysis module and determination of the type of analysis;
- definition of nodes and elements (a process called meshing) and it's editing;
- setting restrictions;
- adding loads for the model;
- performing analysis calculations;
- visualization and interpretation of the results.

A thermal field in the reservoir structures leads to tension and the tension distribution is useful in the design product phase. Distribution and value of tensions are very important in assembly design of the structure of the tank.

Figure 1 shows the schematic of the mechanical structure of the boiler, composed of a reservoir and heating, for heating of water. The assembly of the tank and heating system is made a specific fitting element.

The application aims to determine maximum values of Von Misses stress, to displacement produced by thermal field acting on the system heating temperature at T = 100°C and the gravitational acceleration g = 9.81m/s^2. In this respect, connection with the modeling of the reservoir is achieved through a restriction that requires cancellation of the 6 degrees of freedom.

Analyzed structure is made of steel OL37, with the following mechanical characteristics: longitudinal modulus E = 2.1 x 10^{5}N/mm^2, *Poisson ratio* γ = 0.3 and density ρ=7800kg/m^3.

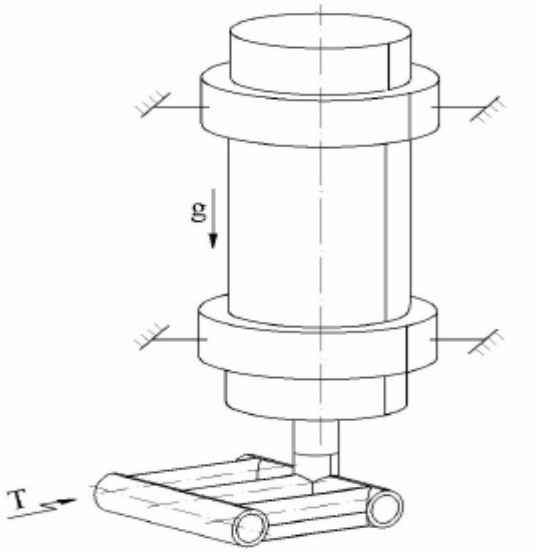

***Fig.1** Boiler 3d model*

2. Geometric modeling

The ensemble consists of two components: the reservoir and heating structure. Using CATIA Part Design and CATIA Sketcher modules the authors designed the two components (Figure 2 and Figure 3).

Fig. 2. *Reservoir*

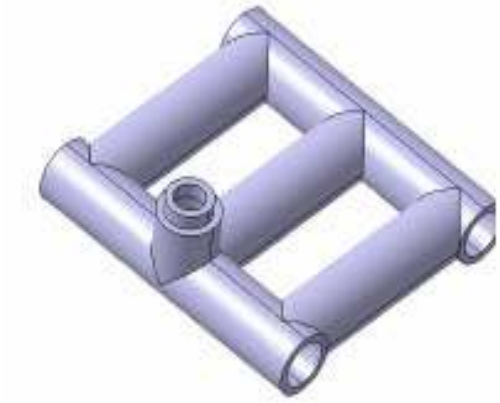

Fig. 3. *Heating structure*

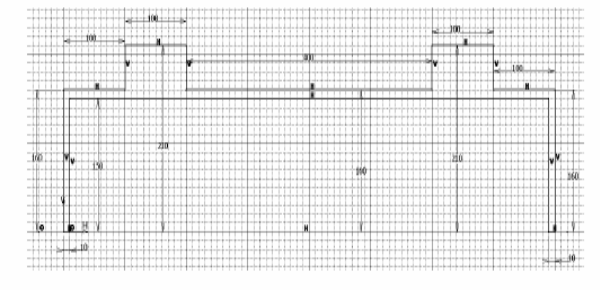

Fig. 4. *Sketch of the reservoir*

Sketch of reference reservoir is done in sketcher module, as seen in Figure 4. Sketch of reference heating structure is presented in Figure 5.

Inserting the component parts are made in CATIA Assembly Design module (Insert / Existing Component) - Figure 6.

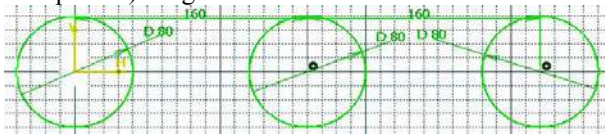

Fig. 5. *Sketch of reference heating structure*

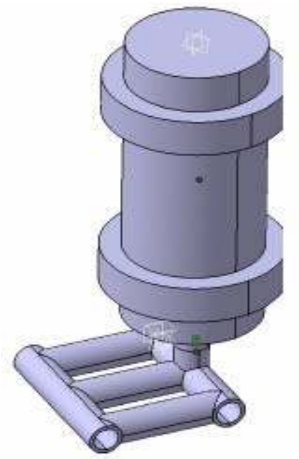

Fig. 6. *Assembly structure*

The assembly is created using geometric constraints between components. *(Contact Constraint and Coincidence Constraint)* Application of material using Apply Material icon. The part is considered carbon steel or alloy steel material, with the following physical properties: thermal expansion coefficient (1.17×10^{-5}K) and admissible strength (2.5×10^{8} N/m^2).

3. Finite element analysis

First step is to access CATIA Generative Structural Analysis module and we set the type of static analysis (static loading), specification tree simultaneously displaying element with the same name and admissible strength.

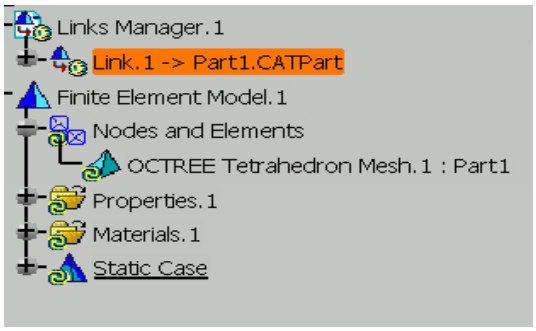

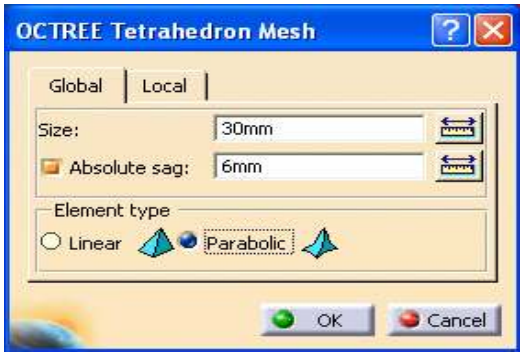

Fig. 7. *Discretization of the part model*

Definition of nodes and elements (a process called meshing). It is determined the size of finite element (Size), the maximum tolerance between discretized model and real model used in the analysis (Absolute sag) type element (element type), etc.

For this, it is executed double click on "Mesh tetrahedron OCTREE" sub-item found in the specification tree.

Figure 7 presents the specification tree and dialog with the same name, which contains the finite element size (30 mm), minimum tolerance (6 mm) and the type of the element as parabolic.

Restrictions definitions

Modeling the interface between the inlet of the hot water tank and heating pipe structure is achieved by selecting the type geometric constraints coincidence of axes of the two tubes (Pressure Fitting Connection).

Contact condition imposed to the model presumes cancellation of the six possible degrees of freedom associated with the side surfaces of the tank).

Stress definitions, using toolbar Load.

Loading is modeled as an acceleration gravity acting on the elements structural components (select the two elements of the sequence, Vector Acceleration: X= 9.81m/s^2, Y= 0N, Z= 0N) and form a thermal field acting on the structure (Temperature Field, Temperature = 373deg) (Figure 8).

Effective step analysis calculation, using "*Compute*" icon.

The display and interpretation of results, with the help on the toolbar *Image*. In Figure 9 is exemplified specification tree, containing a list of three images and their icons. Deformed state of the model is visualized using Deformation command (Figure 10).

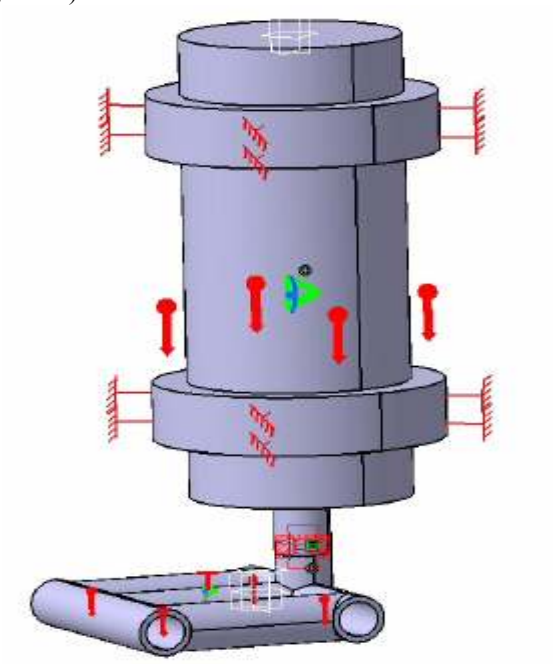

Fig. 8. *Restrictions and stress definitions*

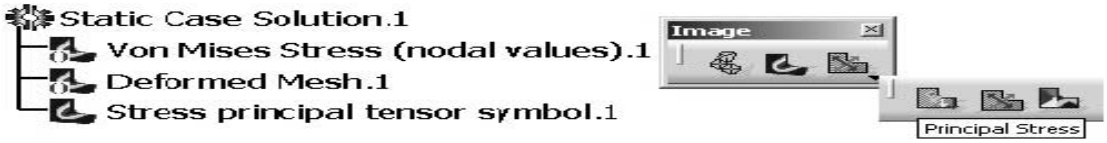

Fig. 9. *The tools of image display and the corresponding menu tree*

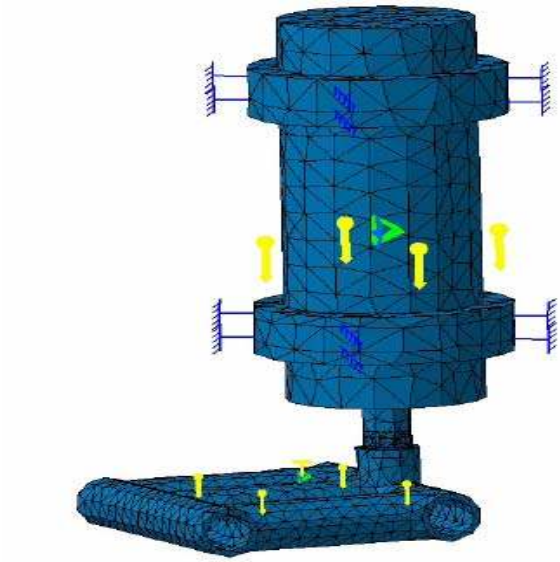

Fig. 10. *Deformed state of the model*

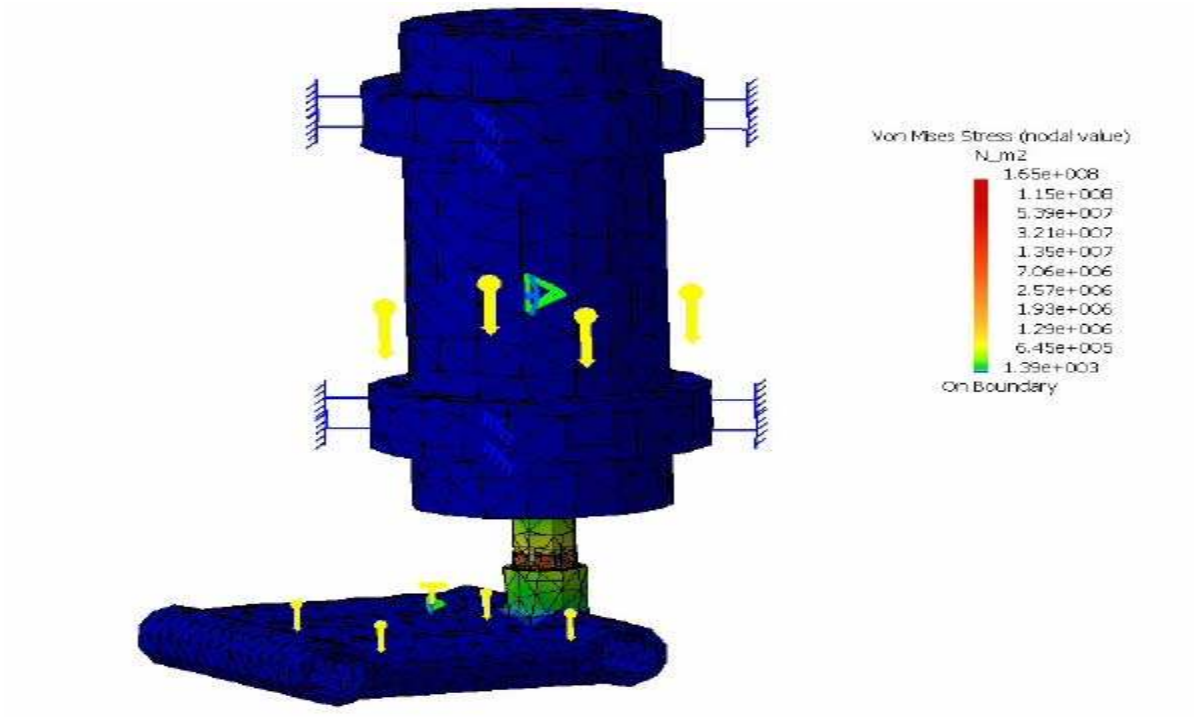

Fig. 11. *Distribution of Von Misses stress*

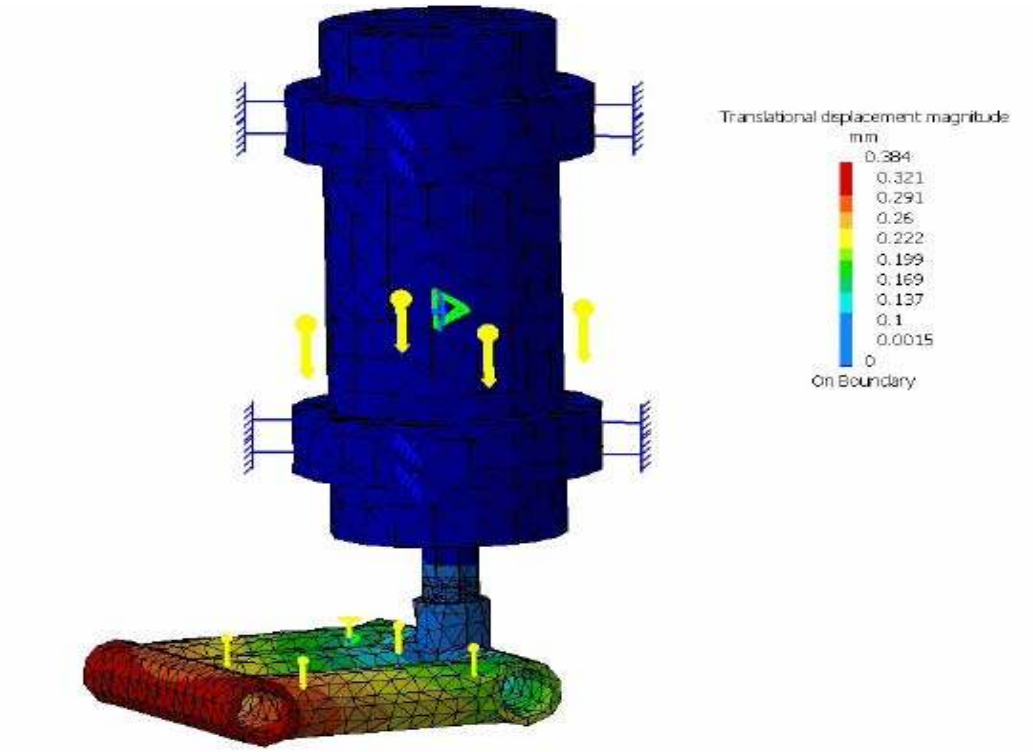

Fig. 12. *Displacement field*

Figure 11 displays the corresponding results Von Misses stress (values of a scalar field energy density obtained from the level of strain). The numerical values of these stresses are displayed along with the Von Misses stress. Also is displayed the nodes location where are located minimum and maximum values of these tensions. To view field trips (in mm) of network nodes as a result of the

imposition of conditions and loading restrictions on the model it is used Image tool bar Displacement. Figure 12 shows the color palette and offset values for the three-way junction for a node.

4. Conclusions

The analysis of displacement field has shown that the maximum displacements are small (0.384 mm). Maximum Von Misses equivalent stress is found in the assembly and has value of 165MPa.

To reduce these tensions there are constructive and / or manufacturing measures to be taken into account, such as increasing area of assembly or the use of materials with superior mechanical properties).

References

[1]. Ionuţ Gabriel Ghionea - *Proiectare asistata în CATIA V5 – Elemente teoretice şi aplicaţii*, Editura BREN, Bucureşti, 2007.
[2]. Mihai Tiberiu Lates - *Metoda elementelor finite. Aplicatii,* Editura Universitatii Transilvania din Brasov, 2008.

THE ANNALS OF "DUNAREA DE JOS" UNIVERSITY OF GALATI.
FASCICLE IX. METALLURGY AND MATERIALS SCIENCE
N^0. 4 – 2013, ISSN 1453 – 083X

RESEARCH REGARDING ON WORK SAFETY IN MAKING STEEL AT LD CONVERTER

Beatrice TUDOR
Faculty of Materials Science and Environment
"Dunărea de Jos" University of Galaţi, 111, Domnească Street, 800201, Galaţi, Romania
email: btudor.ugal.ro

ABSTRACT

This paper presents the tasks and work environment of workers working at the LD converter. Risk factors identified and assessed and suitable measures for reducing or eliminating them, resulting a safer environment for the development of production activities in specific job and decreased risk of work accidents in this sector.

KEYWORDS: environment, risk factors, LD converter

1. Work system components of evaluated

1.1. Workload

The task of the worker at convertizorului LD comprises a number of distinct activities, and for each of them was made a documentation specifies what is described in the technical working instructions provided by the UOR, as follows:

At receipt and handing work jobs should be followed:

- must be present at the work ,least with 15 min. before the beginning of the work program [1];
- at the end of work, surrender next exchange, machinery and equipment and recorded in the report of activity status. [2];
- acknowledgment of the state of operation of machinery and equipment, possible breakdowns [3];
- check the operation of the booth AMC converter [4];
- ensure the smooth running of the plant material and the addition of slag and steel transfercarelor [5];
- check operation with compressed air at lift lance and tipping converter [6].
- before loading iron, execute the following:
  - operation state of the outlet
  - operation state at the converter masonry [7];
- to inform on the status of the installation of heat recovery and dust control, fume removal (boiler) [8];
- check the status of blowing lance and operating parameters of the wires [9];
- depending on many factors, such as temperature and analysis at liquid iron, steel mark,condition of masonry, condition of ladle,will make the determination of the charged,and will send the amount of hot metal, iron and oxigen required [10];
- after the announcement and confirmation from the boiler "ready" (green signal) will give command the smelter worker II of upload converter [11];
- after loading iron, check again the status masonry converter [12];
- after charging "liquid iron walk the convecter, a few times, after that brings upright and locks tilting from the cockpit [13];
- instilling charge as technological instructe, for type steel, following operating parameters, and where appropriate, amend the oxygen, flow and lance position [14];
- during blowing, ordering smelter worker II, the amount of filler material and when it should be added [15];
- after blowing, the converter tilting command fails, the command of cabins [16];
- supervises the tipping of the converter [17];
- supervises the sampling the temperature, from steel and slag then command to the smelter worker,to position convector to the vertical position [18].

1.2. Work environment

The main characteristics of the work environment are specified in analysis reports.

According to analysis bulletins are allowed exceedances of the following pollutants: dust, CO, lime dust, noise.

The work environment is characterized by:

- low light levels at some points of the work and very high in the viewing area of the molten steel;
- the presence of infrared radiation;
- by draft.

2. Research on risk factors, at making steel in convector LD

Risk factors identified in the work areas at making steel in convector LD are divided into:

2.1-Risk factors identified in the use of means of production

2.2 - Risk factors in the workplace

2.3 - Risk factors of the work task

2.4 - Risk factors of the performer

2.5 – Omissions

2.1 Risk factors identified in the use of means of production

The risk factors identified in the production areas are:

2.1.1. Mechanical risk factors

Grip drive by unprotected transmission (eg belt conveyors, etc.).

Flow of steel, pig iron, slag, incandescent ,in the phases of handling ladles;

Flick the automobiles and railways to move through the plant premises (not used warning beep);

Slip of parts, materials, etc. stored without stability;

Roll of parts, materials based cylindrical or stored without stability;

Rolling of cylindrical parts **(**CO_2 extinguishers);

Free fall of parts, tools, parts, materials, the higher altitudes;

Free leak of molten material;

Accidental discharge of incandescent alloy;

Accidental collapse iron and alloying elements stored

Throwing by currents of air or pneumatic installation, of some particles steel, cast iron or slag

Deviation from the normal trajectory of large masses handled with cranes

Balance of ladle, followed by discharge;

Absence of any insurance (wire ties) in case of jet, eruption of molten material, powder, oil under pressure, etc.;

Dangerous contact with surfaces or contours (sharp, slippery, abrasives, adhesives) - unfinished surfaces, contours dangerous;

Working in the vicinity of pressure vessels.

2.1.2. Thermal risk factors

Objects or surfaces with high temperature - splashes of molten material, heated surfaces, trails technological steam, hot water, etc.

Flames - outbursts, thermal process;

2.1.3.Electrical risk factors

Electrocution by direct touch - current paths unprotected;

Electrocution by indirect touch - faulty earthing, accumulation of fluid.

2.1.4. Chemical risk factors

Explosives - mixture of oxygen.

2.2. Risk factors identified in the work environment in making steel in LD converter

2.2.1. Physical risk factors

High temperature of the air - especially in the converter's vicinity;

Low temperature of the air, in the cold weather - especially at elevation + 43m;

Airflow - natural draft, hoods operation, enclosure leakage;

High noise level - according to the attached analysis bulletins determinations;

Vibrations caused by the movement of vehicles (cranes, pushing machine, etc.);

Low level lighting on some routes of travel.

Brightness-focus convector, material incandescent etc;

Radiation - in the vicinity of the converter, ladles etc.

Natural disasters – earthquakes;

Dust excess - especially at higher rates, in the vicinity of the converters - according to the attached analysis bulletins determinations.

2.2.2. Chemical risk factors

Accumulation of toxic gases - from the steelmaking area and weighing area (eg. exhaust gases of forklifts);

Flammable or explosive gases and vapors - gained at steel making (oxygen, acetylene);

2.3. Risk factors of work task

2.3.1. Physical strain

Dynamic effort - long trails at manual handling of heavy masses (eg barrels alloying materials).

2.3.2. Mental overload

- Difficult decisions in a short time - to fix or liquidation situations of "INCIDENT

2.4. Risk factors of contractor

2.4.1. Wrongful

Execution of contingency operations in the work load;

Commands in time, other than those imposed by technology;

Execution of maneuvers, without ensuring compliance with the security conditions;

Wrong positioning of the ladles;

Setting parameters work outside the conditions imposed by technology;

Not ensure synchronization with other workers to teamwork;

Moving and stationary in hazardous areas - the car ways, or taxiways, forklifts, lifting equipment under load, in the face of convector etc.;

Fall on the same level: the imbalance, sliding - uneven surfaces loaded with dust, accumulation of water on access roads;

Falls from heights: by stepping into the void, the imbalance by sliding - handrails missing, technological voids concealed by accumulations of dust, uncovered or unmarked;

Not comply with the code signal crane;

2.5. Omissions

Omission of operations that ensures their safety

Failure personal protective equipment (E.I.P), individual work equipment (E.I.L), and other means of protection provided (which was granted by the employer).

3. Measurements and recordings of specific's area risk factors at making steel in LD converter

After studies and research, targeting the risk factors for the workers at the convector, were measured a total of 47 cases corresponding to specific activities in this area, with level corresponding to the hazard, at the job's analysis; was constructed diagram of Figure 1.

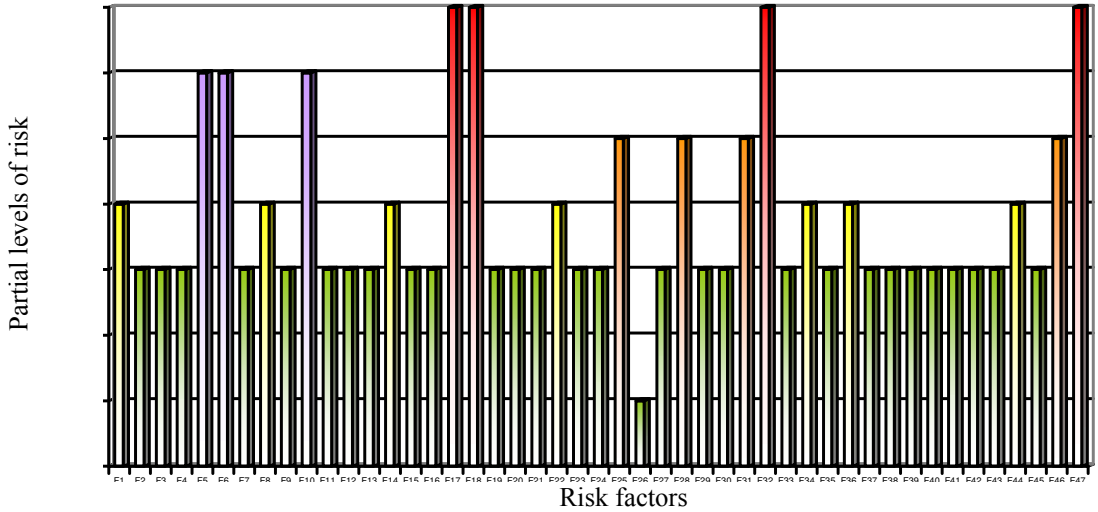

Fig. 1. *Diagram of risk factors for those working in steelmaking in converter (partial levels of risk)*

Explaining risk factors F1 through F47, are given below:

F1-Grip drive by unprotected transmission (eg belt conveyors, etc.).

F2-Flow of steel, pig iron, slag, incandescent ,in the phases of handling ladles

F3-Flick the automobiles and railways to move through the plant premises (not used warning beep)

F4-Slip of parts, materials, etc. stored without stability

F5-Roll of parts, materials based cylindrical or stored without stability

F6-Rolling of cylindrical parts (**CO2** extinguishers)

F7-Free fall of parts, tools, parts, materials, the higher altitudes

F8-Free leak of molten material

F9-Accidental discharge of incandescent alloy

F10-Accidental **collapse fier vechi** and alloying elements stored

F11-Throwing by currents of air or pneumatic installation, of some particles steel, cast iron or slag

F12-Deviation from the normal trajectory of large masses handled with cranes

F13-Balance of ladle, followed by discharge.

F14- Absence of any insurance (wire ties) in case of jet ,eruption of molten material, powder, oil under pressure, etc..

F15-Dangerous contact with surfaces or contours (sharp, slippery, abrasives, adhesives) - unfinished surfaces, contours dangerous

F16-Working in the vicinity of pressure vessels.

F17-Objects or surfaces with high temperature - splashes of molten material, heated surfaces, trails technological steam, hot water, etc.

F18-flames - outbursts, thermal process

F19-Electrocution by direct touch - current paths unprotected

F20-Electrocution by indirect touch - faulty earthing, accumulation of fluid

F21-Explosives - mixture of oxygen

F22-High temperature of the air - especially in the converter's vicinity

F23-Low temperature of the air, in the cold weather - especially at elevation + 43m

F24-Airflow - natural draft, hoods operation, enclosure leakage

F25-High noise level - according to the attached analysis bulletins determinations

F26-Vibrations caused by the movement of vehicles (cranes, pushing machine, etc.)

F27-Low level lighting on some routes of travel.

F28-Brightness-focus convector, material incandescent etc

F29-Radiation - in the vicinity of the converter, ladles etc

F30-Natural disasters - earthquakes

F31-Dust excess - especially at higher rates, in the vicinity of the converters - according to the attached analysis bulletins determinations.

F32-Accumulation of toxic gases - from the steelmaking area and weighing area (eg.exhaust gases of forklifts).

F33-Flammable or explosive gases and vapors - gained at steel making (oxygen, acetylene)

F34-Dynamic effort - long trails at manual handling of heavy masses (eg barrels alloying materials)

F35-Difficult decisions in a short time - to fix or liquidation situations of "INCIDENT"

F36-Execution of contingency operations in the work load

F37-Commands in time, other than those imposed by technology

F38-Execution of maneuvers, without ensuring compliance with the security conditions

F39-Wrong positioning of the ladles

F40-Setting parameters work outside the conditions imposed by technology

F41-Not ensure synchronization with other workers to teamwork

F42- Moving and stationary in hazardous areas - the car ways, or taxiways , forklifts, lifting equipment under load, in the face of convector etc..

F43-Fall on the same level: the imbalance, sliding - uneven surfaces loaded with dust,accumulation of water on access roads

F44-Falls from heights: by stepping into the void, the imbalance by sliding - handrails missing, technological voids concealed by accumulations of dust, uncovered or unmarked

F45-Not comply with the code signal crane

F46-Omission of operations that ensures their safety

F47-Failure personal protective equipment (E.I.P), individual work equipment(E.I.L), and other means of protection provided (which was granted by the employer).

Using the risk factors level, or workers at LD convector,we can calculate the overall risk level at the job using the formula:

$\mathbf{N_{rg11}} = \Sigma R_i r_i / \Sigma r_i$

in which: - $\Sigma R_i r_i$ is the sum of risk factors considered work area; Σr_i - is the sum of the partial workplace risk assessment.

For the worker at LD convector, after the introduction of parameters in formula, results diagram in Figure 1. ***Level of risk achieved is Nrg = 4.3.***

$$\mathbf{N_{rg11}} = \frac{\sum_{i=1}^{47} R_i r_i}{\sum_{i=1}^{47} r_i} = \frac{4(7x7) + 3(6x6) + 4(5x5) + 7(4x4) + 28(3x3) + 0(2x2) + 1(1x1)}{4x7 + 3x6 + 4x5 + 7x4 + 28x3 + 0x2 + 1x1} = \frac{769}{179} = \mathbf{4,3}$$

4. Interpretation of the results of the evaluation of risk factors

Overall risk level calculated for worker at LD convector,equals 4.3, a value that it falls into the category of jobs with unacceptable level of risk. The result is supported by the "Assessment Sheet of worker at LD convector" in which it is observed that out of 47 risk factors identified (Fig. 1), (18 above, as part of the risk level, the 3, 4 falling within the category of high risk factors (NVPR = 7), 3 fits into the category of high risk factors (NVPR = 6), 4 falling the category of high risk factors (NVPR = 5), and the other seven being in the category of environmental risk factors (NVPR = 4). The 18 risk factors, which are situated into unacceptable range are: F17, F18, F32, F47, F5, F6, F10, F25, F28, F31, F46, F1, F8, F14, F22, F34, F36, F44.

To reduce or eliminate the 18 risk factors (which are in the range unacceptable) are required generic measures, listed in "Safety measures proposed" for the worker at LD convector.

Regarding the distribution of the generating sources of risk's factors, the situation is as follows (see Fig. 2):

• 44.68%, factors belonging to the means of production
• 25.53% working environment factors;
• 4.26% work task factors;
• 25.53% factors belonging to the contractor.

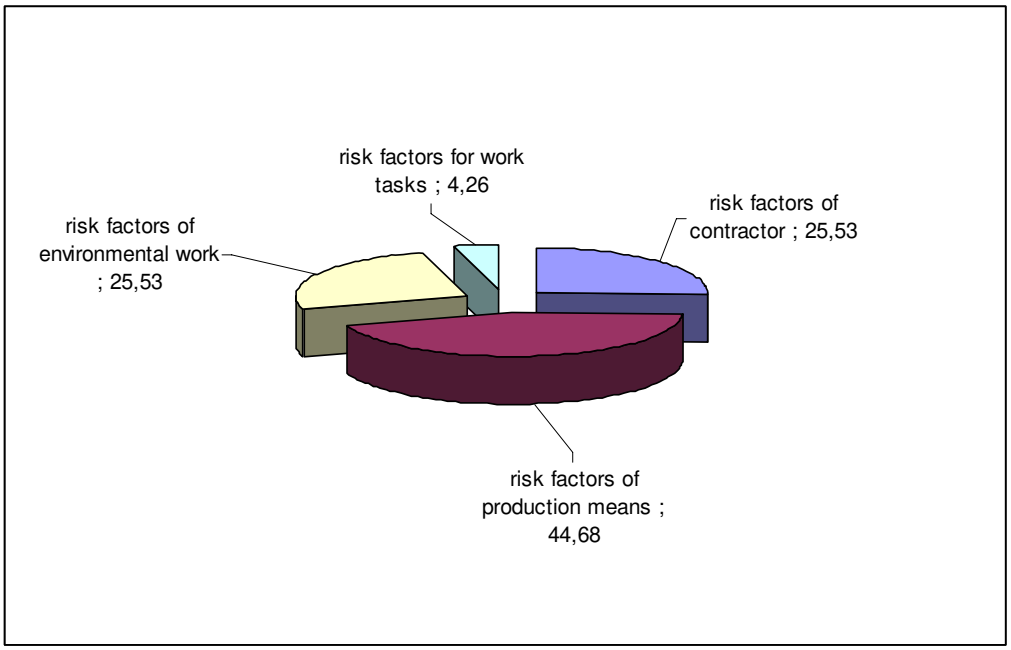

Fig. 2. *Distribution of risk factors identified by elements of the work system*

Analysis of the formular of evaluation, shows that 78.72% of the identified risk factors may have irreversible consequences on the worker.

5. Measures and proposals

To ensure job security in the convector area, measures technical and organizational proposed are:

For high risk factors F17, F18, F32, F47 (NVPR = 7),

-marking hazard areas at contact with surfaces that have high temperatures

-development of optical systems and audible warning of the presence of toxic gases

Equipment required to appropriate activity to be carried, out according to regulations

For high risk factors F5, F6, F10 (NVPR = 6),

Insurance against uncontrolled movement, materials handling, using dangerous procedures

Maximum load allowed by stacking

-Leveling transport routes in the warehouse

-Sizing access roads and removal of all material that prevents the passage

-Insurance against uncontrolled movement of materials through proper fence, anchor handling as hazardous procedures, leveling, anchoring etc.

For high risk factors, F25, F28, F31, F46 (NVPR = 5),

Measures to combat noise's source - is achieved through changes to the technical equipment if possible, or by adopting special attenuators devices, the choice of technical equipment in conditions comparable technology priority, will be given to those that produce noise the lowest

-Measures to combat noise at receiver - consists in isolating the staff working in noise

-Adopt, where possible, working methods with minimal release of dust

For environmental risk factors, F1, F8, F14, F22, F34, F36, F44 (NVPR = 4),

- Repair and installation of all protective devices

- Marked with warning signals, all contact areas with high temperature, with potentially dangerous

- Restriction on possible areas where fluid flow is possible incandescent

- Check all fluid routes, and remedy them

- Restriction on possible areas where there is potential for fluid jets

- Repairing railings and other items to prevent falls from height

- Equipment needed in case of signaling toxic gases and vapors, purchase personal protective equipment, appropriate activity to be carried out according to regulations.

6. Conclusions

-For steelworker job security, as required following main conclusions:

-Training on the risk of accidental contact, with surfaces that have high temperature;

-Training on how to use the means of protection

-Regular training of employees on the consequences of the entry into hazardous areas;

-Potentially marking occurrence of flames, gases or vapors;

-Introduction of mandatory wearing gas mask, in areas where toxic gases or vapors may occur;

-Monitoring health;

-Verifying and the permanent control of the workers;

-Perform periodic measurements of pollutants in the work environment;

-Signaling areas where there is danger of falling from height, marking and completion with anchorages.

References

[1]. Darabonţ, D. - *Evaluarea riscurilor de accidentare şi îmbonăvire profesională*, Editura Virom, Constanta 2005

[2]. Darabonţ, D. - *Managementul securităţii şi sănătăţii în muncă. Ghid de evaluare a confomării cu cerinţele legale,* Bucureşti, Editura AGIR, 2010.

[3]. *** - Instrucţiuni de lucru la masinile de turnare continua TC1-UOR

[4]. *** - Legea 319/2007, Legea securităţii şi sănătăţii muncii;

[5]. *** - HG 1425/2007, Normele metodologice de aplicare a Legii 319/2007;

[6]. *** - HG 955/2010, Modificări la HG 1425/2007;

[7]. *** - SR OHSAS 18001/2008, Sisteme de management al sănătăţii şi securităţii ocupaţionale. Cerinţe;

[8]. *** - SR OHSAS 18002/2009, Sisteme de management al sănătăţii şi securităţii ocupaţionale. Linii directoare pentru implementarea OHSAS 18001/2007;

[9]. *** - SR EN ISO 9000/2006, Sisteme de management al calităţii. Principii fundamentale şi vocabular;

[10]. *** - SR EN ISO 9001/2008, Sisteme de management al calităţii. Cerinţe;

[11]. *** - SR EN ISO 14001/2005, Sisteme de management de mediu. Cerinţe cu ghid de utilizare;

[12]. *** - Sr EN ISO 19011/2011, Ghid pentru auditarea sistemelor de management.

THE ANNALS OF "DUNAREA DE JOS" UNIVERSITY OF GALATI.
FASCICLE IX. METALLURGY AND MATERIALS SCIENCE
N^0. 4 – 2013, ISSN 1453 – 083X

RESEARCH CONCERNING THE INFLUENCE OF LASER CLADDING ON THE OPERATING CHARACTERSITICS OF THE SURFACE LAYERS OBTAINED FROM HIGH-SPEED STEEL POWDER

Simona BOICIUC
"Dunărea de Jos" University of Galaţi,
111, Domnească Street, 800201, Galaţi, Romania email: simonaboiciuc@yahoo.com

ABSTRACT

The paper presents the corrosion behavior of laser cladding layers in 0.5 M NaCl along with a durability test, compared with samples made of clasically hardened HS6-5-2 steel. The higher characteristics of the laser deposited layers have been underlined while recommending the procedure of parts highly required to wear and corrosion.

KEYWORDS: laser cladding, high-speed steel, tool, powder injection, corrosion

1. Introduction

Theoretical and practical studies have lately been established to implement new surface hardening techniques associated with a corresponding increase in resistance to corrosion. Out of them, laser cladding captures the experts' attention as it was found that this leads to ultrafine structures, extremely hard and tenacious, characterized by a mix of properties superior to those obtained by conventional treatments.

In case of making the lathe tool of high-speed steel, an important part of tool body is not used during the facing process but only for setting it into the tool machine. A solution that removes this disadvantage is represented by cladding [1, 2, 3, 4, 5, 6] the high - speed steel in the active area of lathe tool made by carbon steel.

Therefore, the multilayer cladding was made by high-speed steel powder injection in melt bath by CO_2 continuous wave laser connected to x-y-z coordinate table. High-speed steel powder as addition material mainly with 0.82%C, 4.7%Mo, 6.4%W, 4.1%Cr, 2.02%V, 0.3%Mn was used as prior researches emphasized a higher capacity of this material to be quenched since liquid phase, like specific case in laser cladding. Carbon steel with 0.45% C was used like base material. Optimal running found by laboratory testes were used in order to make several lather tools by laser cladding. These lathe tools presented a good behavior when steel facing.

To provide a complete characterization of the laser claddind layers with high-speed steel powder, corrosion behavior was studied using the potentiodynamic method (polarization curves plotting) for determining the corrosion potential (Ecor), maximum corrosion current intensity (Icor) and polarization resistance (Rp).

The potentiodynamic tests aim to plot the polarization curves by varying the current density according to the potential. Proportionality between potential and current density arises from the overlap of the two cathodic and anodic processes, both obeying the logarithmic laws. In a corrosion process, the two reactions occur on the same metal surface, equipotential, so that the experimental measurements will give values that correspond to the potential and anodic and cathodic current density, i.e. mixed values. Mixed potential and corresponding current intensity are also called corrosion potential, and corrosion current density respectively. The potentiodynamic method implies modification of the electrode potential continuously at a preset scanning speed. The paper presents the behavior of laser deposited layers of high-speed steel powder type HS6-5-2 - M2 to corrosion in 0.5 M NaCl solution and a durability test using longitudinal turning with constant cutting speed without using cooling.

The researches were carried out to compare with high-speed steel samples classically treated in volume.

2. Experimental conditions

„M2 Coldstream B-7800, Sweden" powder with 0.82%C, 4.7%Mo, 6.4%W, 0.3%Mn, 4.1%Cr, 0.32%Si, 2.02%V, Fe balance, as chemical composition for cladding was used. By sieving the granulometric fractions, inside the 80÷90μm range, were separated in order to be used as addition material. Powder had spherical shape, therefore, it provided a fluid floating of addition material through the injection system. Powder dried at 110^{o}C for 15 minutes before addition material feeding inside the injection system tank.

Laboratory trials were performed in a CO_2 continuous wave laser installation as GT type of 1400 W (made in Romania), with coordinate working table and running computer program, provided by dust injection system onto laser melted surface.

For laser cladding it was used a 1.8mm diameter laser beam with 1100 W power, 7mm/s sweeping speed, which cladded parallel overlapped stripes with 1.5mm cross travel pass. Addition material flow was 251mg/s. Final thickness of the cladding layer was 3.5 mm resulted by 5 layers overlapping.

Determining susceptibility to corrosion was achieved at room temperature (24°C) using a Voltalab 21 system connected to a computer using a VoltaMaster 4 software for exprimental data processing.

The potentiostate is connected to the electrochemical cell by three electrodes: reference electrode, auxiliary electrode and working electrode. In the experimental determinations as reference electrode was used a saturated calomel electrode Hg/Hg_2Cl_2/ saturated K_2SO_4, (SCE = +241 mV/EHS), and as auxiliary electrode (counterelectrod) a platinum electrode.

The working electrode, that is the laser cladding samples on nickel base have been previouly prepared, polished, made shiny and degreased in accordance with ASTM G1 standard. To study only the behavior of the laser deposited layers, non treated areas were covered with a protective lacquer. Also, the surface submerged into solution was measured and data were entered in program.

Thus polarization curves were obtained to assess the corrosion behavior of the high-speed steel powder laser - cladded layer and volume - thermally treated sample.

For the experimental research to determine the durability of the lathe tool on which powder laser deposition of high - speed was carried out, the method of longitudinal turning with constant cutting speed without cooling was applied. Its behavior was studied in comparison with a lathe tool made from HS6-5-2 steel subjected to special treatment in volume.

The laser deposition with high - speed steel on the lathe leading edge was achieved by a laboratory technology according to the required geometry. After the high - speed steel deposition in a 3.5mm thick layer on each cutting tool, a cooling treatment at -60°C was aplied to reduce the amount of residual austenite. The treatment of double annealing to 550°C was eliminated.

Testings were conducted at three different speeds 40, 60, 80m/min to see how the cutting speed influences the lathe tools durability.

The material subject to cutting was steel 1C45, Ø 42mm diameter, 340mm length, and 2011MPa hardness.

Longitudinal turning test was performed in following conditions: cutting depth t = 0.5mm, feed 0.075mm/rot, speed modified during the test to ensure a constant cutting speed was of the order of 250, 400, 500, 630, 1250rpm.

3. Experimental results and discussions

Corrosion results of the laser cladded layers of high speed steel M2 powder and those classically treated in volume are given in Table 1.

Table 1. *Results of corrosion of the samples*

Samples	Corrosion environment	Parameters achieved							
		E (i=0)	Rp	Icor	Ba	Bc	Corossion	Initial mass	Final mass
		[mV]	[Ω.cm^2]	[mA/cm^2]	[mV]		[mm/an]	[g]	
laser	NaCl, 0.5M	-774.4	12.97	0.0036	199.3	- 144.0	0.04257	2.9565	2.9526
classic	NaCl, 0.5M	-767.8	5980	0.0032	190.4	-133.3	0.03740	2.7708	2.7685

Note: E – corrosion potential; Rp – polarization rezistance; Icor – intensity of corrosion current; Ba, Bc – correspond to constants Tafel for anodic and cathodic reaction

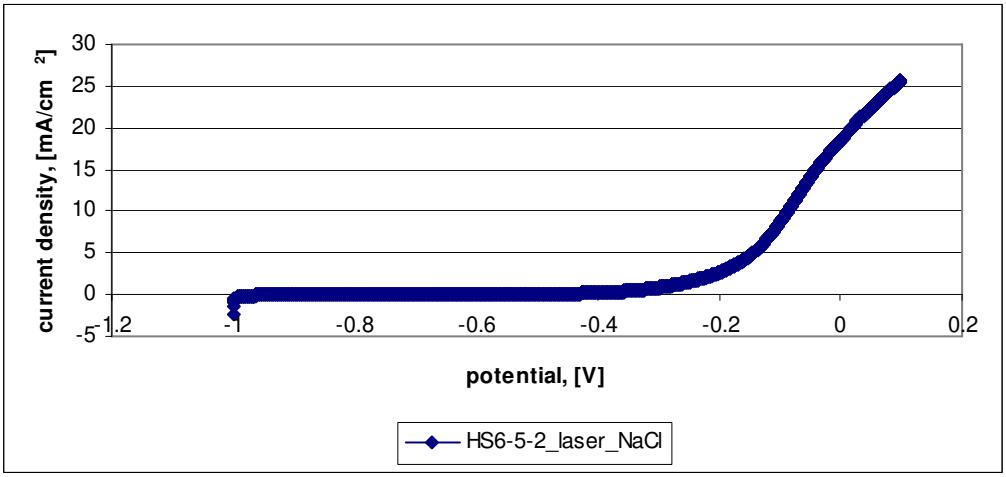

a.

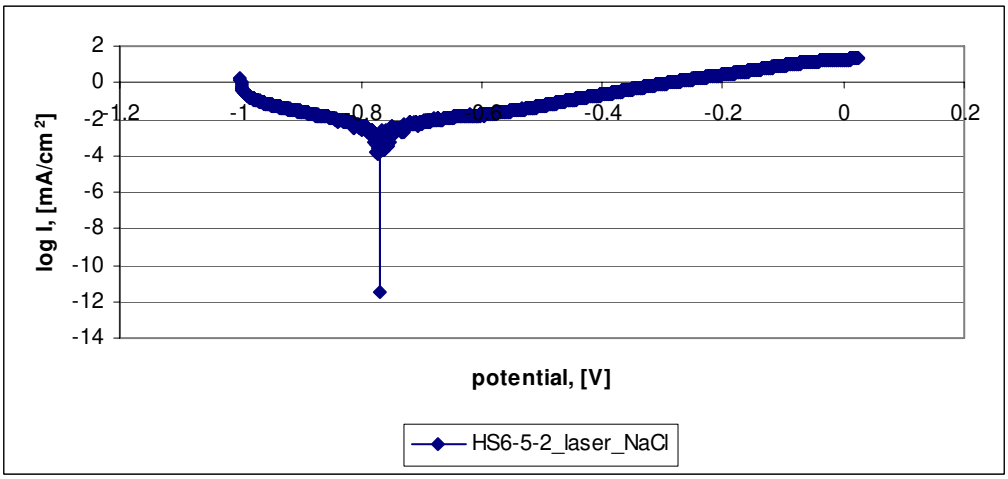

b.

Fig.1. *The potentiodynamic curve – a) and Tafel curve - b) NaCl, 0,5 M environment*

Looking at Figure 1 it can be seen the presence of a passivation sector from potential - 0.9875 V – to potential -0.3844V. Thus the M2 high - speed steel powder deposition resists to corrosion over a wide range of potential. This could be subjected to localized corrosion (pitting) caused by the chloride ions.

Analyzing Table 1 and Figure 1 b we can conclude that the laser deposited alloy is stable to corrosion in NaCl 0.5 M which is also indicated by the corrosion rate obtained.

Polarization resistance Rp is representative for the degree of protection provided by the layer deposited on the steel surface. The higher the polarization resistance, the more resistant the alloy and lower the $I_{cor.}$ Thus we can see that the polarization resistance is higher and the Icor is lower for the volume-treated quick steel sample which indicates that this presents a slightly better corrosion behavior compared with the laser deposited sample which, due to the presence of pores, is more susceptible to corrosion.

However differences between the corrosion rates are relatively small, therefore we can appreciate that the ultra fine structure of the laser deposit provides good corrosion behavior in NaCl 0.5M, medium, which is also seen in Figs. 3 and 4.

Looking at figure 2 it can be seen the presence of a passivation sector from potential from -0.959V – to -0.4282V.

Thus the M2 high -speed powder deposition resists to corrosion over a wide range of potential. This could be subjected to the pitting caused by chloride ions.

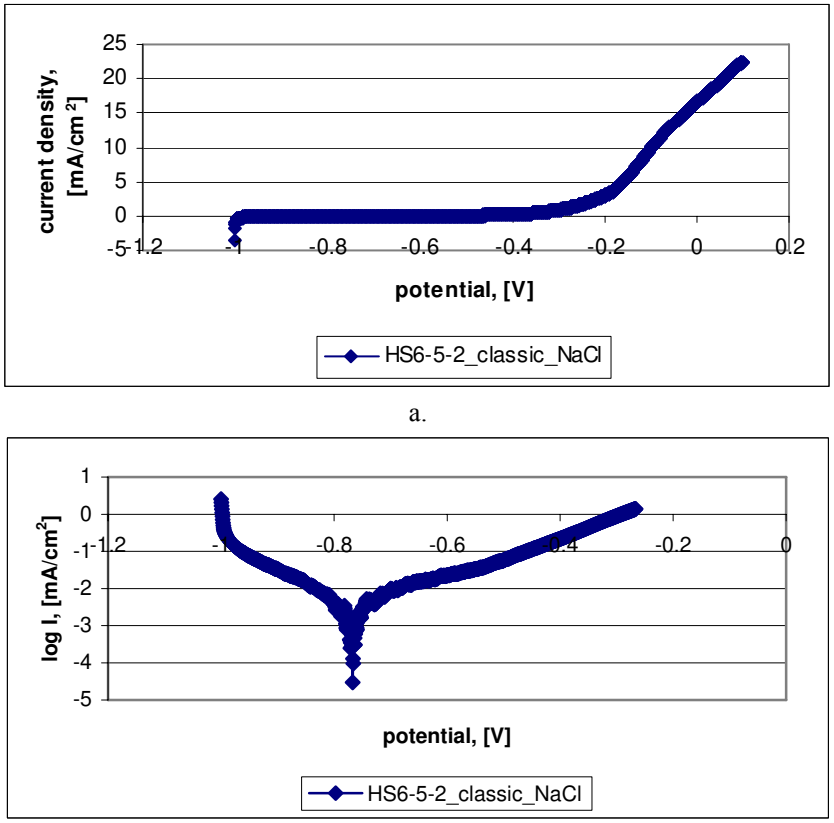

Fig. 2. *The potentiodynamic curve – a) and Tafel curve - b) NaCl, 0,5 M environment*

Analyzing Table 1 and Figure 2 b we can conclude that the high – speed steel classically hardened is stable to corrosion in NaCl 0.5 M which is also indicated by the corrosion rate obtained. Microstructures of the layers subjected to corrosion are given in Figs. 3 and 4.

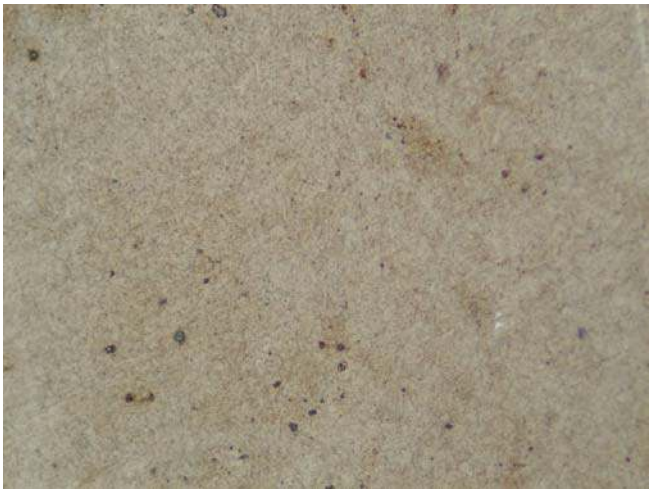

Fig. 3. *Microstructure of the laser cladding layer with powder of high-speed steel, subjected to corrosion in NaCl 0.5 M; (x500), nital attack 2%*

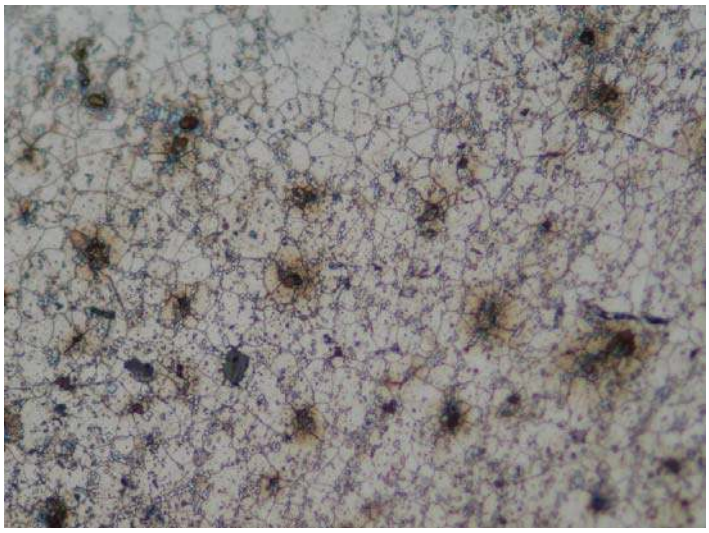

Fig. 4. *Microstructure of the classically treated high speed steel, subjected to corrosion in NaCl, 0.5 M; (x500), nital attack 2%*

Thus we can conclude that the results are comparable to the samples which show stable behavior to corrosion.

As regards durability test, the results provided by wear measurements on the lathe tool seat face are given in Table 2.

Table 2. *Results of durability tests*

No.	Cutting speed, v=40m/min	
	wear of classically quenching tool	wear of laser cladded lathe tool
	[μm]	
1.	49	31
2.	212	107
3.	231	120
4.	267	120
5.	280	136
6.	312	140
7.	488	266
	Cutting speed, v=60m/min	
1.	132	77
2.	180	104
3.	222	137
4.	365	231
5.	420	320
	Cutting speed, v=80m/min	
1.	333	280
2.	440	360
3.	500	420

It should be noted that for every change of speed, the lathe tool were resharpened.

Fig. 5 shows the lathe cutting edge on which laser deposition was conducted, in roughness state, after grinding (Fig. 6) and the longitudinal turning test (Fig. 7).

Fig. 8 illustrates the test results.

Fig. 5. *Semi-product after laser cladding*

Fig. 6. *Lathe tool after sharpening*

Fig. 7. *Longitudinal turning test*

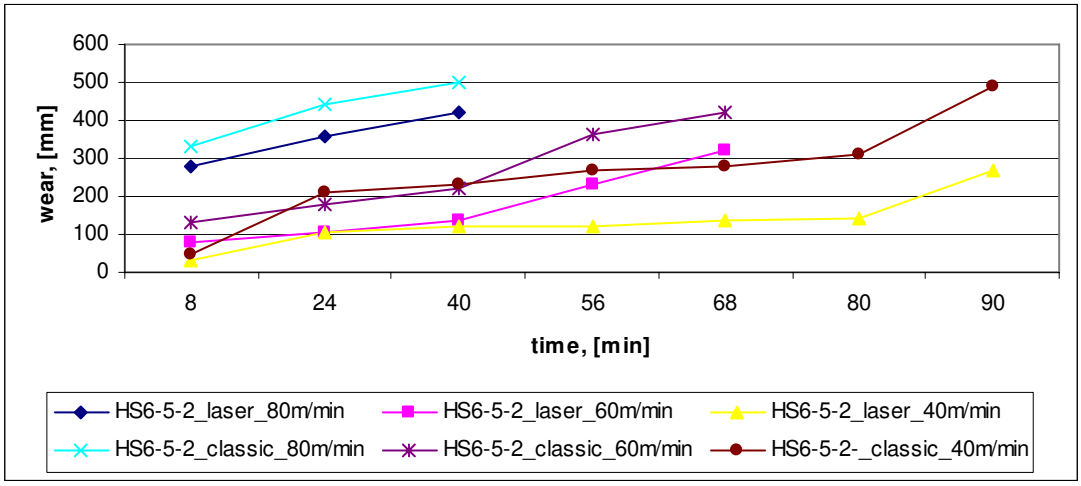

Fig. 8. *Wear vs. time variation of the blades tested to the speeds used during the test*

From Table 2 and Figure 8 the following can be concluded:

- for all speeds achieved the laser deposited lathe tool features higher durability than that of the volume heat-treated lathe tool;
- lathe tool wear increases with higer cutting speed, even more pregnant at 80m/min;
- the higher durability of the high - speed steel powder laser cladded lathe tool is due , on the one hand, to superior hardness to the volume treated lathe tool and on the other hand, due to the highest capacity of the lathe tool body (made from carbon steel) to dissipate heat from the active zone (heat conductivity of steel decreases with increasing alloying);
- the high hardness of the laser deposited lathe tool is due to the structure consisting of ultrafine, tough, tenacious, oversaturated martensite with no chemical non uniformities and a well developed substructure;
- the wear visible on the lathe tool surface concerned is of threshold type.

4. Conclusions

The corrosion behavior of the volume treated samples on which laser cladding was carried out showed that the results obtained are comparable to the samples showing a similarly stable behavior to corrosion.

Comparative durability test carried out on lathe tools classically treated and laser cladded reveals the following: the durability of the laser deposited lathe tool is superior to the classically treated one due to, on the one hand, its high hardness provided by the structure consisting of ultra-fine, tough, tenacious, oversaturated martnesite with no chemical uniformities and a well developed substructure, and on the other hand due to the highest capacity of the lathe tool body (made from carbon steel) to dissipate heat from the active zone (heat conductivity of steel decreases with increasing alloying).

Thus the laser deposition of the M2 high - speed steel powder is intended for parts highly required to wear and corrosion, as it provides a good mix of properties, superior to those obtained by volume heat treatments on the same steel grade (HS6-5-2).

References

[1]. D.T. Levcovici, R. Boiciuc, S.M. Levcovici, C. Gheorhieş – *Laser cladding of M2 steel on a steel substrate*, The International Thermal Spray Conference and Exposition (ITSC), may 15th – 17th, (2006), pp. 1333-1338 Seattle, USA.

[2]. D.T. Levcovici, S.M. Levcovici, I. Onea – *Procedure of laser cladding of high speed steel*, Patent 121477 B1, 30.04.2007.

[3]. S. Boiciuc - *Properties and application of laser cladding with high – speed steel powder, type M2,* Metalurgia International 1, (2010), pag. 5 – 11.

[4]. S. Boiciuc, C. Gheorghieş - *Structural changes in laser cladding layers of powder high - speed steel type HS6-5-2 - M2 heated to different temperatures*, Metalurgia International 2, (2010), pag. 30 – 35.

[5]. M.F. Schneider - *Laser cladding with powder*, Ph. D. Thesis University of Twente, Enschede, Olanda, (1998), http://doc.utwente.nl/fid/1558.

[6]. H. Gedda – *Laser surface cladding - a literature survey*, Lulea University of Technology, Division of Materials Processing, iulie (2000), Suedia, http://epubl.luth.se/1402-1544/2004/41/.

[7]. Levcovici S. M. – *Contributions to the laser surface treatment of tool steel,* Doctoral thesis, Galaţi (1997).

THE ANNALS OF "DUNAREA DE JOS" UNIVERSITY OF GALATI.
FASCICLE IX. METALLURGY AND MATERIALS SCIENCE
N^0. 4 – 2013, ISSN 1453 – 083X

OPTIMIZATION OF THERMOMECHANICAL PROCESSING OF SOME ALUMINUM ALLOYS BY DIMENSIONAL INTERPOLATION METHOD USING THE MATLAB

Marian NEACSU, Doru HANGANU, Elisabeta VASILESCU
"Dunărea de Jos" University of Galaţi, 111, Domnească Street, 800201, Galaţi, Romania
email: uscaeni@yahoo.com

ABSTRACT

This paper presents results of research on optimization of thermomechanical treatment applied to an alloy of the Al-Zn-Mg-Cu system, used in the aviation industry.Optimizing thermomechanical treatment process is based on a mathematical model that establishes the relationships between the main technological parameters of thermomechanical processing and association of physical and mechanical properties of the alloy used. Findings are based on an laborious experimental program to elaborate the mathematical model, an essential element of thermomechanical treatment process optimization applied to the alloy studied for obtaining the required values of mechanical properties with the minimal cost.

KEYWORDS: optimization, mathematical model, aluminum alloy thermomechanical treatments, properties

1. Introduction

Alloys of the system Al-Zn-Mg-Cu 7000 series because they have special characteristics are used first in the aviation industry and engineering.

Are part of wrought aluminum alloys and hardened by the application of heat treatment and (or) Thermo. Some of them have mechanical properties comparable copper-based alloys or steel grades, and even some with titanium, but has the advantage that it has a much lower density [2].

For the aviation industry where alloys are subjected to stresses multidirectional operation alloys must provide an optimal combination of strength, plasticity, toughness, fatigue strength and good resistance to stress corrosion. To achieve this optimum is necessary to replace the coarse grain structure obtained in the process of casting alloys and semi-finished laminated fibrous structure, they are decisive factors to achieve an optimal properties [2].

Like any technical system, metallurgical processes have certain technical performance and economic performance parameters that depend on the conditions and mode of operation of the system. So, the choice of these parameters and conditions at any given time, you select those that will provide the best technical and economic performance of the process (choosing optimal parameters) "[13].

Optimization of the technological process is based on a mathematical model must accurately describe how that process, the mathematical model is the main element in the management process. It follows immense importance to obtain a mathematical model that describes how closely that process, ie between model and describe the process you must be a line as high [14].

Determination of the optimal solution is done by determining the values of the independent variables so as to obtain the best value for the function - objective function (optimized).

The objective function when optimizing thermomechanical processing parameters of the alloy studied is the energy "Q = f (t, τ, ε)" subject to certain restrictions in respect of the mechanical properties investigated.

2. Experimental conditions

Table 1 shows the chemical composition of the alloy from which the samples were made under experimental regimes thermomechanical processing.

Table1. *Chemical composition*

Element / Alloy	Zn	Mg	Cu	Si	Fe	Pb	Cr	Mn	Al
AlZn5,7MgCu	5.76	2.61	1.55	0.15	0.19	0.021	0.19	0.10	rest

Table 2. Properties of alloys according to EN 485-2-2007

Properties / Alloy	Rm, [Mpa]	$Rp_{0.2}$ [Mpa]	A_5 [%]	HB
3 (AlZn5,7MgCu)	540	470	7	161

In table 2 are listed the mechanical properties required by EURONORMA EN 485-2-2007.

Figure 1 shows the schematic thermomechanical processing which were subjected to the aluminum alloy samples studied.

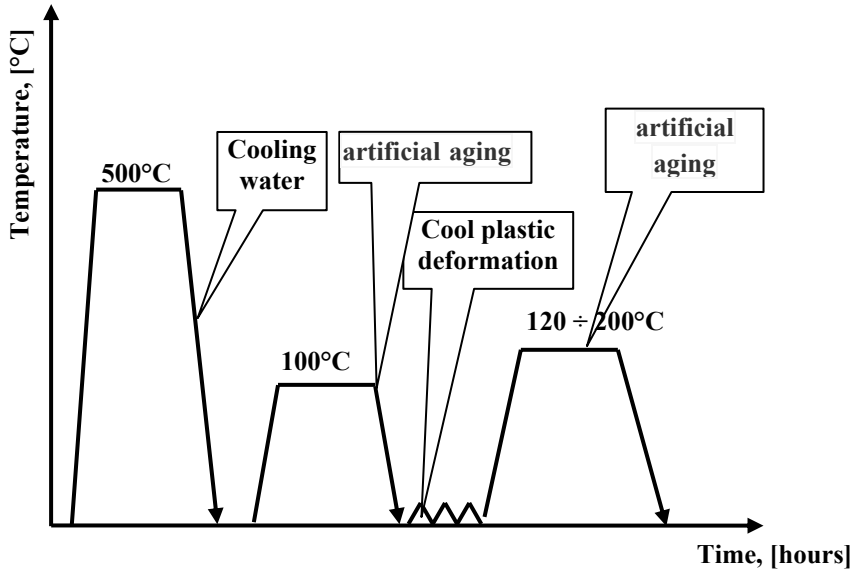

Fig. 1. *Schematic representation of thermal and thermomechanical processing*

After placing the solution annealing at 500 ° C aging is carried out at a temperature of 1000C for 1 hour for structural stabilization of the material. Further samples are subjected to a cold plastic deformation, with three degrees of deformation ε1 = 10%, 20% and ε2 = ε3 = 30% to achieve the set size.

Following this deformation is achieved by artificial aging heat treatment at the following temperatures: T1 = 120°C, T2 = 140°C, T3 = 160°C, T4 = 180°C and T5 = 200°C with the retention times: = 4:00 τ1, τ2 = 8:00, τ3 = 12:00, τ4 = 16 hours τ5 = 20 hours.

For optimization of thermomechanical processing described above we used three-dimensional interpolation using MATLAB software package.

MATLAB software package interpolation function of three variables through the use of specific functions such as ***interp3***.

The interpolation functions interp3 three variables by different laws and calling syntax: vi = interp3 (x, y, z, v, xi, yi, day, 'method') (1) where 'method' may be one of the key words:

• 'Nearest' - for interpolation type nearest neighbor;
• 'linear' - for bilinear interpolation;
• 'cubic' - for Bicubic interpolation;
• 'spline' - for cubic spline interpolation;

The function returns the matrix vi interpolated values corresponding to xi, yi day. Arrays x, y, and z specific data points which are the values of v. If x, y and z are vectors, their values have to be monotonic, equally spaced [1].

vi = interp3(v, xi, yi, zi) (2)

interp3 function implies that x = 1: n, y = 1: m, Z = 1: p where [m, n, p] = size (v) and returns an array with the size you mxnxp, which is data interpolation matrix v [1], [15].

Interpolating through all four mechanical properties studied by three parameters final thermomechanical treatment (t - artificial aging

temperature, τ - ε during artificial aging - the degree of plastic deformation) resulted in a data volume 6069 interpolated values for each property.

Since aluminum alloys are "sensitive" to variations of the temperature of the treatment was determined a change in the temperature of treatment every five degrees, resulting in a total of 17 temperature between 120 ° C and 200 ° C. Artificial aging time was discretized at 4:00 to 8:00 p.m. by step for an hour, resulting 17 values of interpolation. The degree of deformation has been required a total of 21 values increasing with step of 1% in the range of 10-30%.

3. Experimental results and conclusions

After interpolation using the program, resulting 6069 values for each of the four mechanical properties. In these circumstances, the stakes optimization translates into finding of these data, only those that comply with the restrictions simultaneously EN_485-2-2007 regarding property values.

The calculations made in 1648 resulted in a number of cases (combinations of process parameters thermomechanical treatment) for each property in the 6069 possible cases, while fulfilling the requirements for the four mechanical properties:

- mechanical resistance, Rm ≥ 540MPa
- yield, RP0, 2 ≥ 470 MPa;
- elongation at fracture A5 ≥ 7%;
- Brinell hardness, HB ≥.

For each of the 1648 combinations of energy required to calculate the thermomechanical processing.

Calculation of energy as heat (thermal energy) means calculating the total energy consumed to heat treatment furnace that final artificial aging is done according to Figure 1 for mill use, according to the equation below:

Qtotal = Qtotal oven + Qlam, where: Qtotal oven - the amount of heat necessary to achieve and maintain temperature treatment throughout the performing heat treatment; Qlam - the amount of energy consumed for rolling sample.

The program developed in MATLAB shows that any value we impose the limits of the possible in 1648, any property of the four studies, we get a number of options which can be determined by calculating the optimal in terms of energy consumption.

The graphical interface made with the program allows viewing of those possible situations and the choice of a large number of values for each of the four properties as shown in the figure: 2, 3, 4, 5.

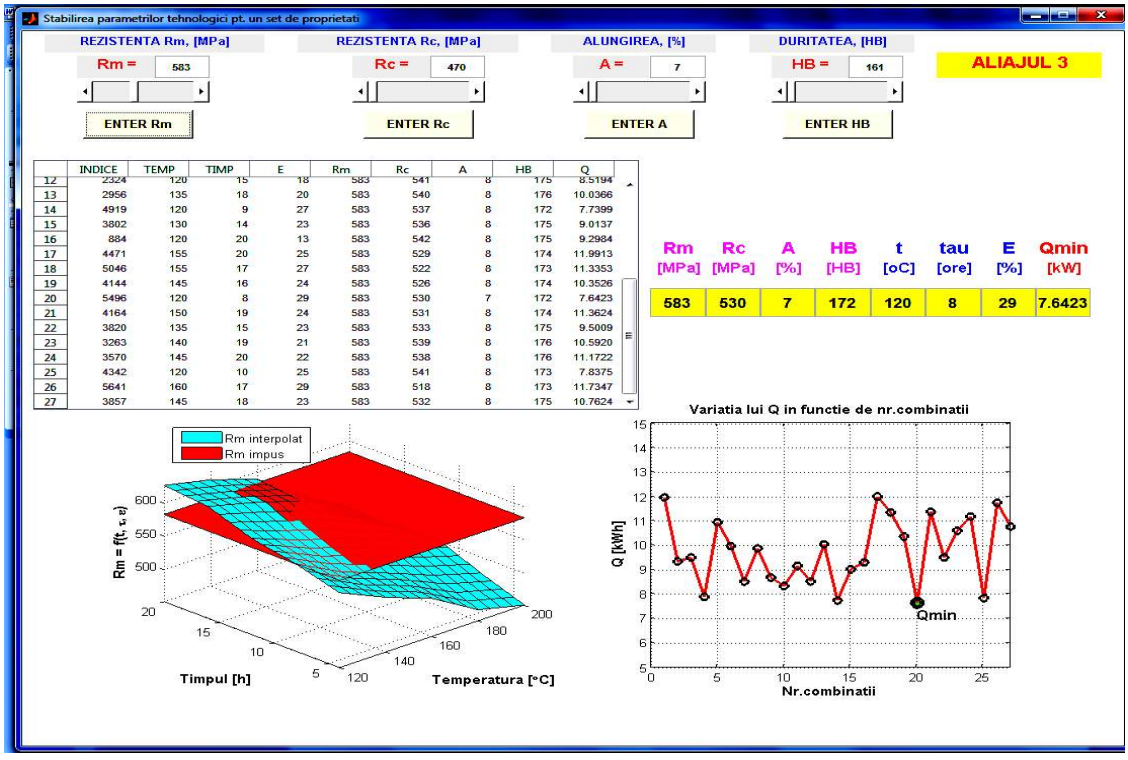

Fig. 2. *The values of thermomechanical treatment to obtain Rm = 583MPa*

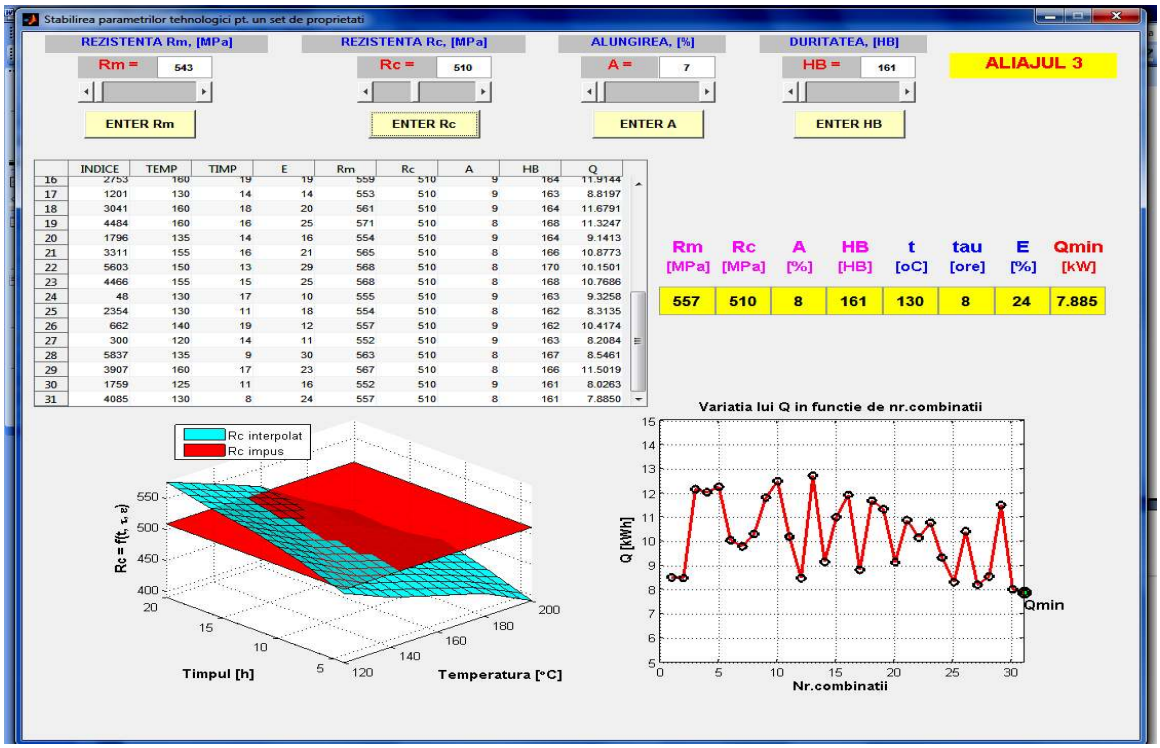

Fig. 3. *The valuesof thermomechanical treatment to obtain* $Rp_{0,2} = 583$ *MPa*

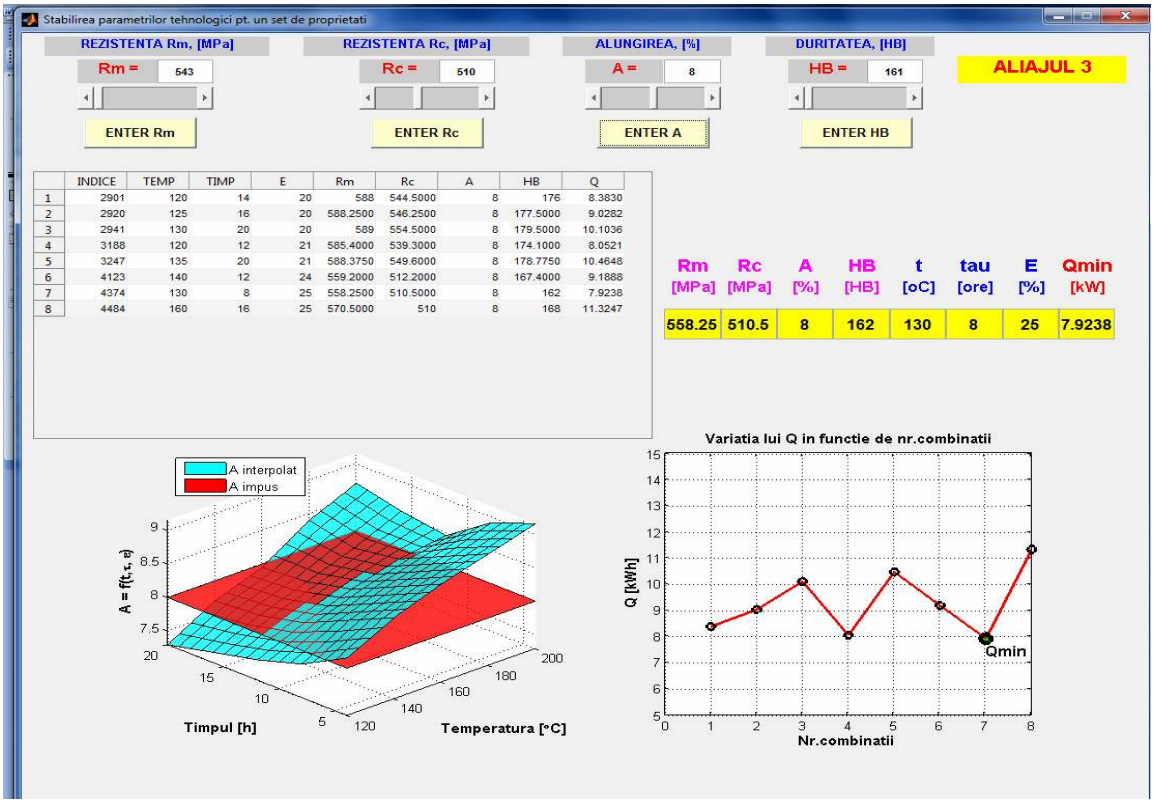

Fig. 4. *The values of thermomechanical treatment to obtain* $A_5 = 8$ *%*

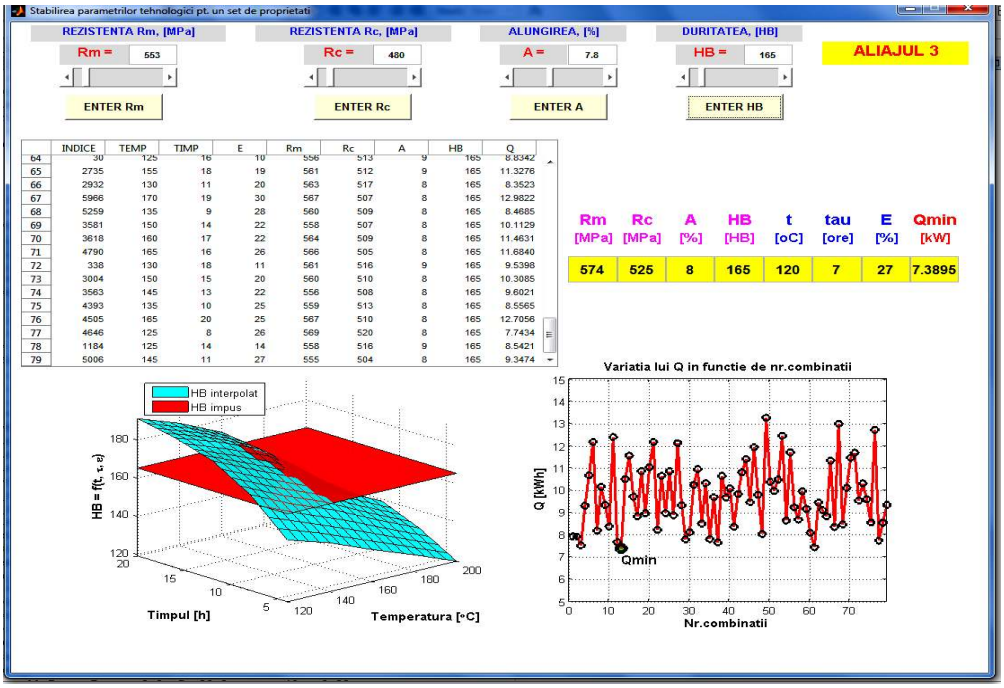

Fig. 5. *The values of thermomechanical treatment to obtain HB = 165*

With the help of the graphical user interfaces can be distinguished, in tabular form, the values of the parameters of thermomechanical processing for those situations where it is desired to obtain a certain amount of one or more of the properties of the study.

Along with calculating these values of thermomechanical treatment process parameters is calculated and the energy needed for these variations. Among them is selected and highlighted one which has the lowest energy consumption, that works best.

In Figures 2, 3, 4, 5 are shown a few examples. Figure 2 shows the situation when the required mechanical strength of 583 MPa, it is apparent that optimal way from the point of view of energy consumption, varying the parameters of thermo-mechanical treatment are the following: T = 120°C, τ = 8:00, ε = 29% with an energy consumption of 7.64kW. Figure 3 shows the situation in which, for a yield strength of 510 MPa, there are 31 possible cases, but of which the most economical is the treatment that has the following parameters: T = 130°C, τ = 8:00, ε = 24%, giving a power consumption of Qtot = 7.88kW.

Elongation 8% is obtained for the optimal parameters shown in Figure 4, with values T = 130°C, τ = 8:00, ε = 25%, leading to a minimum energy Qtot = 7.9kW.

Hardness HB = 165 is obtained for T = 120°C, τ = 7 hours, ε = 27%, as shown in Figure 5, and the minimum value of Qtot = 7.39kW.

References

[1]. Ghinea M., **Fireţeanu V. –** *MATLAB – calcul numeric – grafică – aplicaţii,* Editura Teora, ISBN 973-601-275-1, Bucureşti, 1998;

[2]. Giacomelli I. – *Aspecte privind unele procedee de îmbătrânire accelerată a aliajelor de aluminiu pentru turnare,* revista Construcţia de Maşini, nr.8/1992

[3]. Ciucă I. Dumitriu S. **-** *Modelarea şi optimizarea proceselor metalurgice de deformare plastică şi tratamente termice,* Editura Didactică şi Pedagogică, Bucureşti, 1998;

[4]. Banabic D., **Dorr I. R. -** *Modelarea proceselor de deformare plastică a tablelor metalice*, Editura Transilvania Press, Cluj-Napoca, 1995

[5]. Baron T., **ş.a.**, **-** *Statistică teoretică şi economică,* Editura Didactică şi Pedagogică. Bucureşti, 1995;

[6]. Cazimirovici E. – *Bazele teoretice ale deformării plastice* – Editura Bren Bucureşti, 1999;

[7]. Cănănău N., Tănase D. – *Tehnologia deformării plastice,* Galaţi University Press, 2010;

[8]. Moldovan, P. - *Alliages nonferreux*, Ed. Matrix Rom Bucureşti, 2003;

[9]. Neacşu M., Hanganu D., Vasilescu E. - *Mathematical modeling of thermomechanical treatment process applied to aluminum base alloys for aeronautics,* Analele Universitatii „Dunarea de Jos" din Galati, Fascicula IX Metalurgie şi Ştiinţa Materialelor, nr.4/2011, pag. 70 – 76;

[10]. Popa B., Man E., Popa M. – *Termotehnică, agregate şi instalaţii termice,* Editura tehnică, Bucureşti, 1979;

[11]. Popescu O., ş.a. – *Matematici aplicate în economie,* vol.1 şi vol. II, Editura Didactică şi Pedagogică, Bucureşti, 1993;

[12]. Şerban R., Dumitrescu T. – *Metode de optimizare*, Editura Matrix Rom, Bucureşti, 1998;

[13]. Taloi D. ş.a. – *Optimizarea proceselor metalurgice*, Editura Didactică şi Pedagogică, Bucureşti, 1983;

[14]. Neacşu M. – *Influenţa compoziţiei chimice, a tratamentelor termice şi termomecanice asupra proprietăţilor mecanice ale aliajelor din sistemul Al-Zn utilizate în aeronautică,* Teză de doctorat, Galaţi 2012.

THE ANNALS OF "DUNAREA DE JOS" UNIVERSITY OF GALATI.
FASCICLE IX. METALLURGY AND MATERIALS SCIENCE
N^0. 4 – 2013, ISSN 1453 – 083X

EFFECT OF OXIDATION ON SPECTROPHOTOMETRIC AND RHEOLOGICAL PARAMETERS OF CORN OIL

Liviu Cătălin ŞOLEA, Romică CREŢU
"Dunărea de Jos" University of Galaţi, 111, Domnească Street, 800201, Galaţi, Romania
email: liviu.solea@yahoo.com

ABSTRACT

The aim of this study is the viscosity's evolution depending on the temperature and the shear rate and the analysis of the transmittance spectra of the oxidized corn oil. Corn oil was oxidized of the temperatures of 100°C, 110°C, 120°C, the periods of time of oxidation being 5 to 10 hours. An increase of the viscosity depending on the increase of oxidation temperature and oxidation time is to be noticed. Increasing of the oxidation temperature and the period of oxidation is the cause of the progressing color difference of the oxidized oils comparing to non-oxidized corn oil.

KEYWORDS: transmittance, corn oil, viscosity, shear rate

1. Introduction

Vegetable oils are composed to an extent of 98-99% by fatty acids whose characteristics vary according to the number of carbon atoms, the number of double bonds between carbon atoms and position of these bonds in the fatty acid molecule.

Groups of fatty acids are:

-saturated acids (no double bonds) - myristic acid, palmitic, stearic and so on;

-monounsaturated acids (only one double bond) - oleic acid, erucic acid;

-polyunsaturated acids (with more double bonds) - linoleic acid, linolenic acid;

-fatty species (radicals containing hydroxy, epoxy, etc.).

The most important fatty acids contained in vegetable oils are: oleic acid (C18:1), linoleic acid (C18:2), linolenic acid (C18:3), palmitic acid (C16:0) and stearic acid (C18:0)

Research has shown that oils with a high content of oleic acid (high oleic) are significantly more stable than those with a low content of oleic acid. Oils with long links between carbon atoms indicate a low friction and a low wear compared to oils which have short links between carbon atoms. Oils containing saturated compounds have improved stability to oxidation at high temperature and high pressure compared to the oils containing unsaturated compounds. Free fatty acids have a high degree of polarization and will have a slight reaction with metallic surfaces, forming a layer of adsorption [1], [2].

Corn oil is obtained from corn germs containing 20-30% oil and remaining from degerminating of corn for maize or from starch production, ethyl alcohol, etc. Refined corn germ oil has superior sensory properties, high content in essential fatty acids, being included in the group of dietary product because it helps to reduce cholesterol in the blood, it also has a low free acidity (maximum 0.3% oleic acid) and a low water content.

2. Experimental details

Determination of transmittance spectrum was performed using a spectrophotometer type T60 produced by PG Instruments Limited (EC), determinations were realized in a range of 300-1100nm.

Viscosity was determined by Rheotest 2 system, shear rates ranging between 3.3 and 80s^{-1}, the test temperatures being between 30 and 90°C.

In a first stage we determined the transmittance spectra for non-oxidated corn oil then this oil has been undergone a forced oxidation process to different temperatures and periods of time of oxidation so as to establish the transmittance spectra. Corn oil was oxidized to 100°C and 110°C temperatures, the periods of oxidation time being 5 hours and 10 hours.

To perform forced oxidation process, a system was built in Figure 1. It is composed of 1 - air pump, 2 - air flow meter 3 - air filter, 4 - tube with the sample of oil, 5 - thermostatic bath. For each

oxidation test 25 ml of oil were used. The flow rate of air introduced into the oil sample was 20 l/h.

Also, the samples were measured for colour in the x, y, z or L*, a*, b* and C*, h_{ab} coordinates (CIEXYZ, CIEL a*b* and $CIEC_{ab}$*h_{ab} colour systems). CIE L*a*b* scale is recommended by Commission Internationale de l'Eclairage (CIE), were b* measures the yellowness when is positive, the grayness when zero, and the blueness when negative. In this colour space L* represents the lightness.

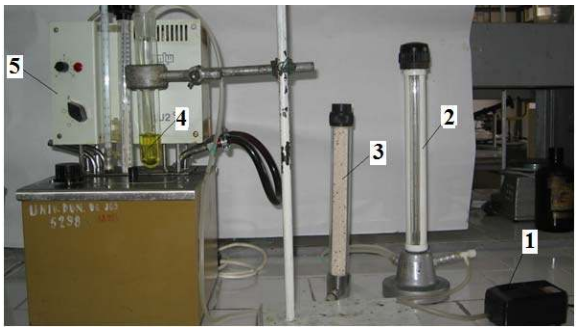

Fig. 1. *Oxidation equipment*

Illumination was performed by C/2^o (standard illuminant defined by CIE). Chroma values denote the saturation or purity of colour. Hue angle values (exprimate in grade) represent the degree of redness, yellowness, greenness and blueness [4].

Dominant wavelength, λ_d was determined as described according to CIE indications [5], [6].

Forced oxidation behavior research of the oxidized and non-oxidized rapeseed oils give us qualitative and quantitative estimations regarding their efficiency in use as lubricants. Trichromatic values are obtained in the case of oils by determination of the transmittance according to the relations:

$$X = 0.21 \cdot T_{445} + 0.35 \cdot T_{550} + 0.42 \cdot T_{625}$$
$$Y = 0.17 \cdot T_{445} + 0.63 \cdot T_{550} + 0.20 \cdot T_{625}$$
$$Z = 0.94 \cdot T_{445} + 0.24 \cdot T_{495}$$

where T is the transmittance measured by the spectrophotometer, when λ is 445, 495, 550 and 625 nm [7], [8].

3. Experimental results

Corn oil was oxidized at the temperatures of 100ºC and 110ºC for 5 or 10 hours. Transmittance spectra of corn oil oxidized at a temperature of 100ºC for 5 and 10 hours are shown in Figures 2 and 3.

It is noted that the transmittance values of 5 or 10 hour oxidized corn oil are not too much changed compared to the transmittance values of non-oxidized oil. Important changes occur for the range of wavelengths between 490nm and 590nm. On the other hand trichromatic parameters established for 100ºC oxidized corn oil, presented in the Tables 1 and 2, certify the presence or absence of the pigments from the macrocyclic pyrrole colorants category.

According to the data from the Table 1, while 100ºC corn oil oxidation, the dominant wavelength vary between 576.5nm and 579.5nm, values that are corresponding to the yellow-orange area in chromatic diagram.

It is noted a slight difference between the dominant wavelength of 5 hour oxidized oils and 10 hour oxidized oils. Oil oxidation can influence the trichromatic parameters beginning with a period of exposal of 5 hours.

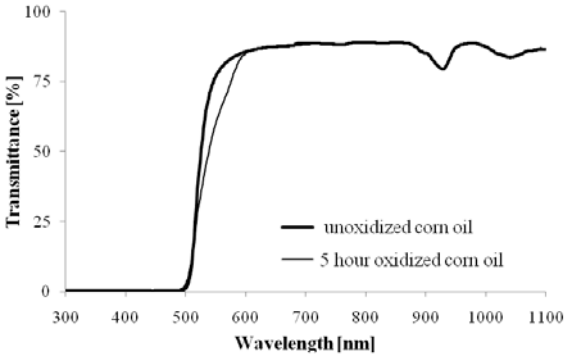

Fig. 2*. Transmittances of unoxidized and oxidized corn oils for 5 hour at a temperature of 100°C*

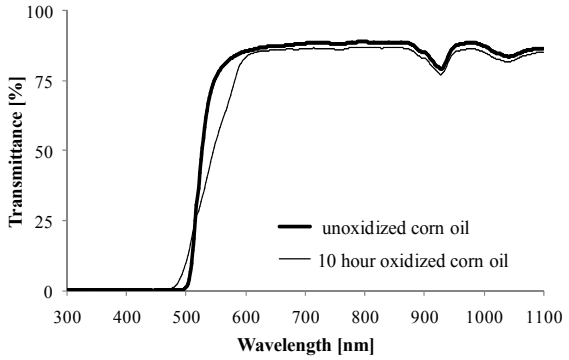

Fig. 3*. Transmittances of unoxidized and oxidized corn oils for 10 hour at a temperature of 100°C*

As shown in Table 2, the parameter b* and brightness of the studied samples decrease as the time of forced oxidation increases. Thus, the trichromatic measurements show a decrease of 8.66% of the brightness compared to non-oxidized corn oil (ΔL^* = -7.35 on 100ºC), probably due to the chromophores destroyed by the effect of the oxygen. Also, the value of the parameter a^* is very small compared to the b^*

parameter, it is clear that the rate of red will tend to subunit values. Chroma, another trichromatic parameter, decreases with increasing of the time of oxidation for the corn oil at 100°C, from 150.41 to 111.95. On the other hand, according to the CIE 1976 (a^*, b^*) chromaticity diagram carried out according to the data from Table 1, the hue angle h_{ab} vary with the time of oxidation from 5 to 10 hours, in quadrant I (0-90 °) to lighter shades of yellow, which is correlated with variation of the other chromatic parameters, in order to elucidate the color change of corn oil during the oxidation. We notice the hue angle migration from the second quadrant of the chromaticity diagram (corresponding to the position of non-oxidized oil color) to the first quadrant (corresponding to oxidized oil).

Increasing the oxidation temperature from 100ºC to 110ºC (Fig. 4 and 5), it is noted that, in the visible area, there are important changes of the transmittance spectra, for 5 hour oxidized oil sample or for 10 hour oxidized oil sample as well. This thing shows that a 10ºC temperature increase, in the same experimental conditions, lead to a sharp oxidation of the corn oil.

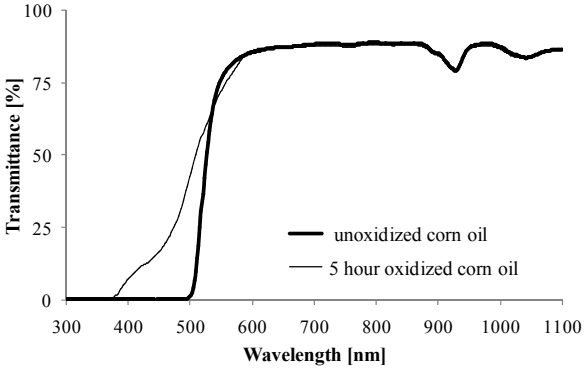

Fig. 4. *Transmittances of unoxidized and oxidized corn oils for 5 hour at a temperature of 110°C*

From Table 3 it is revealed a larger range of values for dominant wavelength of corn oil after 10 hours of oxidation, at 110ºC, compared to its values when the oil was oxidized at 100ºC (Table 1). Also, by color position location in chromatic diagram (trichromatic coordinates x şi y), we deduce the pronounced variability of the oil color in time. Also, corn oil color localization is well defined by the parameters a* and b* (Table 4).

According to these the color of this oil is localized in the quadrant II (90º - 180º), unlike the case when the oil is oxidized at 100ºC. Also, from the data in Table 4 it is revealed a rapid decrease of the color intensity while oxidation, by the variation of chroma from 150.41 to about 9. Meanwhile the angle hue is increasing in the quadrant II up to shades of yellow-green.

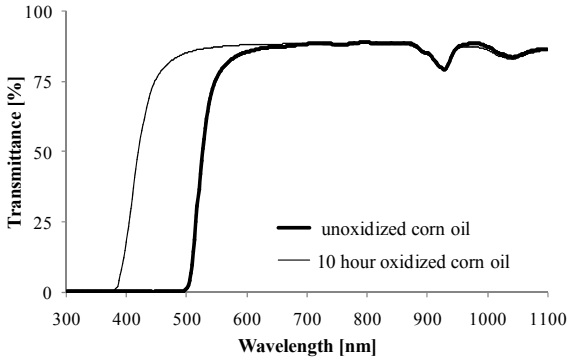

Fig. 5. *Transmittances of unoxidized and oxidized corn oils for 10 hour at a temperature of 110°C*

Based on the results above we determined the differences of color for each chromatic parameter analyzed, by calculating the color difference between the recorded values during 10 hour and 5 hour oxidation and the initial one (Table 5). Trichromatic measurements show an increase of brightness as compared to non-oxidized oil, to both periods of oxidation time for which the experiments were performed, ΔL^* = 2.03 after 5 hour oxidation time, or ΔL^* = 9.94 after 10 hour oxidation time at 110°C. This is due to the fact that even after 5 hour oxidation time are some of the oil pigments are destroyed, in 10 hour oxidation time peroxides and hydroperoxides are both formed in the stage of oxidation phenomena propagation.

Much sharper turns out to be b^* parameter variation by its decrease comparing to the initial sample. Thus, in corn oil case, the degree of yellow is decreasing with about 25.8% (100ºC) and 94.35% (110ºC). In the presence of oxygen, no matter the study temperature might be, the corn oil becomes a little yellow, meaning the grade of yellow is decreasing ($-\Delta b^*$). This occurs because, as a consequence of oxidation, oil pigments disappear, and the light corresponding to the blue area in the spectrum is less distributed than that corresponding to the yellow area (leading to a decrease of the yellow degree).

The hue angle (tonality angle) vary in a range of values much wider the oxidation temperature for corn oil increases (Table 5). As in the case of 100ºC oxidation of the corn oil, the analysis of the chromatic parameters at 110ºC oxidation, leads to the same conclusions as information provided by the transmittance spectra regarding oil oxidation reaction. Further on, using Rheotest 2 equipment, we determined the viscosities of oxidized corn oil and

non-oxidized corn oil as well. In the graphs shown in Figures 6 and 7 there are represented the temperature variation with shear rate, for non-oxidized corn oil and oxidized corn oil at a temperature of 110°C and 120°C, the period of oxidation time being 5 and 10 hours respectively.

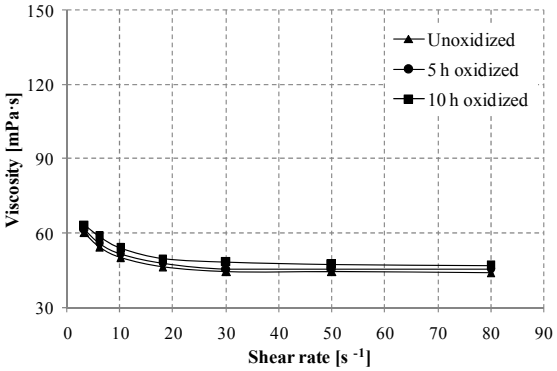

Fig.6. *Variation of viscosity with shear rate, for the unoxidized and oxidized corn oil at the temperature of 110°C*

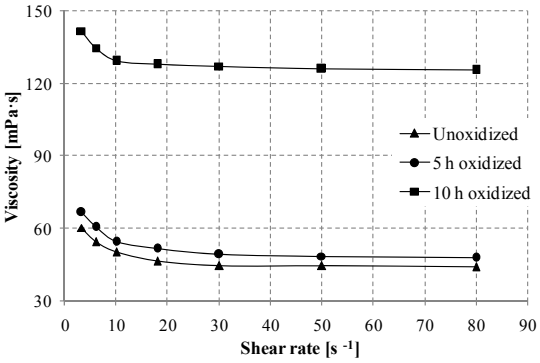

Fig.7. *Variation of viscosity with shear rate, for the unoxidized and oxidized corn oil at the temperature of 120°C*

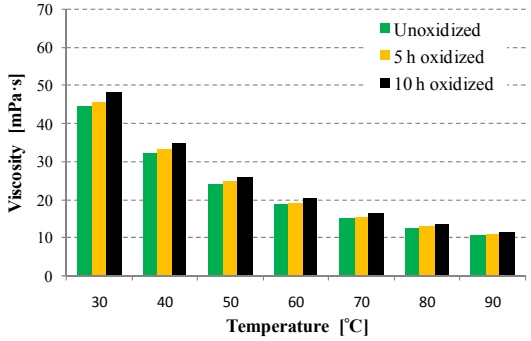

Fig. 8. *Variation of viscosity with temperature, for the unoxidized and oxidized corn oil at the temperature of 110°C*

Viscosity decreases with the shear rate for both oxidation temperature values, meanwhile one can notice a high increase of viscosity for the oil that was oxidized for 10 hours at a temperature of 120°C.

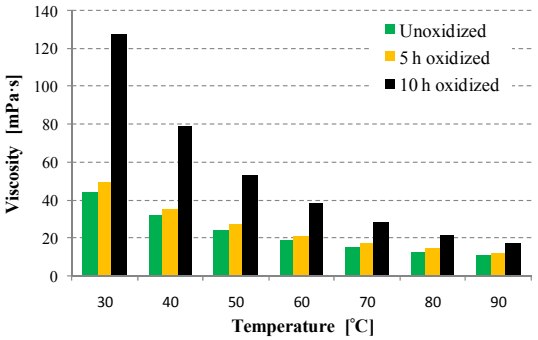

Fig. 9. *Variation of viscosity with temperature, for the unoxidized and oxidized corn oil at the temperature of 120°C*

In Figures 8 and 9 we represented the variation of viscosity with temperature for non-oxidized corn oil and for corn oil that was oxidized at 110°C and 120°C for 5 hours and 10 hours respectively. Viscosity is decreasing with temperature for all oil samples in both cases of temperature and periods of testing time.

It is noted a sharp increase of the viscosity for 10 hours oxidized oil at the temperature of 120°C. Thus for a testing temperature of 30°C it is recorded an increase of the viscosity with 187.16% compared to non-oxidized oil viscosity, in the case of recorded testing temperature the increase is 104.17%, the percentage increase observed for 90°C testing temperature is 66.67%. The percentage increase of oxidized oil at a temperature of 120°C for 10 hours decreases with the increase of testing temperature.

4. Conclusions

Using spectrophotometer analysis of corn oil, oxidized in various conditions, it was found that the transmittance spectra and chromatic parameters are changing. The color differences of oxidized oils compared to non-oxidized oils, increase with the temperature and the period of time of oxidation.

Analysis of viscosity evolution with temperature and shear rate for corn oils also show that this parameter is an indicator of oil oxidation. Viscosity decreases with increase of the temperature and shear rate.

Following these viscosity tests we noticed an increase of viscosity with the increase of oxidation temperature and the period of time for oxidation.

Viscosity evaluation with temperature and shear rate, correlated with oxidized oils transmittance variation analysis, respectively trichromatic analysis shows that these parameters are good indicators of oil oxidation.

Table 1. *Experimental results for corn oils oxidized at a temperature of 100ºC*

Corn oil	Trichromatic components			Trichromatic coordinates			λ_d [nm]
	X	Z	Z	x	y	z	
Unoxidized	63.245	65.666	0.19	0.4898	0.5086	0.0014	576.5
5 hours oxidized	57.456	55.249	0.43	0.5078	0.4883	0.0038	579
10 hours oxidized	54.831	52.327	1.798	0.5032	0.4802	0.0165	579.5

Table 2. *Chromatic characteristics (systems: CIELAB, CIELCH) for corn oils oxidized at 100°C*

Corn oil	Chromatic coordinates			a^*/b^*	$(a^*/b^*)^2$	C^*_{ab}	h_{ab}
	L^*	a^*	b^*				
Unoxidized	84.825	-2.507	150.395	-0.01668	0.0002	150.416	90.95
5 hours oxidized	79.18	8.2005	133.334	0.06150	0.00378	133.586	86.48
10 hours oxidized	77.475	9.0922	111.582	0.08148	0.0066	111.952	84.91

Table 3. *Experimental results for corn oils oxidized at a temperature of 110ºC*

Corn oil	Trichromatic components			Trichromatic coordinates			λ_d [nm]
	X	Z	Z	x	y	z	
Unoxidized	63.245	65.666	0.19	0.4898	0.5086	0.00147	576.5
5 hours oxidized	65.247	69.703	23.81	0.4109	0.4390	0.1499	574
10 hours oxidized	83.08	87.057	89.63	0.31982	0.33513	0.34504	564

Table 4. *Chromatic characteristics (systems: CIELAB, CIELCH) for corn oils oxidized at 110°C*

Corn oil	Chromatic coordinates			a^*/b^*	$(a^*/b^*)^2$	C^*_{ab}	h_{ab}
	L^*	a^*	b^*				
Unoxidized	84.825	-2.5079	150.395	-0.0166	0.00027	150.416	90.955
5 hours oxidized	86.851	-6.7254	60.0226	-0.11205	0.01255	60.3982	96.393
10 hours oxidized	94.762	-4.2072	8.48755	-0.4956	0.24570	9.47306	116.367

Table 5. *Experimental values of color differences when studied corn oils during forced oxidation*

Corn oil	Time [hours]	ΔL^*	Δa^*	Δb^*	ΔC^*_{ab}	Δh_{ab}	ΔE^*_{ab}
Oxidized oil to 100ºC	5	-5.64	10.71	-17.06	20.92	-4.475	20.92
	10	-7.349	11.61	-38.82	-38.47	-6.037	41.172
Oxidized oil to 110°C	5	2.03	-4.21	-90.37	-90.02	5.438	90.49
	10	9.94	-1.699	-141.91	-140.95	25.412	142.261

References

[1]. Gülsüm, P. - *Bio-based Lubricants*, Opet Petrolcülük A.Ş., AOSB-Izmir, (2008).
[2]. Stachowiak, G.W., Batchelor A.W. - *Engineering Tribology*, Butterworth-Heinemann, Team Lrn, (2005).
[3]. Iliuc, I. - *Tribology of Thin Layers*, Elsevier Scientific Publishing Co., Amsterdam, Oxford, New-York, (1980).
[4]. *** - CIE Technical Report., Colorimetry, 3rd ed., Publication 15, Central Bureau of the CIE, Vienna, (2004).
[5]. *** - CIE Technical Report: *Improvement to Industrial Colour-Difference Evaluation,* (2001).
[6]. *** - CIE Pub. No. 142, Vienna: Central Bureau of the CIE, (2001).
[7]. Zgherea, **Gh**. - *Analize Fizico – Chimice*, Ed. Fd. Universitare "Dunărea de Jos" Galaţi, pp. 74-80, (2002).
[8]. Florea, T., Creţu, R., Zgherea, Gh. - *Studiul afinităţii unor coloranţi alimentari faţă de fracţiile majore ale laptelui, Buletin de Informare Pentru Industria Laptelui (BIIL)*, Editura Academica, 19 (2), II, pp. 86-101, (2004).

THE ANNALS OF "DUNAREA DE JOS" UNIVERSITY OF GALATI.
FASCICLE IX. METALLURGY AND MATERIALS SCIENCE
N^0. 4 – 2013, ISSN 1453 – 083X

ANALYSIS OF DENTAL ALLOYS CHARACTERISTICS (MICROSTRUCTURE AND CORROSION RESISTANCE) FOR DIFFERENT OBTAINING METHODS

Ionuţ ŞTIRBU, Petrică VIZUREANU, Nicanor CIMPOEŞU
Technical University "Gh. Asachi" Iaşi
e-mail: nicanornick@yahoo.com

ABSTRACT

A dental alloy was studied by electro-chemical polarization method, scanning electrons microscopy (S.E.M.) and X-ray dispersive energy analysis (EDAX) equipments analyzing the influence of casting process on microstructure and corrosion behaviour. These studies present that in natural aerated Afnor solution saliva this alloy behaves as a corrosion resistant alloy. By casting, this alloy undergoes a significant modifications of both internal microstructure and corrosion resistance. Using over-potentials bigger than five hundred mV (SCE) in artificial saliva this alloy exhibits a generalized corrosion, the surface morphology being dissimilar for commercial and as-cast samples. EDAX studies point out that corrosion takes place especially by cobalt dissolution.

KEYWORDS: dental alloy, Co-Cr-Mo, potentiometry, EDX analysis, surface morphology

1. Introduction

The base-metal alloys have received recently considerable attention in biomedical field, because such alloys provide excellent strength, toughness and wear resistance. Cobalt-Chromium alloys are well used for biomedical applications such as fixed and removable partial denture framework and orthopaedic implants owing to their excellent mechanical properties, wear resistance and biocompatibility /1, 2/. Besides the economic advantage over gold, owing to their low cost, these alloys are attractive because they are less than half the density and are considerable stronger than gold. Co-Cr dental alloys have an excellent corrosion resistance, which is provided by a thin adherent layer of chromium-based oxides on the surface /3, 4/. The most used Cobalt base alloys for dentistry is Co-Cr-Mo with carbon content about 0.5 percent. Chromium and Molybdenum are substantial elements while Carbon is well known as interstitial element. It was stated that corrosion resistance of metallic denture prostheses depends on many factors, among other things on the chemical composition, surface structure and microstructure. Many of microstructure aspects such as: elements segregation and cast homogeneity, shrinkage and pores, sizes of grain boundaries or precipitates are directly subjected to the production engineering and manufacture of casts /5, 6/. Venugopalan and Gaydon /7/, in a review of the corrosion behaviour of surgical implant alloys, observe that cobalt alloys do not show the traditional active-passive transition as they were also in a passive state prior to testing. The wrought and cast alloys do not exhibit a hysteresis loop in a potentiodynamic polarization curve, indicating that they can repair damage to their oxide/passive layer faster/better. The casting of these alloys is easily performed by the use of a gas-oxygen flame with a blowtorch. Nevertheless, the gas-air combustion in the blowtorch exposes the worked alloy to oxidation through the inclusion of carbon which might change the physical and corrosion properties of the alloy /8, 9/.

The aim of this study is to evaluate the influence of the casting process on the microstructure and the corrosion behaviour of a Co-Cr dental alloy

2. Experimental part

For these studies a "CH" trade mark dental alloy, produced and purchased by VASKUT Kohaszati Kft - Hungary, was used. This is a Co-Cr type dental alloy for prosthesis, crown, bridges and round bridges, having the composition:

Co = 62%, Cr = 30%, Mo = 5%, Si = 1%, C = 0.5%, Mn = 0.5%, W = 0.5%

The manufacturer indicates that the Co-Cr-Mo base alloys are suitable for producing corrosion resistant long life metal frameworks and plate casting, easy to process and polish providing an aesthetic outlook. The material meets ISO 6871-1, ISO TR 7405 and 93/42/EEC Council Directive prescriptions. From this commercial material a casting sample was obtained by melting in butane/oxygen flame and manual horizontal centrifugal machine, in a non-controlled casting environment.

Corrosion behavior was realized by rapid electrochemical tests, particularly by dynamic potentiometry. The measurements of open potential circuit and potentiodynamic polarizations were performed on a VoltaLab 21 Electrochemical System (PGP201 - Radiometer Copenhagen) equipped with the acquisition and processing data software VoltaMaster 4. A three-electrode electrochemical cell was used. From commercial and as-cast materials, the working electrodes were performed in cylindrical form and mounted in a Teflon support to enable the connection to rotating port-electrode of the electrochemical cell.

The free area was precisely measured before embedding in the Teflon support. A saturated calomel electrode (SCE) was used as a reference and platinum as auxiliary electrode.

Each specimen was polished with SiC paper, gradually, down up to 4000 grit specification, degreased with acetone and washed in distilled water.

As corrosion medium an aerated solution of Afnor artificial saliva (Carter-Brugirard AFNOR/NF (French Association of Normalization) 591-141) was used, having the composition: NaCl – 0.7 g/l, KCl – 1.2 g/l, $Na_2HPO4H2O$ – 0.26 g/l, $NaHCO_3$ – 1.5 g/l, KSCN – 0.33 g/l, urea – 1.35 g/l, and pH = 8.

Linear polarization measurements were performed, in aerated solution, at potentials near the E_{corr}, in the potential range ± 150 mV against the open circuit potential and a potential scan rate of 0.5 mV/s. The polarization resistance (R_p) was calculated as tangent slope at the electrode potential vs. current density curve in the E_{corr} point. The cathodic Tafel slope (b_c) was calculated as the potential change over one decade (one order of magnitude) decrease in the current density at potentials near the E_{corr}. The anodic Tafel slope (b_a) was determined in a similar way.

Linear polarization method is used to determine when a test electrode is at its steady state. Polarization resistance is used to estimate the general corrosion rate of the metal.

On the basis of these data, the corrosion current density (J_{corr}) - which is a measure of the corrosion rate, was calculated with the Stern-Geary equation:

$$J_{corr} = \frac{b_a b_c}{2{,}3R_p\left(b_a + b_c\right)} \qquad (1)$$

The corrosion rate, expressed as penetration rate - the layer thickness of the metal removed from the alloy surface in the time unity, was evaluated with the relation:

$$v_p = 3{,}27.\overline{\left(\frac{A}{z}\right)}.\frac{J_{cor}}{\rho} \quad \text{, μm/year} \qquad (2)$$

where: A – is the atomic mass of the corrodible metal (g/mol), z – number of electrons changed in the corrosion process, ρ - density of the removed component (g/cm^3) and J_{corr} – instantaneous current density (μA/cm^2).

Three additional corrosion parameters: corrosion potential in dynamic conditions (E_{cor}), breakdown potential (E_{BD}) and re-passivation potential (E_{RP}), were determined from the cyclic potentiodynamic polarization curve, performed at a potential scan rate of 10 mV/s, on the electrode potential range: –1500 to +1500 mV:

To evaluate the influence of the casting on the corrosion process and the surface morphology, an electrochemical treatment, consisting in five successive cyclic polarizations, was performed in 0…+1500 mV potential range, with a 10 mV/ potential scan rate. First cycle was beginning on -1500 mV, view to electrochemical cleaning of the surface.

To study the microstructure of the two alloys samples their surface was chemically treated in agreement with standard procedures /10/. The treated surface was examined with using a XJP-6A type metallurgical microscope (China). After the electrochemical treatments, a study of the modifications of the alloys surface was performed on a VEGA-TESCAN Scanning Electron Microscope equipped with QUANTAX Bruker AXS Microanalysis system.

3. Results and discutions

The microstructures obtained for the two studied sample are shown in Figure 1.

For the wrought sample one can identify large amounts of precipitate along the interdendritic regions. Considering the ternary phase diagram of Co-Cr-Mo alloy, the precipitate in this high chromium alloy can be a mixture of Mo-concentrate R ($Co_{49}Cr_{21}Mo_{30}$) and μ(Co_7Mo_6) phase, or, more probable, chromium carbides like Cr_7C_3 or $Cr_{23}C_6$ due to presence of the C in alloy composition. The image for as-cast sample reveals a quite different aspect, a relativelly ordered broken dendrite structure with large interdendritic zones. Using the QUANTAX Bruker AXS Microanalysis (GmbH, Berlin, Germany) the compositions of the commercial and casting „C" alloy, both before and after

electrochemical treatment, were evaluated. The obtained values are presented in Table 1.

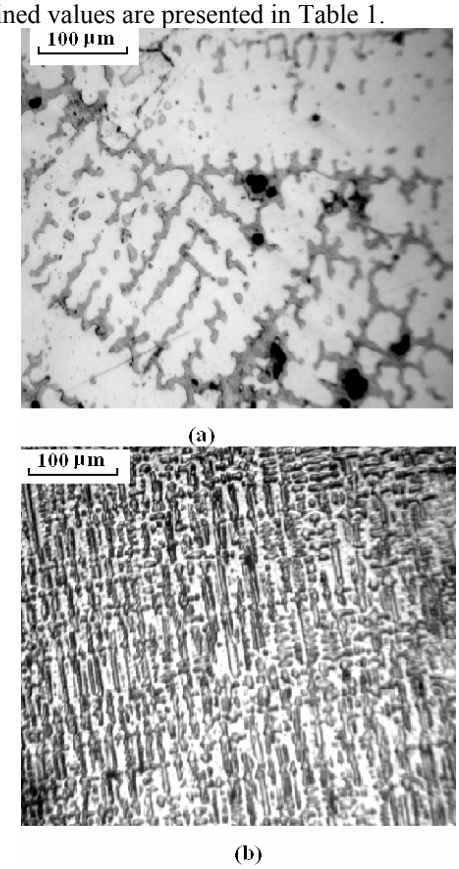

Fig. 1. *Optical micrographs of commercial Co-Cr sample (a) and as-cast sample (b)*

The composition of the commercial sample differs slightly comparing to the one indicated by manufacturer, the quantity of Cobalt being approximately 3% higher while the quantity of Chromium is more than 3% smaller. The performed microanalysis did not evidence the presence of Manganese (Mn) and Tungsten (W).

By casting, the alloy loses out more than 2% of Chromium, while the percentages of Mo, Si and C practically remain unchanged. The loss of Chromium percentage is reflected in a corresponding increase of the Cobalt percentage.

The five cycles of polarization in Afnor saliva lead to a superficial corrosion which produces a modification of the superficial composition of the alloy. This modification consists in a pronounced decrease of the Cobalt; about 24% for the commercial sample and 19% for the casting sample. This denotes that the corrosion process takes place by anodic dissolution of the Cobalt from the alloy.

More unlike the non-electrochemically treated sample, the microanalysis indicates that on both commercial and casting electrochemically treated surfaces a quantity of almost 12% Oxygen is present on alloy surface. This is probable due to formation of Cr_2O_3 and MoO_3 oxides, which assure the higher resistances to corrosion at over-potentials lower than 700 mV (SCE).

The linear polarization curves, in semi-logarithmic coordinates (Evans diagram), and the cyclic polarization curves for the two studied samples are presented comparatively in figure 2.

Table 1. *Superficial compositions of „CH" alloy, no processed and as cast, before and after electrochemical treatment in artificial Afnor saliva*

Surface state	Sample	Element (wt %)					
		Co	Cr	Mo	Si	C	O
Non-corroded	Commercial alloy	65	26	6.0	0.5	1.5	-
	Casting alloy	67	24	6.0	0.5	1.3	-
Electrochemically processed	Commercial alloy	50	27	7.3	0.7	2.0	12
	Casting alloy	54	24	7.0	0.6	1.5	12.

From Evans diagram the corrosion parameters corresponding to the equilibrium state were evaluated. Corrosion potential ($E_0 \equiv E$ (I=0)) - namely the potential where the total corrosion current is zero) and, Tafel constants (b_a and b_c), polarization resistance (Rp), instantaneous corrosion current density (J_{cor}) and corrosion rate (v_{cor}). From cyclic polarization curves the corrosion potential (E_{cor}), breakdown potential (E_{BD}) and re-passivation potential (E_{RP}) were evaluated. Table 2 collates these parameters.

The corrosion potential in quasi equilibrium conditions (obtained at lower potential scan rate), $E_{0,}$ is more negative for commercial sample than for the as-cast sample, this indicating a higher tendency of corrosion when the alloy is immersed in Afnor saliva. This is only an apparent situation because of the polarization resistance of commercial alloy in this artificial saliva is five time higher than that of the casting alloy. Accordingly, the instantaneous current density and corrosion rate are lower in the case of the wrought alloy. However, the differences regarding the corrosion behaviour of the two samples in Afnor saliva are not relevant. More, the values of the corrosion rates are very small, indicating a high corrosion resistance of this alloy.

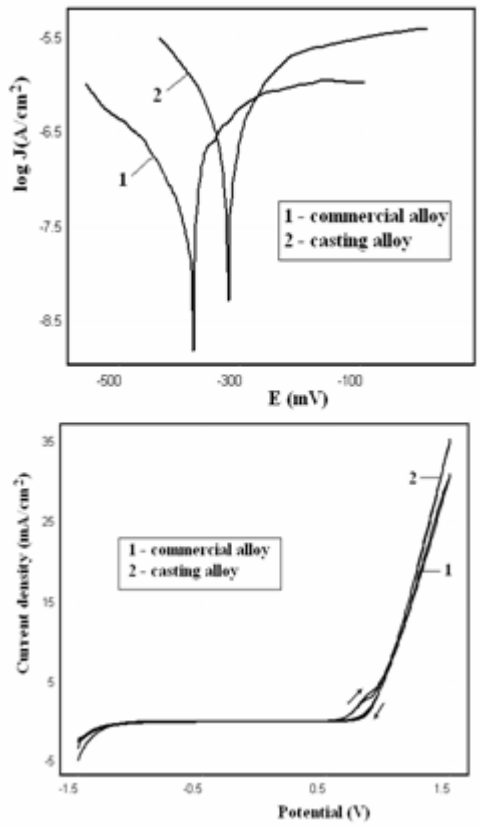

Fig. 2. *Linear potentiodynamic polarization curve (a) and single cyclic polarization curve (b) for commercial (curve 1) and as-cast (curve 2) alloys*

The cyclic voltammograms of the two sample showed a very close similarity (Fig. 2(b)); the two curves practically overlap. The two recorded curves revealed the passive region over a large domain of potential, from negative value to the breakdown potential situated at 557 and 523 mV (SCE) respectively. At over-potentials higher than the breakdown potential the corrosion currents increase appreciably and vary linearly with electrode over-potential, indicating a direct dependence between corrosion current and over-potential. The anodic and cathodic branches of the polarization curve in this domain practically overlap, excepting the potential range between E_{BD} and E_{RP}, where a small hysteresis loop appears. The slopes of the linear portions are 47.6 mA /(cm^2.V) for the non-casting sample and 54.7 mA/(cm^2.V) for the casting sample.

The current densities at 1500 mV potential electrode were 30.9 mA/cm^2 and 35.4 mA/cm^2 these values indicating higher corrosion rates of the alloy.

Table. 2 *Corrosion parameters evaluated from linear and cyclic polarization curves*

Sample	Linear polarization						Cyclic polarization		
	E_0,mV	b_a,mV	b_c,mV	R_p kΩ.cm^2	J_{cor} μA/cm^2	v_{cor} μm/an	E_{cor} mV	E_{BD} mV	E_{RP} mV
Commercial	-383	244	-441	366.7	0.262	3.07	-622	557	452
As-cast	-318	136	-121	68.7	0.378	4.42	-662	523	343

The voltammogram shapes indicate rather a general corrosion not a pitting corrosion.

This assertion is confirmed by Scanning Electron Microscopy (SEM) studies. Figure 3 shows SEM micrographs of the "C" alloy after the five cycle electrochemical treatment.

Figure 3 illustrates the generalized corrosion taking place as a result of the electrochemical treatment performed.

The surface morphology is very dissimilar for the two samples. In the case of the commercial sample, the surface is corroded in a proportion of over 90%, it is heterogeneous, showing at least three distinct regions; the surface is grooved with irregular shallow channels which delimitate continuous dark portions and is dotted about with small prominent and bright islands (Figure 3, (a) and (b)).

In the case of the casting sample, the entire surface is covered with irregular deep ditches. Very small bright stoppers are randomly buried in these ditches (Figure 3 (c) and (d)).

In order to better understand the qualitative composition of the corroded surface, the EDX line scans were taken at cross sections of surfaces containing different zones. The EDX line scan along lines A-B and B-C of figure 3, shown in figure 4, indicate an enhanced Chromium signal and a decreased Cobalt signal at positions of bright regions, both for commercial and casting samples.

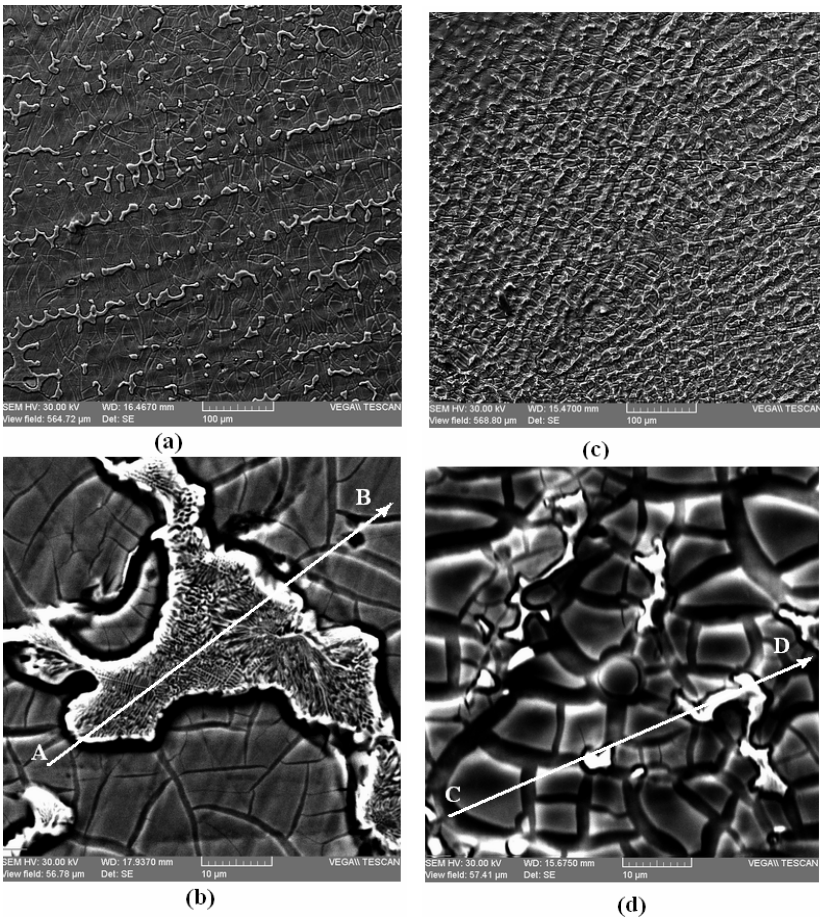

Fig. 3. *SEM micrographs for CH alloy electrochemically corroded in Afnor saliva by five successive cyclic polarization processes between 0 and 1500 mV; a)- non-casting sample (500 x), (b) – non-casting sample (5000x) (c)- as-cast sample (500x), (d) - as-cast sample (5000x)*

These spectra indicate the fact that the Cobalt dissolution during the repeated cyclic polarization treatment takes place only from limited portions of the alloy surface, most probable at the interdendritic regions along with large amounts of precipitate. The dark portions are most probable chromium oxide, responsible for good resistance to corrosion of this alloy in Afnor saliva. Similar structural modifications for a co-Cr-Mo biomaterial also were reported by Giacomelli et al. [11].

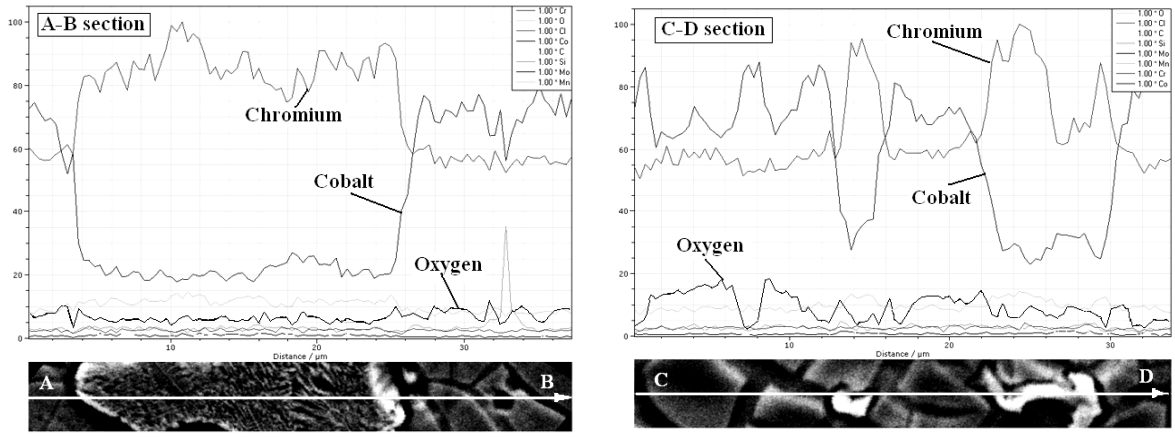

Fig. 4. *EDX line scan along lines A-B and C-D of figure 3*

4. Conclusions

The influence of the casting process on microstructure and corrosion behaviour of a Co-Cr-Mo alloy was studied by linear and cyclic polarization method, Scanning Electron Microscopy and EDX analysis. These studies reveal that in natural aerated Afnor S90-701 artificial saliva, the studied alloy behaves as a corrosion resistant material. In linear and cyclic polarization studies this alloy showed a passive behaviour with a large potential independent region up to a potential of about 500 mV (SCE), followed by a region with significant increase in current density.

By casting, this alloy undergoes a significantly modifications of both internal microstructure and corrosion resistance. At over-potentials greater than 500 mV (SCE) in Afnor saliva this alloy exhibits a generalized corrosion, the surface morphology being dissimilar for commercial and as-cast samples. EDX studies point out that corrosion takes place especially by cobalt dissolution.

References

[1]. Wulfes H., *Precision milling and partial denture constructions*, Bremen: Academia Dental; 2003. p. 259–60; 115–9; 108–13.
[2]. Wataha J. C., *Alloys for prosthodontic restorations*, J Prosthet Dent. 87, 2002, p. 351–63.
[3]. Dong H., Nagamatsu Y., Chen K. K., Tajima K., Kakigawa H., Shi S., *Corrosion behavior of dental alloys in various types of electrolyzed water*, Dent Mater J, 22 2003, p. 482–93.
[4]. Luthy H., Marinello C. P., Reclaru L., Sharer P., *Corrosion considerations in the brazing repair of cobalt based partial dentures*, J Prosthet Dent, 75, 1996, p. 515–24.
[5]. German R., *The role of microstructure in the tarnish of low-gold alloys*, Mettallography, 14, 1981, p. 253-266.
[6]. Hero H., Jorgensen R., *Tarnishing of low/gold dental alloy in different structural states*, J. Dent. Res., 63, 3, 1983, p. 371-376.
[7]. Venugopalan R., Gaydon J., *A review of corrosion behaviour of surgical implant alloys*. Dept. of Biomedical Engineering, University of Alabama at Birmingham, Technical Review Note, Princeton Applied Research, USA, 2001.
[8]. Strandman E., *Influence of different types of acetylene-oxygen flames on the carbon content of a dental Co-Cr alloy*, Odontol Revy, 28, 3, 1976, p. 223-238.
[9]. Oliveira Bauer J. S., Logueriçio A. D., Reis A., Filho L. E. R., *Microhardness of Ni-Cr alloys under different casting conditions*, Braz Oral Res, 20, 1, 2006, p. 40-46.
[10]. Bane M., *Analiza structurii materialelor metalice (The analysis of the structure of metallic materials)*, Editura Tehnică, Bucharest, 1991, p. 184.
[11]. Giacomelli F. C., Giacomelli C., Spinelly A., *Behaviour of a Co-Cr-Mo Biomaterial in simulated body fluid solutions studied by electrochemical and surface analysis techniques*, J. Braz. Chem. Soc., 15, 4, 2004, p. 541-547.

THE ANNALS OF "DUNAREA DE JOS" UNIVERSITY OF GALATI.
FASCICLE IX. METALLURGY AND MATERIALS SCIENCE
N^0. 4 – 2013, ISSN 1453 – 083X

RADIAL FORGING MACHINE. TECHNOLOGY FOR AXLE TYPE PARTS

Doru HANGANU, Marian NEACSU
"Dunărea de Jos" University of Galaţi, 111, Domnească Street, 800201, Galaţi, Romania
email: uscaeni@yahoo.com

ABSTRACT

This paper presents three types of radial forging machines to produce the axle type pieces. The new types of radial forging machines are presented cinematically. The movement of the deformation tools at these types of machines is compared with the motion at the existing machines.

KEYWORDS: hot plastic deformation, radial forging, axle type parts

1. Classical forging on machines with two tools used in parallel

When forging blanks of round section between plain tools, when the hammer or press ram reaches the blank, it does not result a contact surface as in the case of the extent of semi-square-section, but a contact line whose length is equal to the gripping length.

As the ram goes down, the deformation of the blank takes place on both sides of the contact line, at the same time, the contact line changing into contact surface. Once the top and bottom surfaces occur, the zones with difficult deformation occur too, which, together with the contact surfaces increase as the ram goes down. In contrast to the square section blanks forging, where in the zones with difficult deformation the material pervades in a non-deformed state, when forging round section blanks the zones with difficult deformation are formed on the account of the volume of metal that was previously subject to plastic deformation.

The outside friction between the tools and the deforming material has an influence in this case too as it has when forging square section blanks, only this time the plastic deformation occurs before the forming of the difficult deformation zone.

It should also be noted that while forging blanks of square cross section the material deformed is entirely under the influence of tools (Figure 1), at the forging of round blanks only a part of the deformed material is under the direct influence of the tools, that is the shaded area (Figure 1 b). The escape of a portion of the workpiece from the influence of tools changes substantially the stress state scheme.

In the case of round section blanks forging, the plastic deformation zones, the non-uniformity of deformation and the plastic deformation stress depend to a great extent on the tools type, which can be plain or profiled, and on the degree of unitary deformation.

***Fig 1**. Deformation zones that were produced under the direct influence of tools at the forging of square and round section blanks*

In Figure 2 are shown the plastic deformation zones which are formed during forging round section blanks between plain tools, with small degrees of unitary deformation, under 3%. [1]

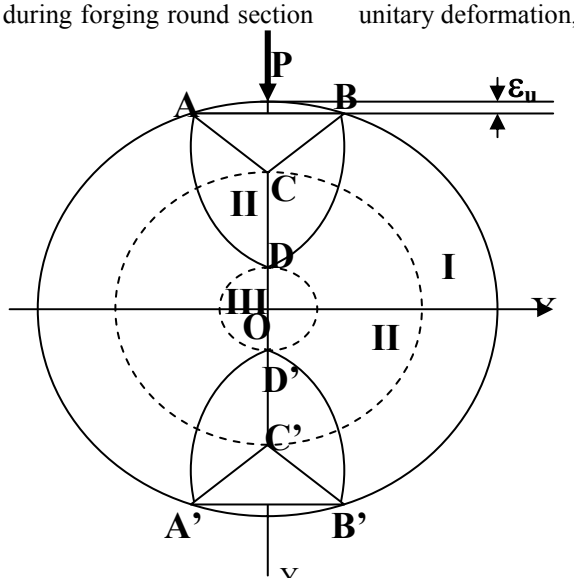

***Fig. 2**. The plastic deformation zones which are formed during forging round section blanks between plain and*

As the difference between the extreme tensions is much higher in zone II than in the difficult deformation zone, the plastic deformation zone is more easily produced in zone II. When rotating the blank, Zone II expands and forms the ring between the OD radius circle and the maximum radius circle, overlapping zone I in the exterior zone of this ring. It results that the maximum and minimum deformation zones are overlapping and in the interior ring situated between the OD and OC radius circles, the plastic deformation takes place only at maximum intensity.

In zone III, that is inside the OD radius circle, the plastic deformation takes place at medium intensity, but under the influence of tensile stress.

Compared with the tension and deformation state at the forging of square section blanks, at forging round blanks between plain tools, the non-uniformity of the deformation ε Δ is lower in value, but the heterogeneity of plastic deformation is more obvious. When forging round section blanks is done with small degrees of deformation, the central area is deformed by stretching and the amount of mechanical characteristics is reduced. This explains why in many cases the values of the mechanical characteristics of the parts and semi-products forged after the scheme square - rectangle - square are better than in the case of forging on the scheme round - round.

After forging, for the purpose of decreasing the diameter and increasing the length of the disk, the dimensional change of the pins and of their holes took place in a different way. Thus, while the peripheral pin has reduced its diameter and become elongated, the central pin has not undergone any change and its hole widened and shortened. The intermediate pins underwent different changes. Increasing the central pin hole diameter, while the disc diameter decreased, confirms the presence of radial tensile stresses in this area. Shortening the length of the disk in the axial zone and its elongation in the peripheral zone proves the presence of longitudinal tensile stress in the center.

The way in which the radial tensile stress is formed is presented in Figure 3, which shows the decomposition and composition of the forces acting on the round blank during forging between plain tools. [1].

In the ABC difficult deformation zone, which is formed under the influence of external friction forces T, the tension state is space compression S1 and the difference between the extreme voltages is minimal, virtually negligible. Due to the reduced difference between σ3 and σ1, the material in the ABC zone does not deform. Due to lack of material deformation of the ABC, the plastic deformation force is transmitted to the blank through this area that enters the material just like a ripping spike.

In the case of forging round blanks between flat tools to reduce tension stress and cracking or fracture tendency, as well as to improve the mechanical characteristics, forging must be run with deformation degrees higher or at least equal to 8%. Increasing uniform deformation over 8% makes difficult the forging operations in order to maintain the round shape of the blank section.

This is why in the case of forging round blanks from metals and alloys with low plasticity it is recommended using profiled tools or at least combined tools.

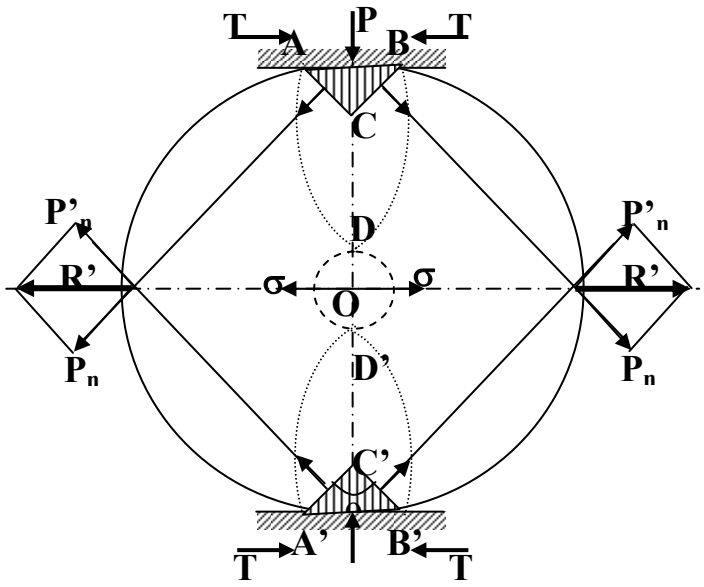

***Fig. 3**. Scheme and the tension forces during forging blanks between tools round flat*

2. Radial forging - working principle of classic machine

Radial forging is the operation of stretching by forging in which the deformation forces, of the same size, acts on the blank simultaneously from two or more diametrically opposed directions. In the moments of pause, when the forming tools (hammer pairs) are executing the withdrawal motion, the blank runs an advance and rotation movement (Figure 4). Radial forging is currently an advanced process for the series manufacturing of cylindrical, conical or mixed step axis, made of semi-round, square or hollow blanks, both hot and cold. Pieces like: rods for steering rods, axes from gear boxes and differentials, tube axles for serial production of cars, wagon axles, connecting sleeves for the oil industry, hard rolling special steel bars, are executed by radial forging with good results.

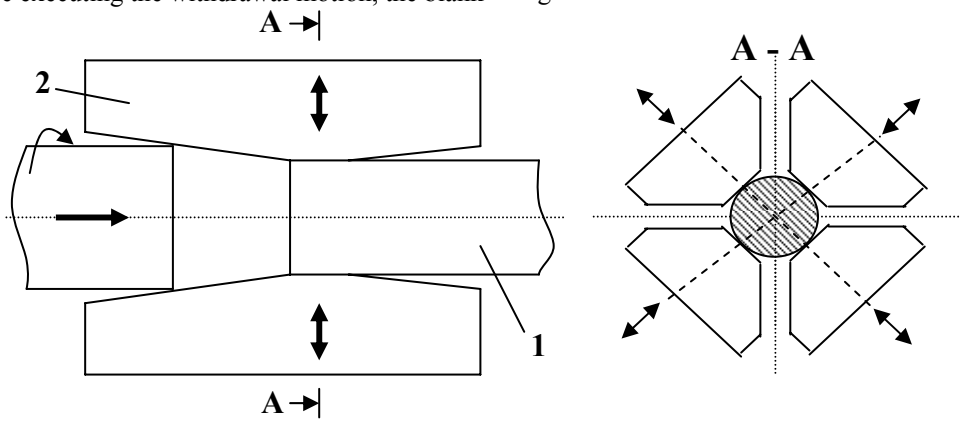

***Fig. 4.** Scheme of radial forging of round blanks with two pairs of tools: 1 – blank; 2 – sledge*

The radial forging process is performed on vertical or horizontal machines. Because the vertical stroke is limited by the size of the machine, vertical radial forging machines can forge blanks and parts with lengths up to 2 ... 3 m. Horizontal machines can get parts or elements up to 12 m. The most known radial forging machines worldwide are manufactured by GFM (Austria). Radial forging machines for executing long bars are equipped with two manipulators supporting the blank at both ends. In both cases, the forward movements of the manipulator and the rotating movements of the clamp that holds the blank are synchronized with the movements of the hammers carrying the plastic

deformation. In forging square, rectangular or hexagonal profiles, the manipulator or the grip head achieves only an advance movement without turning the blank.

The machine has the advantage of rapid deformation (within one minute / cycle), which permits to maintain the temperature of the piece almost constant during plastic deformation.

The main disadvantage of the conventional radial forging machines is that for parts with small diameter, it is necessary that the forming tools to be changed for each size.

3. Working principle of new radial forging machine and construction variants

Reducing the section of the material takes place due to the simultaneous movement of the four forming tools driven two by two by two hydraulic cylinders.

The tool movement during contact with the material actually consists of two movements that occur at the same time: one perpendicular on the direction of the main deformation and the other parallel and in the same direction with it. This last movement has the effect of the automatic advance of the forged blank. Material deformation is made without limitation of widening, requiring small capacity of installed power and forces (Figura 5).

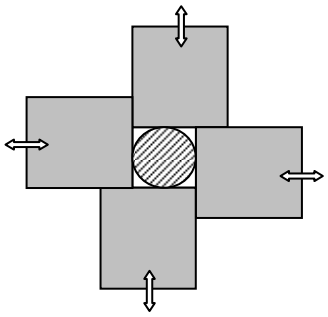

Fig. 5. *Working principle of radial forging machine*

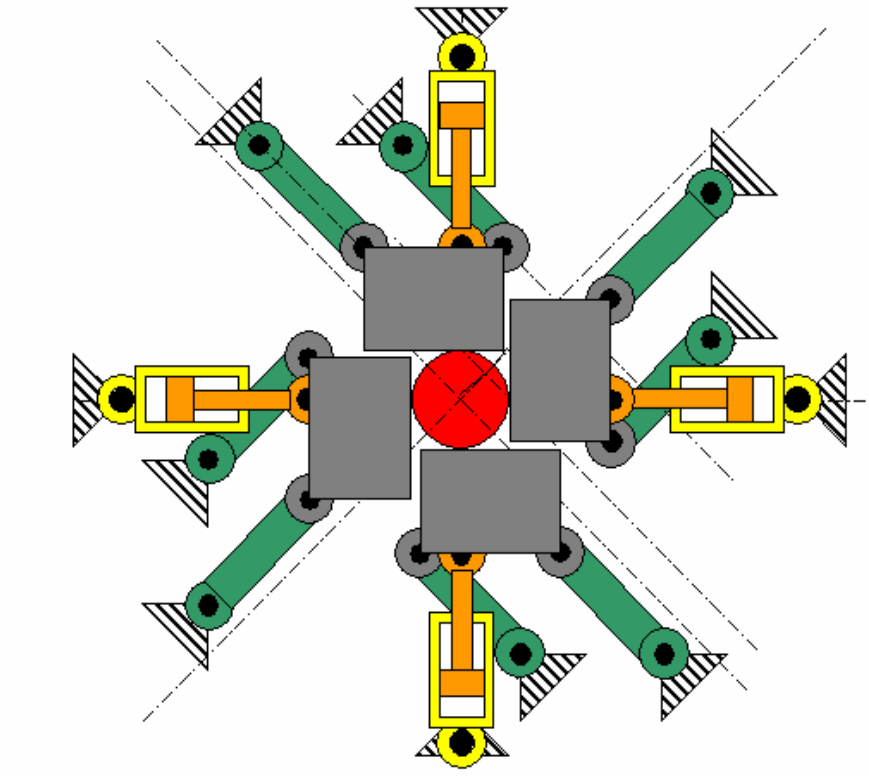

Fig. 6. *Kinematic scheme of new radial forging press (Option 1)*

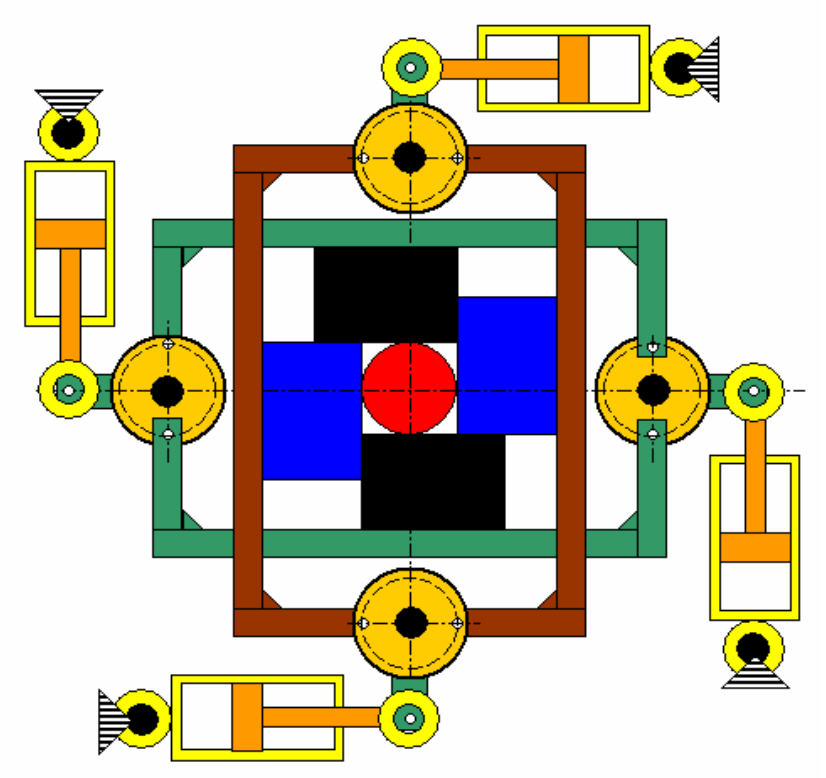

Fig. 7. *Kinematic scheme of new radial forging press (Option 2)*

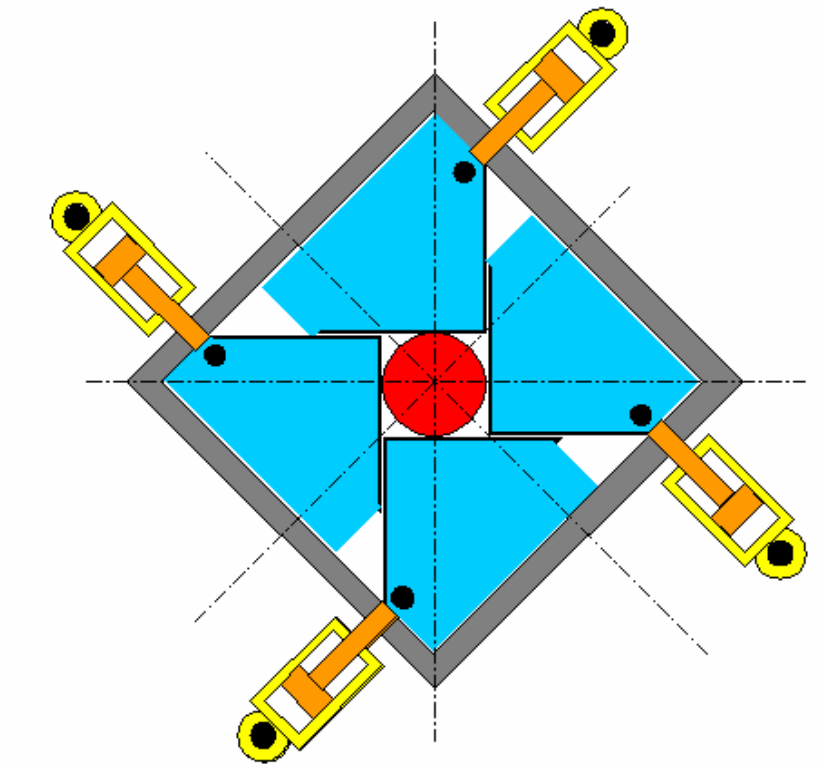

Fig. 8. *Kinematic scheme of new radial forging press (Option 3)*

4. Concluzion

1. The number of presses in the case of radial forging is considerably smaller than in the case of forging between two plain tools (63 to 400) because in the case of radial forging there is no widening and a higher degree of deformation per pass is possible.

2. The small number of presses involves a higher productivity and a reduced duration of the operation. In this way the number of reheating operations reduces, so there are heat savings too..

3. The possibility of using a higher degree of deformation per pass involves a smaller number of passes.

4. The lack of widening creates a state of tension and triaxial deformation, state in which there is no stress tension, only compression tension. As there is no tensile stress, there is no central cracking either, as it is found in most cases of forging round section blanks between two parallel plane tools.

5. To forge with high degrees of deformation per pass for radial forging machines, forming tools present an angle of adjustment to avoid overlapping.

6. The radial forging machine model presented in this paper has the advantage that, unlike other types of radial forging machines, allows extension of semi-round or polygonal blanks in a wide range of diameters without having to change the forming tools.

References

[1]. Popescu V., Drăgan I., Alexandru T. - *Tehnologia forjării* Ed. Tehnică Bucureşti, (1982)
[2]. Tălpăşeanu N. - *Tehnologia Materialelor* Editura Tehnică, Bucureşti, (1967)
[3]. Vlădescu M., Ancuţ R., Scorţea C. – *Îndrumar Metalurgic,* Editura Tehnică, (1988)
[4]. Hosford W. F., Caddell R. M. - *Metal Forming***:** Mechanics and Metallurgy, Cambridge University Press, 3rd edition, (2007)
[5]. Domblesky J. P., Shivpuri R. - Painter B. - *Application of finite-element method to the radial forging of large diameter tubes*, J.M.P.T., vol. 49, (1995), pp. 57-74.
[6]. Kurtaran H. - *Dissertation, design optimization of structures under impact loading with approximation methods*, George Washington University, Washington, DC, USA, (2001).

THE ANNALS OF "DUNAREA DE JOS" UNIVERSITY OF GALATI.
FASCICLE IX. METALLURGY AND MATERIALS SCIENCE
N^0. 4 – 2013, ISSN 1453 – 083X

EVALUATION OF THE OCCUPATIONAL RISK ASSOCIATED TO WORK ENVIRONMENT IN FERROUS METALLURGY

Tamara RADU, Anișoara CIOCAN
"Dunărea de Jos" University of Galați, 111, Domnească Street, 800201, Galați, Romania
email:tradu@ugal.ro

ABSTRACT

Work environment present risk factors due to chemical pollution of ambient air with dust, smoke, fumes, vapors, mists and gases. Moreover physical risk factors (related to noise, lighting, temperature, vibration, humidity, radiation) lead to hazards with varying degrees of significance. In this paper were identified the hazards associated with the work place for a maintenance worker who works in all sectors of metallurgical plant. The risk assessment was made in terms of severity and probability, combining these two factors in a risk matrix. From the analysis the significant hazards (unacceptable) related to work environment resulted. These are caused by the presence of the following pollutants: toxic gases (VOCs, PAHs, dioxins, furans), explosive flammable gases (methane gas, blast furnace gas, bigaz, oxygen), carbon monoxide and particulate matter.

KEYWORDS: risk factors, hazards, work environment, integrated steel plant

1. Introduction

The work environment presents the following important risk factors: chemical factors (dusts, gases, vapours, mists, fumes etc.); physical factors (noise, vibrations, radiation, excessive humidity, lighting etc.); thermal factors (high or low temperatures, abrupt changes of temperature). The raw materials, the energy sources, the technologies and the processes in ferrous metallurgy sector lead to a work environment with significant risk [1, 2]. This paper proposes to identify the factors of occupational risk and the hazards which they may generate. It also proposes to assess which of the risks are major through the significantly consequences on the workers health from steelmaking plant and what measures may apply for their minimization. All judgments shall relate to work environment and they do not deal with other risk factors that can be taken into account for assessment of a workplace and that are related to means of production, work obligations, execution of operations etc.

Firstly, work environment in ferrous metallurgy presents the risk of air pollution with: dust particles (coarse, fine and very fine), smoke, steam, vapours, mists and gases (CO, CO_2, SO_2, NO_x, H_2S, NH_3, VOC_s, CH_4) [3]. Also there are present the physical risk factors such as noise (continuous, intermittent, impulse), lighting (excessive, shine, incorrect, inappropriate), temperature (heat or extreme cold, heat shocks), vibrations, humidity, radiations. The hazards are principally related to the fugitive emissions (diffuse) and less to the controlled emissions. Fugitive emissions may be continuous andare produced mainly by imperfect seals (loading systems, conveying lines, furnaces doors, manholes, refractory lining etc.) or uncontinuous (loading and unloading, maintenance of facilities, damages, accidents and others) [4].

2. Risks related to the work environment in ferrous metallurgy

Environmental pollutants that impact upon work security are different (in terms of amount and type of pollutant) or common to steel plants. For example, the dust and VOCs appear on all metallurgical flow, while the ammonia is present only in coke production sector. Significant quantities of particulate matter are to be found in the sectors of raw materials, of coke production and sinter and less in the other sectors. From a certain level of pollution or by storage in the body, most environmental pollutants from steel work can cause diseases.

The most common work-related ailments in ferrous metallurgy and their causes are shown in Table 1. The routes of exposure are the inhalation, skin absorption (or percutaneous absorption) and ingestion [5-10].

Table 1. *Diseases associated with work environment and with risk factors that produce them*

Diseases associated with profession	Potential risk factors
Respiratory ailments	Low temperatures, air courses, air polluted with dust, toxic and irritant gases, smoke, fly-ash, vapours, nickel and manganese.
Ischemic heart disease	Noise, vibrations, high temperatures, heat radiations
Nervous system diseases and neuropsychiatric disorder	Noise, vibrations, NO_x, VOCs, manganese
Ophthalmic diseases	Dusts, irritating gases, smoke, vapours, H_2S, inadequate lighting, shining
Skin ailments	Particulate matter, nickel, chromium, acids vapours, SO_2, NH_3, VOCs
Acute and subacute intoxications	CO (most common), CH_4, smoke
Cancer	Dusts, VOCs, heavy metals
Digestive ailments	Toxic fumes, noise, high temperatures, SO_2
Deafness	Noise

2.1. Chemical risk factors

Air pollutants with risk resulting from the metallurgical activities and processes are: particulate matter, CO, SO_2, NO_x, H_2S, NH_3, VOCs, vapours of acids. Depending on the duration of exposure, for all these pollutants there are limit values and maximum permissible concentrations in ambient air. There are also systems for pollutants treatment which are continuously improved and upgraded. Their utilisation at optimum regime keeps ambient air in the workplaces and in neighbourhood areas at the recommended parameters by reference standards from the environment legislation. Although new solutions are looked for permanently, the complete elimination of the pollutants emissions is not possible. The risks associated with them must be communicated and understood by all those who work or come into contact with the work environment from the ferrous metallurgical plants. At the same time must be taken all specific security measures.

Particulate matter. In the ferrous metallurgy the major sources of particulate matter are: stock piles of raw materials (ores, coals, limestone etc.); operations for materials preparation (crushing, sieving) and transport; coke production; sinter production; pig iron castings and slag; pig iron pretreatments (desulphurization etc.); loading and unloading of converters; oxygen blowing; maintenance and cleaning of the equipments of the air quality control; demolition and reconstruction of refractory linings. The particulate matter are more dangerous if they are finer and if are associated with the heavy metals, SO_2, NO_2, NH_3. As seen in Table 1 many diseases associated with occupation may be caused by the presence in the breathed air at workplace of dust, smoke, mist or ash-fly. The particulate matter can mainly give respiratory diseases and diseases of the liver, skin, brain, eyes too.

Carbon monoxide results from incomplete oxidation of carbon, generally from combustion processes and from certain metallurgical processes. The sources of diffuse or controlled emissions include almost all sectors of the metallurgical plants: coking batteries, sintering, blast furnaces, basic oxygen furnaces (BOF) and the operations from the secondary metallurgy. Carbon monoxide is a very dangerous gas because it is colourless, odourless and tasteless. Therefore it can not be seized by the victims. It enters the body through the respiratory tract. From lungs it passes into blood where it leads to blocking the haemoglobin (suffocation), disruption of the muscle metabolism (especially to the heart) and to blocking of some enzymes. The most severely affected organs are the heart, brain and lungs. Harmful actions occur at concentrations of 0.06 % CO in air. The acute and subacute intoxications and death can occur depending on the concentration and exposure time.

Carbon dioxide is not a harmful gas for human health but it is strongly responsible for climate changes that present a major risk for environment. It is present on whole flow of steelmaking plant as a result of the combustion processes and of the metallurgical processes.

Sulphur dioxide has as main source of emission the coke production, sintering and various combustion processes of fuels with sulphur content. It is part of irritant gases category, its presence is felt because of its suffocating odour, and its odour becomes perceptible from 6 - 15 % SO_2 in breathable air. The short term exposure at an average of 10 - 30 min (24 hours) and the long-term exposure (years) irritate respiratory tracts, eyes and can cause premature death. For example, an exposure for 10min at 1000μg/Nm^3 at workplace causes severe effects (bronchitis, tracheitis). Effects of the SO_2 differ from one person to another. These are more serious for persons who already have respiratory problems and for older persons. Also sulphur dioxide can give digestive problems because it is dissolved in saliva and so can be swallowed. In addition, skin is directly affected because by dissolving into sweat it is

transferred into the body in the form of acid. The SO_2 association with particulate matter has a synergetic effect that leads to the penetration and deposition of particles in the human respiratory tract and the lungs determine serious respiratory and cardiac diseases.

Nitrogen oxides are formed in the iron and steel production processes that involve the presence of air and of the high temperatures. One of these is sintering of ferrous ores. Also the fuels combustion in diverse installations may be mentioned. In this case the NO or NO_2 are formed in accordance with the conditions of combustion and NO formed is further transformed into NO_2, a brown irritating gas. This is the precursor of ozone and by reaction with water from atmosphere is partially transformed into nitric acid. If NH3 exists into atmosphere has formed NH4NO3 as particulate matter (PM2.5 fraction). Workers may be affected directly by NOx or by secondary pollutants what have been formed (ozone, photochemical fog, and particulate matter). Human body is affected by the nitrogen oxides, especially by quantity and less by the exposure period or by accumulation. They lead to respiratory or cardiac diseases, in blood oxide has a similar effect as CO. In lungs the effects may be reversible or irreversible.

Hydrogen sulphide is released mainly from granulation of blast furnace slag. This gas has an unpleasant odour which can cause various diseases in human body depending on its concentration and exposure time. The main diseases are those respiratory, from the irritation of respiratory tracts, pneumonia, lung injury, until death. Also eyes are affected and hydrogen sulphide can cause the temporary loss of smell.

Ammonia has as potential significant sources the coke-oven plant and the chemical installations for extraction of the chemical products from coke gas. It is an irritant gas that can create serious problems because of its odour (which may be felt from 18.5 mg/Nm^3). Permissible occupational exposure limit in accordance with WHO regulations is 70mg/Nm^3 for 8 hours. The exposure for 30 minutes at 2800mg/Nm^3 causes death. Ammonia affects upper respiratory tract, eyes and skin.

Volatile organic compounds (VOCs) may be emitted from all stages of production processes from the steel manufacturing plant. They are present in the off gas resulted in the sintering process because of the to oil content from input materials (mainly from mill scale), from coke ovens and from installations for chemical processing of coke gas. They may act on the human body directly or by their transformation products. The main compounds resulted from coking processes and from coke gas processing are aromatic hydrocarbons (benzene, xylene, toluene) which by skin contact or inhalation on short-term exposure cause various ailments of respiratory tract, nervous system, skin diseases and narcotic effect. A long-term exposure to benzene affects central nervous system (fatigue, insomnia, loss of memory) and the blood (anaemia, leukaemia).

Polynuclear aromatic hydrocarbons (PAHs) include the benzo(a)pyrene and naphthalene. If naphthalene is formed specifically at the coke plant, benzo(a)pyrene is present in many sectors of integrated steel work: coke plant, blast furnaces, steelmaking sector. This compound is extremely dangerous and is prohibited by the rules of occupational safety and by the security work normative. There are serious both short-term exposures (skin irritation and upper respiratory tract, dizziness, headaches) and long-term exposures and high concentrations (respiratory collapse, cancer, damage to liver, kidneys, lungs, and blood and lymphatic systems).

Acid vapours are specifically from the sectors of stripping (in rolling mills and galvanization sectors), maintenance, repairs and laboratories. The most used acids are: HCl, H_2SO_4, HF. These emissions affect upper respiratory tract, lungs, kidneys, liver and the skin.

2.2. Physical risk factors

Along with chemical risk factors there are important risks related to the exposure to physical agents: noise, vibration, temperature.

Noise is almost ubiquitous in steelmaking industry. The most important noise sources are: operation for gas evacuation from the blast furnace by opening a relief valve for the pressure equalization; exhaust fans for installations of the air quality control; pretreatment of iron scrap; handling, crushing and sieving of input materials, products and by-products. As example, the noise in the vicinity of exhaust fans with high capacity from sinter belts can reach values of 100-110 dB. The noises may also appear due to abnormal functioning (explosion to the slag tapping). Depending on the characteristics and propagation mode these noises affect the population surrounding the metallurgical plant. The main characteristics of noise affecting human body are: the intensity and the frequency. Endurance limit of human hearing is 65 dB. Occupational safety regulations impose safe exposure level of 75 dB for 8 hours and of 85 dB as action threshold.

Vibrations lead to health problems at long-term exposure. They are generated by the use of vibrating tools, the mobile components and equipment that operate by pneumatic, hydraulic and electrical actuators. If the vibrations are associated with humidity and cold the health effects are higher.

High temperatures at workplace are common in the steel industry. Many operations and equipments are the sources of high temperatures: coke ovens;

unloading, conveying, crushing, sieving and quenching of hot coke; tapping and conveying of the pig iron and blast furnace slag; pouring of the steel and BOF slag; other pyrometallurgical processes from BF and BOF sectors; hot rolling of the steels; thermal treatment furnaces etc. Temperature exposure affects the human body (syncope, oedema, dehydration, rash) and thermal shocks give thermoregulatory difficulties. Equally dangerous are low temperatures and air currents at unprotected workplaces (raw materials stock yards, dump slag).

Shine of the molten alloys and glow of products and by-products are also often situations frequently in work places from steel industry that directly affect (eye diseases) or indirectly (reduced visibility) the safety.

Radioactivity was detected as a result of accidental introduction of scrap with radioactive sources. Also it is considered for laboratories and the handling of radioactive sources related to control systems (smoke detectors, measuring apparatus for level, humidity and thickness).

3. Risk assessment and risk analysis

The risk assessment is made in terms of severity and probability, by combination of the two factors in risk matrices. Severity refers to the consequences of hazard occurrence and the probability refers to the frequency with which these may occur. In our country, the risk assessment is evaluated by the method of determining the level of risk which shows seven grades of severity, six grades of probability and six levels of risk [11]. Grades of severity are related to the following possible consequences of risk production:

- 1st class: negligible consequences; (incapacity for work less than 3 days)
- 2nd class: small consequences; (incapacity of between 3 - 45 days, which requires medical treatment);
- 3rd class: medium consequences; (disability of 45 - 180 days, medical treatment and hospitalization);
- 4th class: high consequences (disability grade III);
- 5th class: serious consequences (disability grade II);
- 6th class: very serious consequences (disability grade I);
- 7th class: maximum impact death.

In terms of probability classes it was opted for the following form:

- 1st class of probability: event frequency over 10 years;
- 2nd class: generation frequency – once in 5 ÷10 years;
- 3rd class: once in 2 ÷ 5 years;
- 4th class: once in 1 ÷ 2 years;
- 5th class: once in 1 year ÷ 1 month;
- 6th class: once in less than a month.

According to the 7 classes of severity there were established 7 risk levels, in ascending order, because the severity is a more important element in terms of environmental and labour protection and it was admitted that it has a greater impact on the level of risk than the frequency:

- N_1 - minimal risk level; s-p couples: (1,1) (1,2) (1,3) (1,4) (1,5) (1,6) (2,1);
- N_2 - very small risk level; s-p couples: (2,2) (2,3) (2,4) (3,1) (3,2) (4,1);
- N_3 - small risk level; s-p couples: (2,5) (2,6) (3,3) (3,4) (4,2) (5,1) (6,1) (7,1);
- N_4 - moderate risk level; s-p couples: (3,5) (3,6) (4,3) (4,4) (5,2) (5,3) (6,2) (7,2);
- N_5 - high risk level; s-p couples: ((4,5) (4,6) (5,4) (5,5) (6,3) (7,3);
- N_6 - very high risk level; s-p couples: ((4,5) (4,6) (5,4) (5,5) (6,3) (7,3);
- N_7 - maximum risk level; s-p couples: (6,6) (7,5) (7,6).l ;

If were considered all possible combinations of specified variables, taken two, was obtained a risk matrix, $M_{s,p}$, with 7 lines - s, which will represent severity classes, and 6 columns - p for probability classes:

$$M_{s,p} = \begin{Vmatrix} (1,1) & (1,2) & (1,3) & (1,4) & (1,5) & (1,6) \\ (2,1) & (2,2) & (2,3) & (2,4) & (2,5) & (2,6) \\ (3,1) & (3,2) & (3,3) & (3,4) & (3,5) & (3,6) \\ (4,1) & (4,2) & (4,3) & (4,4) & (4,5) & (4,6) \\ (5,1) & (5,2) & (5,3) & (5,4) & (5,5) & (5,6) \\ (6,1) & (6,2) & (6,3) & (6,4) & (6,5) & (6,6) \\ (7,1) & (7,2) & (7,3) & (7,4) & (7,5) & (7,6) \end{Vmatrix}$$

The formula for calculating the overall risk level is:

$$Nr = \frac{\sum_{i=1}^{n} r_i \cdot R_i}{\sum_{i=1}^{n} r_i} \quad (1)$$

where: Nr is the global risk level on the workplace; r_i is the risk factor rank "i"; R_i is the risk level for the risk factor "i"; n is the number of risk factors identified at the workplace.

For the assessment of the occupational risk that is associated with the workplace have been identified the hazards correlated with the workplace for a maintenance worker (e.g. a welder) because they are all steel sectors which were previously assessed risk factors. To identify the hazards the have been established class of the level, class of probability and risk level.

The results are given in Table 2.

Table 2. *Severity class, probability class and risk level for identified hazards*

Code.	Hazard	Severity	Probability	Risk level
1.	Particulate matter (fine and very fine fractions) in ambient air of the workplaces (interventions at cleaning systems for gases)	3	6	4
2.	Irritant gas resulted from the production processes (NH_3, SO_2, H_2S)	3	6	4
3.	Presence of carbon monoxide in some areas of workplaces	7	3	5
4	VOCs, PAHs, PCDDs/F in ambient air of workplaces	7	1	3
5.	Toxic gases arising during welding or oxy-fuel cutting of metals	7	6	7
6.	Working in areas where toxic substances are present (mineral oils, acids, greases)	7	1	3
7.	Working in areas where corrosive substances are present (mixture of water and phosphates from cooling installations)	7	1	3
8.	Possibility of accumulation of flammable gases and vapours and/or explosives to some workplaces (accumulation of methane, oxygen in closed spaces), fire hazard and/or explosion	7	6	7
9.	Working with flammable substances and/or explosives or at installations that use flammable (oxygen, methane, oils, greases)	7	1	3
10.	Leakage of methane, oxygen by cracking of supply systems, oil jet from accidental cracking of hydraulic circuits, hot water jet or steam from process lines	6	1	3
11.	Working in the vicinity of pressure vessels	7	1	3
12	Flames and fires from the process or as a result of ignition of flammable substances, damages of the electrical installations in the work area (burn or fire hazard)	6	1	3
13	High temperature of the objects, materials, surfaces from the work environment or of the products and by-products resulted from the manufacturing process	2	6	3
14	High temperature of ambient air in some work areas (near furnaces and other thermal aggregates)	2	6	3
15	Low temperature of the metal surfaces in cool season	2	5	3
16	Low temperature of ambient air in cool season	2	5	3
17	High humidity of the air at making works in the household water	2	5	3
18	Air Currents (defective enclosures, doors open)	2	6	3
19	High level of noise	4	6	5
20	Low level of lighting in some areas of workplaces	2	6	3
21	High contrast between background material and general lighting of the working place	2	6	3
22	Non-ionizing radiations (IR and UV) from the process or near furnaces, rolling lines etc.	2	6	3
23	Working in areas where there is risk of drowning (cooling towers, tanks, basins, clarifiers etc.)	7	1	3
24	Natural disasters: earthquake, lightning, hail, storm etc.	7	1	3

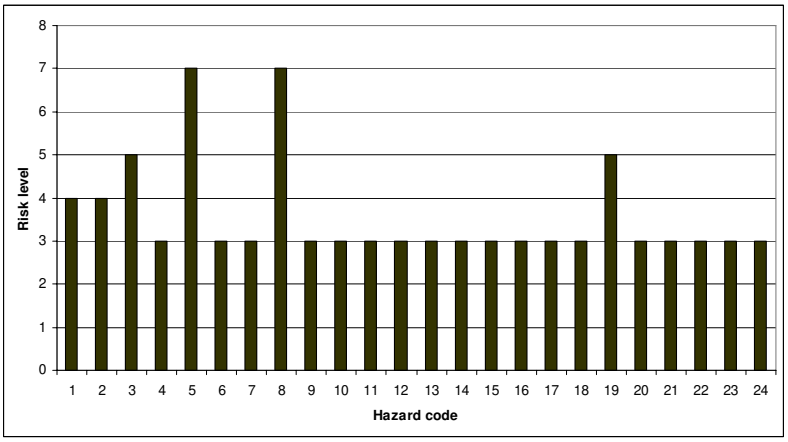

Fig 1*. Level of analyzed risk hazards as function of severity and probability*

The level of risk for each hazard identified in the work environment is shown in Figure 1. In any assessment action, significance will be attributed to considerable risks with a great impact on workers and environment. To identify these risks, the ranking scale of risks at the workplace is made (Table 3).

This gives the possibility to establish the priority of prevention and protection, according to the risk factors that have the highest risk level.

Table 3. *Ranking scale of risks*

Risk level	Hazards code
7 - Maximum risk level	5 and 8
5 - high risk level	3 and 19
4- moderate risk level	1 and 2
3- small risk level	5, 6, 7, 9-18, 20-24

The level of global environmental risk calculated in accordance with relation (1) is 3.84. From risk assessment results a total of seven significant hazards (unacceptable) related to workplace. Other risks associated with the work environment shows a low level of risk that is considered acceptable. The most dangerous workplaces are those that generate toxic gases that accumulate into enclosed spaces, also the flammable gases with potentially explosive or fire. The carbon monoxide in the work environment has a high risk level and requires protective measures for monitoring such as the audible warnings. A level of high-risk shall submit and the noise. Measures that may apply to this risk factor consist in minimization by isolation of the sound sources or utilization of soundproofing materials. Also there may be applied the individual protection measures with special equipment (for protection of ears) associated with alternative periods of exposure and rest. The presence of the irritant gases and the particulate matter in the work environment requires a set of measures to reduce the risk associated with them. These emissions can not be eradicated in the steel plant but can be significantly minimized by using the best technologies that ensure a clean work environment. Unfortunately a barrier in taking such measures is the high costs.

4. Conclusions

- Risk assessment associated to work environment in steelmaking emphasizes several dangers to workers through: pollution of air with toxic gases and with the potential of explosion and fire; uncontrolled emissions of CO; fine and very fine particles in the ambient air; high noise.

- Toxic gases (VOCs, PAHs, PCDDs/F) that are potentially flammable and explosive (methane gas, blast furnace gas, oxygen) have the maximum risk level. They can cause death and present the potential hazards with high probability.

- The presence of CO in the work environment are also very serious consequences (death) but this gas emission hazards are well monitored and have a lower probability of occurrence. The level of risk is still high requiring continuous monitoring.

- Releases of the particulates and the gases to the work environment from diffuse sources or controlled sources are impossible to be eliminated in the steel industry but by application of the best technologies they can be much reduced.

- Work environment may involve important problems of work security that requires implementing an occupational risk management.

References

[1]. Moraru R., Băbuț G. - *Cadrul general al managementului riscului de mediu*, Buletinul AGIR nr. 3/2006, iulie-septembrie, p. 103-107

[2]. Ozunu A., Anghel C. I. - *Evaluarea riscului tehnologic şi securitatea mediului*, Editura Accent, Cluj-Napoca, 2007

[3]. * -** *European Commission. 2000. Reference Document on Best Available Techniques for the Production of Iron and Steel*. BAT Reference Document (BREF). European IPPC Bureau, Seville, Spain. eippcb.jrc.es.

[4]. *** - *Sustainability Report of the world steel industry*,2008, http://www.worldsteel.org

[5]. * -** *Hazard Prevention and Control in the Work Environment*, World Health Organization, Geneva, August 1999, http://www.who.int

[6]. * -** *National Emission Standards for Hazardous Air Pollutants: Integrated Iron and Steel Manufacturing*: Final Rule. 40 CFR Part 63, Federal Register 68:97. EPA, 2003, Washington, D.C. www.epa.gov.

[7]. Alvarez F., et.al. - *Physical speciation of arsenic, mercury, lead, cadmium and nickel in inhalable atmospheric particles,* Analytica Chimica Acta 524, 2004, pp.33–40

[8]. Popescu L.G., Manea D., Savin D. - *Compuşi organici volatili. caracteristici fizico-chimice, efecte asupra mediului şi sănătăţii umane, măsuri de control poluare atmosferică*, Gepropol 2009, p.282

[9]. Chang E.E., et.al. - *Health risk assessment of exposure to selected volatile organic compounds emitted from an integrated iron and steel plant*, Inhalation Toxicology, December 2010, Vol. 22, No. S2: pp. 117-125

[10]. Van den Berg et.al. - *The 2005 world health organization re-evaluation of human and mammalian toxic equivalency factors for dioxins and dioxin-like compounds*. Toxicological Sciences, 2006, pp. 223-241

[11]. * - SR EN 292-1/1996.**

THE ANNALS OF "DUNAREA DE JOS" UNIVERSITY OF GALATI.
FASCICLE IX. METALLURGY AND MATERIALS SCIENCE
N^0. 4 – 2013, ISSN 1453 – 083X

ELECTRODEPOSITION AND CHARACTERIZATION OF Ni-Si NANOCOMPOSITE COATINGS

Gina Genoveva ISTRATE
"Dunarea de Jos" University of Galati, Faculty of Materials Science and Environment
email: gistrate@ugal.ro

ABSTRACT

In this paper is presented morphological aspects and corrosion behaviour of composite coatings having nickel as metal matrix and silicon as dispersed phase obtained during electrodeposition process of nickel. Silicon mean diameter size of particles particles by 50 nm. The Ni-Si composite coatings were electrodeposited from a suspension silicon particles in aqueous nickel sulphate electrolyte by adding 10g/L and 20g/L of silicon particles in the electrolyte solution. The morphological aspects of the coatings and inclusion on particles were investigated using SEM and EDX. As test solution NH_4OH 0.5M (specific coke industry) was used in a three electrode open cell with nickel based nanostructured composite coatings as working electrode (WE), a platinum electrode as counter electrode (CE) and an Ag/AgCl electrode as reference electrode (RE).

KEYWORDS: nanocomposite coatings, silicon, nickel, polarization resistance

1. Introduction

Composite materials have been designed to replace a growing proportion, ferrous and non-traditional materials, which are characterized by some shortcomings on the performance, processes for obtaining and processing, dimensions, weights, geometric complexity, usage and costs.

Applications of composite coating technology can now be found in general consumer products and more applications are on the horizon.

Electrodeposition of ceramic, polymer and metal powders within metal, ceramic or polymer matrix produces composite coatings with attractive properties such as microhardness, polarization resistance, wear-resistance [1]. The production of composite coatings can be achieved through electrochemical deposition of the matrix material from a solution containing suspended particles such as: oxides (TiO_2 [2], Al_2O_3 [3], CeO_2 [4], ZrO_2 [5]), carbides (SiC, WC), nitrides, metal powder (Si [6, 7], P [8], Co [9], W, B [6]).

Nickel matrix composites containing particles like oxides, carbides, nitrides or diamond have been developed for their improved wear resistance and dispersion strengthening.

Among the solid particles used for reinforcement, SiC is the most frequently studied and applied [9-11].

Considerable researches have been mainly focused on the fundamental conditions of the electrolysis such as composition and pH of the electrolyte, the presence of additives, temperature agitation rate, density and type of the current, surface properties of particles, their size and concentration in the bath [12].

The present study aims to codeposit Si into nickel matrix. The effects of Si concentration in the suspension, current density, temperature and pH of the plating bath on silicon inclusion into the deposit were studied. Microhardness and corrosion behaviour of nickel–silicon (Ni–Si) composite in NH_4OH 0.5 M solution have been studied. Microstructure of the composite has also been investigated and reported.

The novelty of the work is the use of nanometer silicon as disperse phase.

2. Experimental procedure

The coating was plated on carbon steel plates (measuring 100x30x2 mm). The nickel matrix was prepared from sulphate electrolyte with the following composition $NiSO_4 \cdot 7H_2O$ 110g/L + Na_2SO_4 x $10H_2O$ 110 g/L + NH_4Cl 25g/L+ H_3BO_3 15g/L, at cathodic current density 2 A/dm^2 and 3 A/dm^2 with electrolyte stirring. The stirring rate in the electrolyte was 500, 750 and 1000 rpm. The electrodeposition was carried out for one hour. Silicon powder (dispersed phases) with a concentration 10 g/L and 20 g/L were introduced into the bath to obtain the composite coatings. The mean diameter size of particles of

silicon powder was 50 nm. The pH of solution was in the range 5-6, the temperature was kept at 293K.

The morphologic aspects of the coatings were investigated by scanning electron microscopy method. The experimental measurements of the Vickers microhardness of composite deposits are described in [13].

Also this paper present the electrochemical corrosion behavior of nanostructured composite coatings using potentiodynamic polarization method.

As test solution NH_4OH 0.5 M (specific coke industry) was used in a three electrode open cell with nickel based nanostructured composite coatings as working electrode (WE), a platinum electrode as counter electrode (CE) and an Ag/AgCl electrode as reference electrode (RE) (E_{RE} = +200 mV/ENH). For potentiodynamic polarization measurements was used initial potential (I. P.) – 1000mV (Ag/AgCl), final potential (F. P.) + 600mV (Ag/AgCl) and a scan rate of 2 mV/s. The polarization potentiodynamic curves were recorded after 60 minutes of immersion. The corrosion current density (i_{corr}) for the particular specimens was determined by extrapolating the anode and cathode Tafel curves.

3. Results and discussion

In Fig. 1 is presented the thicknesses of composite coatings obtained by electrodeposition at 2A/dm^2 and 3A/dm^2 current density, 60 minutes deposition time and various stirring rate of the electrolyte.

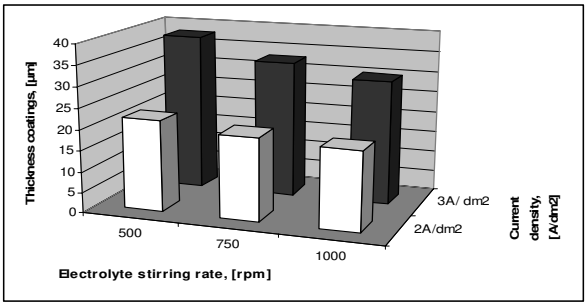

Fig. 1. *The thickness of Ni-Si composite coatings function current density and stirring rate*

From fig. 1 we can observed that deposited layer thickness increases with current density and decreases with increasing electrolyte stirring rate. The higher thickness of the composite coating was observed at these conditions of electrodeposition: current density 3A/dm^2 and 500 rpm electrolyte stirring rate.

Fig. 2 show the minimum variation of the silicon content in the nanocomposite coatings according to the electrolyte stirring rate (current density 2A/dm^2, 60 minutes deposition time).

As it can be observed from figure 2 the content of Si nanoparticles is highest at a stirring rate of 500 rpm and a dispersed phase containing 20 g/L (2.7% wt). It is also noted that at higher agitation rates (750, 1000 rpm) the content of Si included is lower (except composite coating obtained at 750 rpm and a dispersed phase containing 10 g/L).

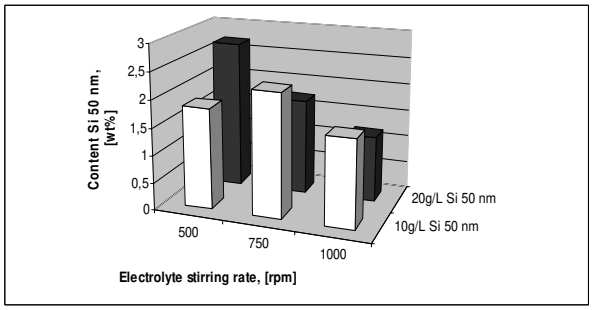

Fig. 2. *Content of silicon wt% in the nickel matrix*

Figs. 3 – 4 compares morphological aspects of Ni-Si composite coatings by scanning electron microscopy method.

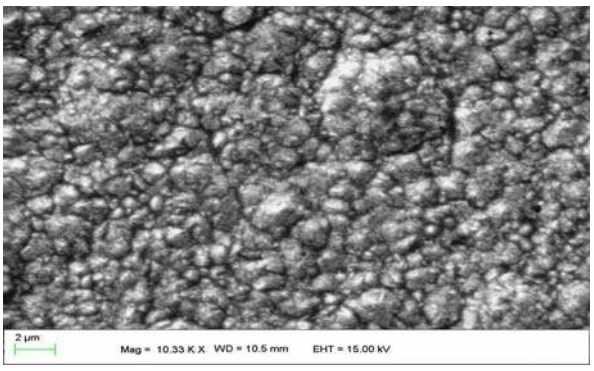

Fig. 3. *SEM surface morphology of Ni-Si composite coatings (20g/L Si, 2A/dm^2, 500 rpm, 60 min.) (x 10000)*

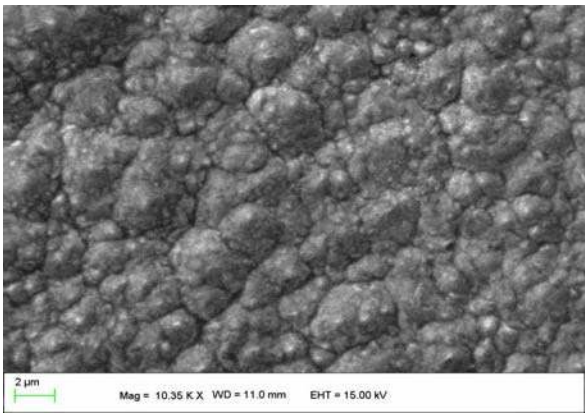

Fig. 4. *SEM surface morphology of Ni-Si composite coatings (20g/L Si, 3A/dm^2, 500 rpm, 60 min.) (x 10000)*

It has been found by SEM that with increasing current density, nodular structure is more pronounced, crystal size becomes larger. At a current density of 2A/dm^2 finer structure indicates a greater number of nucleation centers and thus a more homogeneous coating. The electrochemical investigation of each sample began with monitoring the open circuit potential (OCP). OCP changes immediately after the immersion into the testing solutions till reaching relatively stable stationary values.

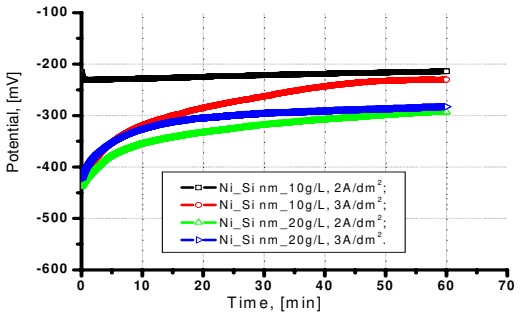

Fig. 5. *Open circuit potential Ni-Si composite coatings in NH_4OH 0.5 M*

Fig. 5 show that potential value of composite coating Ni-Si obtained at 3 A/dm^2 with 20 g/L silicon nano in electrolyte is more positive suggesting a more noble the deposit. This may be associated with an inhibition of the anodic reaction and therefore a higher resistance to corrosion

The typical anodic potentiodynamic polarization curves of various nanocrystalline Ni-Si coatings measured in NH_4OH 0.5 M solutions are shown in Fig. 6.

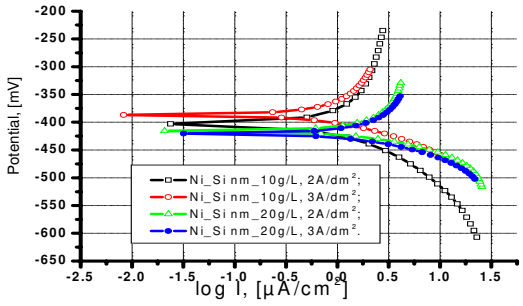

Fig. 6. *Polarization curves of Ni-Si composite coatings in NH_4OH 0.5 M*

Corrosion rates of the coatings were derived from the Stern–Geary equation:

$$i_{corr} = \frac{1}{2.303 R_p}\left(\frac{\beta_a \cdot \beta_c}{\beta_a + \beta_c}\right) \quad (1)$$

- i_{corr} is the corrosion current density in Amps/cm^2;

- R_p is the corrosion resistance in ohms cm^2;

- β_a is the anodic Tafel slope in Volts/decade or mV/decade of current density;

- β_c is the cathodic Tafel slope in Volts/decade or mV/decade of current density;

- the quantity, $(\beta_a \cdot \beta_c)/(\beta_a + \beta_c)$, is referred to as the Tafel constant.

The polarization resistance, Rp, was determined from the slopes of the potential-current plots measured by the linear polarization curve (LSV) at a scanning rate of 2 mV/s.

The corrosion potential (E_{corr}), corrosion current density (i_{corr}) and polarisation resistance (R_p), which were obtained from the potentiodynamic polarisation curves are summarized in Table 1.

Table 1. *Corrosion parameter values determined from polarization curves*

Composite coatings [500 rpm, 60 min]	**E_{cor}, mV Ag/AgCl**	**β_a mV/dec**	**β_c mV/dec**	**i_{cor}, µA/cm²**	**R_p kΩ·cm²**
Ni-Si, 2A/dm^2, 10g/L Si nm	-384.0	139.8	123.4	0.8864	32.10
Ni-Si, 2A/dm^2, 20g/L Si nm	-406.0	145.0	67.8	1.5464	12.97
Ni-Si, 3A/dm^2, 10g/L Si nm	-383.3	154.5	73.5	0.9429	22.93
Ni-Si, 3A/dm^2, 20g/L Si nm	-414.8	194.1	75.0	2.0888	11.24

From the data presented it can be seen that the corrosion potential tends to negative values for composite coating Ni-Si obtained with 20 g/L silicon nano in electrolyte solution.

From potentiodynamic polarization curves the polarization resistance for composite coating Ni-Si obtained at 3 A/dm^2 with 20 g/L silicon nano in electrolyte was 11.24 kΩ·cm^2. For composite coating Ni-Si obtained at 2A/dm^2 with 10 g/L silicon nano in electrolyte the polarization resistance was 32.10 kΩ·cm^2.

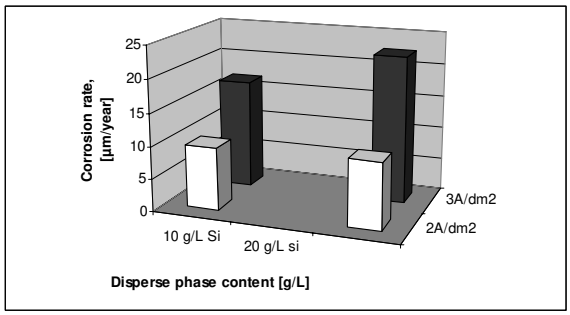

Fig. 7. *The variation of corrosion rate with the content of the disperse phase and current density*

The better corrosion resistance coating Ni-Si obtained at 2A/dm^2 could be due to the fine surface structure of composite coating compared with coating Ni-Si obtained at 3A/dm^2. Microhardness measurements were carried out using a Vickers microhardness tester, applying 20 g load for 10 s time [11].

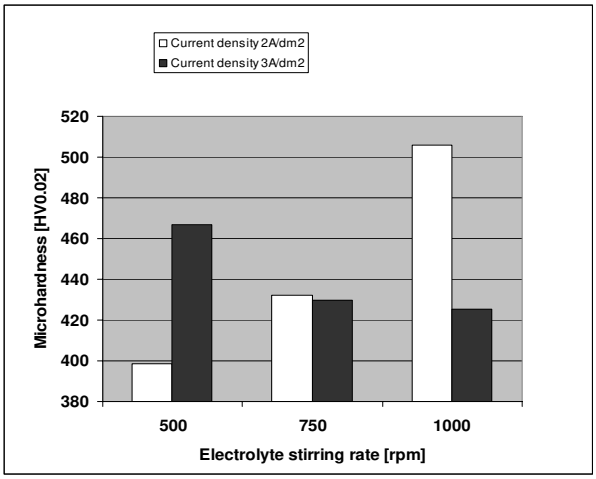

Fig. 8. *Microhardness as a function of electrolyte stirring rate (10 g/L Si) [13]*

The mean value of Vickers microhardness of pure nickel coatings has been found of about 300 $HV_{0.02}$ while composite coatings Ni-Si obtained at 2A/dm^2 with 10 g/L silicon nano in electrolyte is about 505 $HV_{0.02}$. This result shows that the codeposition of Si nanoparticles ameliorates the mechanical properties by 70% microhardness increase.

4. Conclusions

Nano-sized Si particles were successfully co-deposited in the nickel matrix by electrodeposition technique with a current density of 2 A/dm^{2}and 3 A/dm^2. Deposited layer thickness increases with current density and decreases with increasing electrolyte stirring rate. It is also observed that the Ni–Si nanocomposite sample deposited from electrolyte with a current density 2A/dm^2 and with 20 g/L silicon nano in electrolyte solution has the highest corrosion resistance. This is due to the fact that it has the smallest crystallite.

Highest microhardness value was obtained for composite coating Ni-Si at 2A/dm^2 with 10 g/L silicon nano in electrolyte.

References

[1]. R. W. Messler Jr. - *Joining Composite Materials and Structures: Some Thought-Provoking Possibilities,* Journal of Thermoplastic Composite Materials, vol. 17(1), p. 51, 2004.

[2]. S. Ranganatha, T.V. Venkatesha, K. Vathsala - *Development of electroless Ni–Zn–P/nano-TiO_2 composite coatings and their properties*, Applied Surface Science 256 (2010) 7377–7383.

[3]. Alina–Crina Ciubotariu, Lidia Benea, Magda Lakatos–Varsanyi, Viorel Dragan - *Electrochemical impedance spectroscopy and corrosion behaviour of Al_2O_3–Ni nano composite coatings*, Electrochimica Acta 53 (2008) 4557–4563.

[4]. Yu-Jun Xue, Xian-Zhao Jia, Yan-Wei Zhou, Wei Ma, Ji-Shun Li - *Tribological performance of Ni–CeO_2 composite coatings by electrodeposition*, Surface & Coatings Technology 200 (2006) 5677 – 5681.

[5]. Katarzyna Zielinska, Alicja Stankiewicz, Irena Szczygiel - *Electroless deposition of Ni–P–nano-ZrO_2 composite coatings in the presence of various types of surfactants*, Journal of Colloid and Interface Science 377 (2012) 362–367.

[6]. P. Fellner, Phuong Ky Cong, *Ni-B and Ni-Si composite electrolytic coatings*, Surface and Coatings Technology 82 (1996) 317-319.

[7]. G. I. Desyatkova, L. M. Yagodkina, I. E. Savochkina, and G. V. Khaldeev - *Composite Nickel-Based Electroplates*, Protection of Metals, Vol. 38, No. 5, 2002, pp. 466–470.

[8]. S. Afroukhteh, C. Dehghanian, M. Emamy - *Preparation of the Ni–P composite coating co-deposited by nano TiC particles and evaluation of it's corrosion property*, Applied Surface Science 258 (2012) 2597– 2601.

[9]. Babak Bakhit, Alireza Akbari - *Effect of particle size and co-deposition technique on hardness and corrosion properties of Ni–Co/SiC composite coatings*, Surface & Coatings Technology 206 (2012) 4964–4975.

[10]. H. Gül, F. Kilic, M. Uysal, S. Aslan, A.Alp, H. Akbulut - *Effect of particle concentration on the structure and tribological properties of submicron particle SiC reinforced Ni metal matrix composite (MMC) coatings produced by electrodeposition*, Applied Surface Science 258 (2012) 4260–4267.

[11]. Mohsen Rostami, Abbas Fahami, Bahman Nasiri-Tabrizi, Reza Ebrahimi-Kahrizsangi, Ahmad Saatchi - *Characterization of electrodeposited Ni–SiC–C_g nanocomposite coating*, Applied Surface Science 265 (2013) 369–374.

[12]. Jothi Sudagar, Jianshe Lian, Wei Sha - *Electroless nickel, alloy, composite and nano coatings – A critical review*, Journal of Alloys and Compounds 571 (2013) 183–204.

[13]. G. Istrate, P. Alexandru, O. Mitoseriu, M. Marin - *Morphology of nickel matrix composite coatings with nano-silicon dispersion phase,* The Annals of "Dunarea de Jos" University of Galati. Fascicle IX Metallurgy and Materials Science, N°. 3, 2011, p. 38 – 41, The journal is indexed in Cambridge Scientific Abstract, http://www.fmet.ugal.ro/Anale/Anale%203-2011.pdf..

MANUSCRISELE, CĂRŢILE ŞI REVISTELE PENTRU SCHIMB, PRECUM ŞI ORICE CORESPONDENŢE SE VOR TRIMITE PE ADRESA:

MANUSCRIPTS, REVIEWS AND BOOKS FOR EXCHANGE COOPERATION, AS WELL AS ANY CORRESPONDANCE WILL BE MAILED TO:

LES MANUSCRIPTS, LES REVUES ET LES LIVRES POUR L'ECHANGE, TOUT AUSSI QUE LA CORRESPONDANCE SERONT ENVOYES A L'ADRESSE:

MANUSCKRIPTEN, ZIETSCHRITFTEN UND BUCHER FUR AUSTAUCH SOWIE DIE KORRESPONDENZ SID AN FOLGENDE ANSCHRIFT ZU SEDEN:

After the latest evaluation of the journals achieved by National Center for the Science and Scientometry Politics (**CENAPOSS**), as recognition of its quality and impact at national level, the journal is included in B^+ category, 215 code (http://www.cncsis.ro/2006_evaluare_rev.php).

The journal is indexed in:
CSA: http://www.csa.com/ids70/serials_source_list.php?db=mechtrans-set-c
EBSCO: http://www.ebscohost.com/titleLists/a9h-journals.pdf
Copernicus: http://journals.indexcopernicus.com/karta.php

The papers published in this journal can be visualized on the "Dunarea de Jos" University of Galati site, the Faculty of Materials and Environmental Engineering, page: www.fimm.ugal.ro.

Publisher's Name and Address:
Contact person: Antoaneta CĂPRARU
Galati University Press - GUP
47 Domneasca St., 800008 - Galati, Romania
Phone:+40 336 130139, Fax: +40 236 461353
Email: gup@ugal.ro

Editor's Name and Address:
Prof. Dr. Eng. Marian BORDEI
Dunarea de Jos University of Galati, Faculty of Materials and Environmental Engineering
111 Domneasca St., 800201 - Galati, Romania
Phone: +40 336 130223, Phone/Fax: +40 236 460750
Email: mbordei@ugal.ro

AFFILIATED WITH:

- *ROMANIAN SOCIETY FOR METALLURGY*
- *ROMANIAN SOCIETY FOR CHEMISTRY*
- *ROMANIAN SOCIETY FOR BIOMATERIALS*
- *ROMANIAN TECHNICAL FOUNDRY SOCIETY*
- *THE MATERIALS INFORMATION SOCIETY (ASM INTERNATIONAL)*

Annual subscription (4 issues per year)

Edited under the care of
Faculty of
MATERIALS AND ENVIRONMENTAL ENGINEERING

Edited date: 31.12.2013
Issues number: 200
Printed by
Galati University Press
accredited CNCSIS
47, Domnească Street, 800036
Galati, Romania